



UNIVERSITÀ DEGLI STUDI DI PADOVA

Dipartimento di Fisica e Astronomia “Galileo Galilei”

Master Degree in Physics

Final Dissertation

Mathematical modeling of phasic calcium dynamics in HaCaT
cells

Thesis supervisor

Prof. Fabio Mammano

Thesis co-supervisor

Prof. Morten Gram Pedersen

Candidate

Nazli Shojaei Barjouei

Academic Year 2022/23

(This page is intentionally left blank)

Acknowledgments

I would like to express my sincere gratitude to my supervisor Prof. Fabio Mammano for his invaluable assistance and support during the course of this thesis. He provided valuable guidance and mentorship, and his insights and expertise were instrumental in the success of this project. I'm deeply grateful for his time and effort in helping me to complete this thesis.

I would also like to thank Prof. Morten Gram Pedersen for the patient guidance, encouragement and advice that he has provided throughout my time as his student. I have been extremely lucky to have a supervisor like him who cared so much about my work, and who responded to my questions and queries so promptly.

Finally, I must express my very profound gratitude to my parents for providing me with unfailing support and continuous encouragement throughout my years of study and through the process of researching and writing this thesis. This accomplishment would not have been possible without them. Thank you.

(This page is intentionally left blank)

Abstract

Background: Connexin (Cx) channels are ubiquitous, providing pathways for movement of molecules between cells and for release of molecular effectors into the extracellular environment (plasma membrane hemichannels (HCs)). To maintain an adequate permeability barrier, HCs are tightly regulated by normal extracellular calcium ion (Ca^{2+}) to be closed under most conditions. Cx mutations that disrupt HC regulation by Ca^{2+} cause human pathologies, due to aberrantly open HCs. These pathological conditions including cardiac infarct, stroke, deafness, cataracts, epilepsy, Alzheimer's disease, and skin diseases. Therefore, Cx HCs have emerged as a valid therapeutic target. Cx HCs activity has been explored indirectly by the release of adenosine triphosphate (ATP) and other metabolite, as well as by electrophysiological methods and/or using HC-permeable dye uptake measurements. Recently, all-optical assay based on fluorometric measurements of Ca^{2+} uptake with a Ca^{2+} -selective genetically encoded indicator (GCaMP6s), that permits the optical tracking of cytosolic Ca^{2+} concentration changes with high sensitivity, was presented, the assay in stable pools of HaCaT cells overexpressing Cxs of interest, under control of a tetracycline (Tet) responsive element (TRE) promoter (Tet-on), for the characterization of new monoclonal antibodies targeting the extracellular domain of the HCs.

Aim: Developing a mathematical model of Ca^{2+} dynamics with the aim of simulating the complex responses measured experimentally by fluorescence microscopy in HaCaT cells challenged by a sudden increase of the extracellular Ca^{2+} concentration. Moreover, the model aims to explain the observed damping effects caused by increasing concentrations of different HC blockers, including monoclonal antibodies targeted at the HC extracellular domain.

Method: Open source ImageJ software as well as Vimmaging (a custom-made software developed under the MATLAB environment) were used to derive Ca^{2+} uptake traces in HaCaT-Cx26-GCaMP6s cell cultured bathed in extracellular medium and exposed to CaCl_2 bolus concentrations to reach final extracellular Ca^{2+} concentrations of 2mM, 1mM, 560 μM , 260 μM , and 100 μM . A set of previously derived differential equations that successfully modeled epidermal Ca^{2+} dynamics in vivo was adapted to the peculiar toolset of ion channels and transporters expressed in HaCaT cells to generate an original model variant account quantitatively for the insurgence of a biphasic

elevation of intracellular Ca^{2+} when the extracellular Ca^{2+} concentration overcomes a critical threshold.

Conclusion: Our mathematical simulation of Ca^{2+} dynamic has revealed that the first elevation phase of Ca^{2+} observed experimentally is due to the release of Ca^{2+} from endoplasmic reticulum to cytosol, whereas the second peak is the result of influx of Ca^{2+} from extracellular milieu to cytosol through HC.

Table of contents

1	Introduction and aims	12
	1.1 Calcium in human's body	12
	1.1.1 Ca ²⁺ signaling	12
	1.1.2 Calcium stores and pumps	14
	1.2 ATP as a signaling molecule	18
	1.3 Skin	19
	1.3.1 Keratinocytes differentiation	20
	1.3.2 Connexin HCs	25
	1.3.3 Inhibitors of Cx HCs	34
	1.4 Aim and structure of this thesis work	35
	1.5 References	37
2	Materials and methods	51
	2.1 A short review of the experimental work	51
	2.2 Calcium imaging overview	52
	2.2.1 Optical measurement of ion concentration	52
	2.2.2 Linking fluorescent to ion concentration	54
	2.2.3 Confocal microscopy	58
	2.2.4 Two photon microscopy	60
	2.3 Image processing	61
	2.4 References	64
3	Mathematical model	67
	3.1 Introduction	67
	3.2 Regulation of cytosolic Ca ²⁺	67
	3.3 Hemichannel model	71
	3.4 References	73
4	Results and discussion	76
	4.1 Results	76
	4.2 Discussion	84
	4.3 Conclusion	88
	4.4 References	89

List of Figures

Figure 1.1 :	Schematic model of intracellular Ca^{2+} homeostasis	13
Figure 1.2 :	Ca^{2+} channels, pumps and exchangers and important regulatory domains	15
Figure 1.3 :	Schematic diagram of some of the interactions between Ca^{2+} and IP_3 dynamics	17
Figure 1.4 :	Scheme of skin layers	19
Figure 1.5 :	An evidence-based or potential association between epidermal Ca^{2+} gradients and the epidermal barrier	22
Figure 1.6. :	Extracellular Ca^{2+} concentration-stimulated signaling responses in keratinocytes	24
Figure 1.7 :	Schematic representation of the role of HCs in development, cell survival and death	26
Figure 1.8 :	Overall structure of Cx26 GJ channel in ribbon representation	28
Figure 1.9 :	Cx26 topology and mutant residues	28
Figure 1.10 :	Cxs expression profiles through epidermis	29
Figure 1.11 :	Main pathophysiological changes associated with human diseases	32
Figure 1.12 :	Experimental results of Ca^{2+} uptake in HaCaT-Cx26-GCaMP6s cells.	35
Figure 1.13 :	Dose-dependent effect of the abEC1.1h-IgG for concentration in the range 0.001nM- 10 μM	36
Figure 2.1 :	Chemical structure and pH dependence of Ca^{2+} affinity of BAPTA and EGTA	53
Figure 2.2 :	Spectral properties that can be used to measure Ca^{2+} concentration.	53
Figure 2.3. :	Graphical representation of the single wavelength $[\text{Ca}^{2+}]$ -measurement formula	56
Figure 2.4 :	Excitation spectra of fura-2 for the indicated values of the free Ca^{2+} concentration	57
Figure 2.5 :	Components of a confocal microscope	58
Figure 2.6 :	Scheme of the confocal microscope system.	60
Figure 2.7 :	Photobleaching correction for an individual cell exposed to CaCl_2 to reach 2mM final Ca^{2+} concentration	62

Figure 2.8 :	Ca ²⁺ uptake of HaCaT-Cx26-GCaMP6s cells exposed CaCl ₂ bolus concentration to reach different final Ca ²⁺ concentrations	63
Figure 3.1 :	Components of computational model	68
Figure 3.2 :	HC model	71
Figure 4.1 :	Simulation results for HC without blocker	76
Figure 4.2 :	Simulation results for HC with blocker	77
Figure 4.3 :	Simulation results for fluoresce signal as a function of time for changing individual parameter	78
Figure 4.4 :	Simulation results for ER Ca ²⁺ concentration as a function of time for changing individual parameter	80
Figure 4.5 :	Results of different final Ca ²⁺ concentrations, when HC is open for parameters with specific values.	82
Figure 4.6 :	Results of different final Ca ²⁺ concentrations, when HC is blocked for parameters with specific values	83

List of tables

Table 1.1 :	Functions of elements in organisms	12
Table 1.2 :	Regulation of HCs activity.	25
Table 1.3 :	Clinical phenotypes of Cx skin diseases	31
Table 3.1 :	Cytosolic Ca ²⁺ model parameters	72
Table 3.2 :	HC model parameters	72

(This page is intentionally left blank)

1 INTRODUCTION AND AIMS

1.1 Calcium in human's body













Apart from four elements, which are responsible for more than 96% of the organisms' mass, oxygen, carbon, hydrogen, and nitrogen, other elements including calcium, phosphorus, potassium, and magnesium, are also present. The lists of elements that make up organisms and the importance of each in typical plants and animals are described in (Table 1.1).

Calcium is the most abundant mineral in the body. Almost all calcium in the body is stored in bones and teeth, giving them structure and hardness. Ca^{2+} are involved in regulating almost all biological functions of the body such as nerve-information transmission, heart and muscle contractions, learning and memory, embryo formation and development, cell proliferation and apoptosis, cell division and differentiation, cell energy metabolic, protein phosphorylation and dephosphorylation, and gene expression and regulation [2,3].

1.1.1 Ca^{2+} signaling

The process of Ca^{2+} signaling consists of a series of molecular and biophysical phenomena that link the external stimulus to the expression of some appropriate intracellular responses via an increase in cytoplasmic Ca^{2+} as a signal [4]. The most common external signal is a neurotransmitter, hormone or growth factor; however, for excitable cells, the initial chemical stimulus is about membrane excitation, which in turn activates a Ca^{2+} -signaling pathway. The signaling machinery of the cell is composed of multiple discrete units, including ryanodine receptor (RyR), inositol 1,4,5-triphosphate (IP_3) receptor (IP_3R),

Table 1.1 Functions of elements in organisms (from ref. [1])

Functions of Elements in Organisms	
Element (chemical symbol)	Functions
 Oxygen	Required for cellular respiration; present in most organic compounds; component of water
 Carbon	Forms backbone of organic molecules; each carbon atom can form four bonds with other atoms
 Hydrogen	Present in most organic compounds; component of water; hydrogen ion (H^+) is involved in some energy transfers
 Nitrogen	Component of proteins and nucleic acids; component of chlorophyll in plants
 Calcium	Structural component of bones and teeth; calcium ion (Ca^{2+}) is important in muscle contraction, conduction of nerve impulses, and blood clotting; associated with plant cell wall
 Phosphorus	Component of nucleic acids and of phospholipids in membranes; important in energy transfer reactions; structural component of bone
 Potassium	Potassium ion (K^+) is a principal positive ion (cation) in interstitial (tissue) fluid of animals; important in nerve function; affects muscle contraction; controls opening of stomata in plants
 Sulfur	Component of most proteins
 Sodium	Sodium ion (Na^+) is a principal positive ion (cation) in interstitial (tissue) fluid of animals; important in fluid balance; essential for conduction of nerve impulses; important in photosynthesis in plants
 Magnesium	Needed in blood and other tissues of animals; activates many enzymes; component of chlorophyll in plants
 Chlorine	Chloride ion (Cl^-) is principal negative ion (anion) in interstitial (tissue) fluid of animals; important in water balance; essential for photosynthesis
 Iron	Component of hemoglobin in animals; activates certain enzymes

*Other elements found in very small (trace) amounts in animals, plants, or both include iodine (I), manganese (Mn), copper (Cu), zinc (Zn), cobalt (Co), fluorine (F), molybdenum (Mo), selenium (Se), boron (B), silicon (Si), and a few others.

phospholipase C (PLC), and sarcoplasmic/endoplasmic reticulum ATPase (SERCA.) These elements frequently exist in cluster or are distributed through the cell and this leads to local or polarized Ca^{2+} .

Concentration of the Ca^{2+} in the cytosol should be maintained at nanomolar, which is 10-fold lower than that of extracellular milieu. Increases in Ca^{2+} concentration can be achieved by both entry of that ions from the extracellular space through plasma membrane (PM) channels and also release from intracellular stores (figure 1.1).

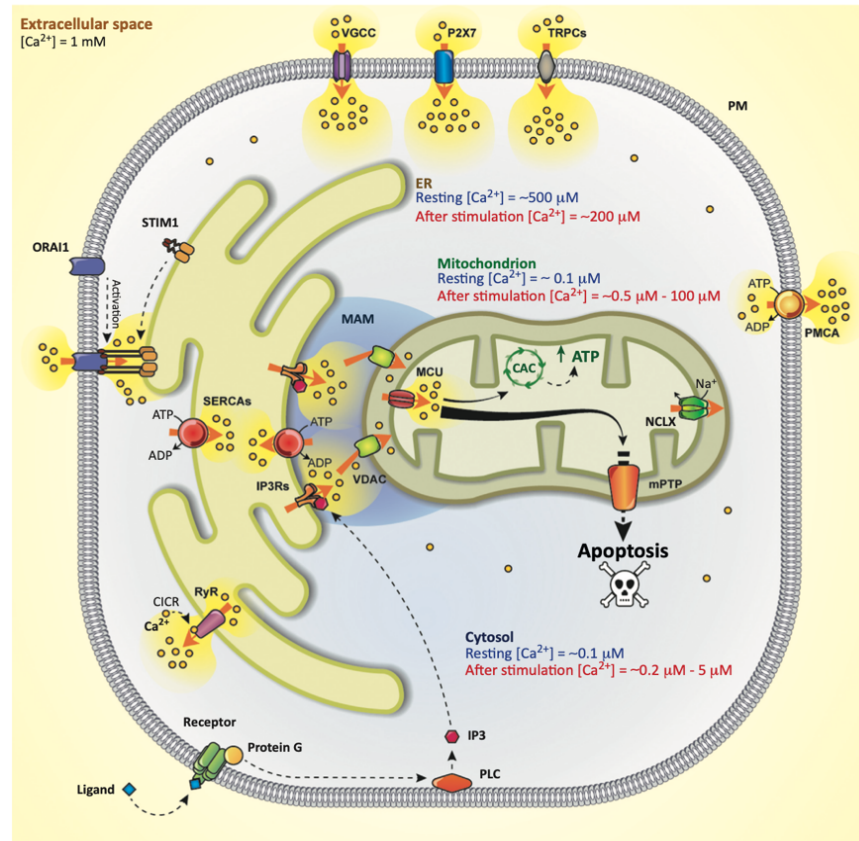


Figure 1.1 Schematic model of intracellular Ca^{2+} homeostasis.

The Ca^{2+} concentration [Ca^{2+}] inside cells under resting conditions is maintained at a low concentration (Ca^{2+} levels are indicated in blue). Ca^{2+} enters the cell via different channels [voltage-gated Ca^{2+} channels (VGCC), P2X7, and transient receptor potential channels (TRPCs)] that are located on the PM. The binding of ligands to plasma membrane G-protein-coupled receptors activates PLC to initiate the generation of IP₃ and the release of Ca^{2+} from the ER and the Golgi apparatus into the cytosol (the Ca^{2+} levels reached in stimulated cells are indicated in red). Mitochondria are prone to take up great quantities of Ca^{2+} due to their interaction with the ER through contact sites defining hotspot Ca^{2+} signaling units (MAMs). After agonist stimulation, Ca^{2+} is released from the ER to mitochondria, where it triggers an increase in cellular metabolism and ATP production. By contrast, the mitochondrial Ca^{2+} overload induced by apoptotic stimuli or ER stressors sensitizes the mitochondria to apoptosis, leading to mitochondrial permeability transition pore (mPTP) opening. Ca^{2+} backs to its resting levels through the concerted action of channels and pumps, such as plasma membrane PMCA and the $\text{Na}^{+}/\text{Ca}^{2+}$ exchanger (NCX), which permit ion extrusion in the extracellular milieu. SERCA pump re-establishes basal Ca^{2+} levels in intracellular stores. STIM1 and ORAI1 are the major proteins responsible for the SOCE mechanism. (from ref. [3])

1.1.2 Calcium stores and pumps

A key characteristic determining how Ca^{2+} serves as a signaling molecules is that, unlike organic messengers (i.e. cyclic adenosine monophosphate (cAMP), $\text{Na}^+/\text{Ca}^{2+}$ exchanger (NCX)), Ca^{2+} cannot be created or metabolized. Consequently, cell signaling with Ca^{2+} requires a strategy of accumulation or storage coupled with Ca^{2+} release (figure 1.2). The cell exploits major Ca^{2+} stores, the extend environments that contains a virtually infinite supply of Ca^{2+} of concentration of about 1-2 mM and internal stores usually contained within endoplasmic reticulum (ER) or muscle-equivalented sarcoplasmic reticulum (SR). The storage capacity of SR/ER is increased by the presence of Ca^{2+} buffering proteins. For example, calsequestrin and calretinin, that can bind large quantities of Ca^{2+} [5,6]. The free Ca^{2+} concentration in the ER is in the 10-100 μM range. Mitochondria can serve as a Ca^{2+} reservoir, taking up Ca^{2+} in times of excess and releasing Ca^{2+} when cytosolic Ca^{2+} falls.

To maintain the necessary electrochemical gradient that derives Ca^{2+} release from these stores, the cell membrane must be relatively impermeable to Ca^{2+} . In addition, the cell must be able to reduce the cytoplasmic Ca^{2+} concentration and reload the stores to turn off the signal to reset the system. This is achieved by energy-dependent Ca^{2+} -pump (Ca^{2+} ATPase) or Ca^{2+} exchanger located in cell membrane. There are two basic form of Ca^{2+} ATPase, PMCA and SERCA pumps. The over expression of these two pumps has an obvious effect on the Ca^{2+} influx across the PM elicited by the emptying of intracellular Ca^{2+} store [7].

PMCA is a transport protein in the PM of cell and functions to remove Ca^{2+} from the cell. As one of the P-type pumps family, it has 10 transmembrane helix and two cytosolic loops. The most striking feature of it is a C-terminal tail that include most of regulatory sites including that for calmodulin. The calmodulin contains four Ca^{2+} binding sites. The binding of Ca^{2+} to calmodulin causes a conformational change that permits Ca^{2+} /calmodulin to bind various target proteins, thereby switching their activity on and off. Overall, PMCA and NCX are together the main regulators of the intracellular Ca^{2+} concentration.

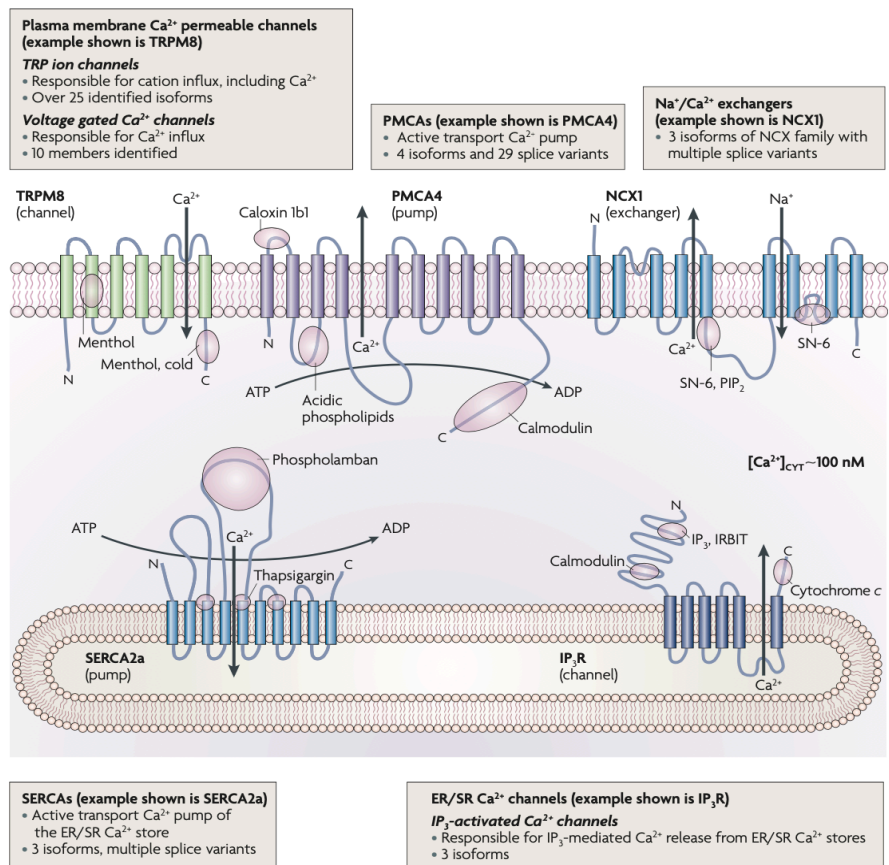
The SERCA pump is a 110-kDa transmembrane protein that has been identified both in prokaryotes and eukaryotes cells. Even though its primary function is to control cytosolic Ca^{2+} , it plays a crucial role in many cellular functions such as cell growth and differentiation. The crystal structure of SERCA confirmed the existence of 10 transmembrane helices (M1–M10), three cytoplasmic domains, an A domain, a P domain (phosphorylation domain), and an N domain where ATP binds. Moreover, there are two Ca^{2+} binding sites located near the cytoplasmic surface of the lipid layer.

They are accessible just from the cytoplasm and not from the SR lumen. As ATP phosphorylate the enzyme, a series of conformational changes initiates that, through long-range interactions, causes change the conformation of the transmembrane helices and repercussion is that the access of bound Ca^{2+} to the cytoplasm is lost, whereas access to the lumen is gained, resulting in Ca^{2+} transport to the lumen. For each molecule of ATP hydrolyzed, the pump transports two molecules of Ca^{2+} ions. Since the SERCA pump is highly abundant in the SR, Ca^{2+} ion reuptake takes only a few milliseconds. However, there are number of factors can affect SERCA pump activity which are including Ca^{2+} ion concentration, ATP level, pH, and adenosine diphosphate (ADP) and inorganic phosphate level [8].

Figure 1.2 Ca^{2+} channels, pumps and exchangers and important regulatory domains.

Arrows show possible directions for Ca^{2+} transport (note that the $\text{Na}^+/\text{Ca}^{2+}$ exchanger (NCX1) can transport Ca^{2+} in either direction depending on the concentration gradients for K^+ , Na^+ and Ca^{2+} across the plasma membrane). Pink shapes show binding sites of modulators. Depictions of Ca^{2+} transporters are schematic; some channels such as TRPM8 and IP_3R are functional as multimers. The schematic representation is not intended to reflect the stoichiometry of ion or co-ion transport, nor the precise domains that are involved in the transport of Ca^{2+} . Plasma membrane Ca^{2+} permeable channels such as TRPM8, which allow Ca^{2+} influx, include: the voltage-gated Ca^{2+} channels (subdivided into L-type, T-type, P/Q-type, R-Type and N-Type); and the TRP ion channels that differ in selectivity for Ca^{2+} (subdivided into classes: A, C, M, ML, P and V). TRPM8 is permeable to Ca^{2+} and has specific domains associated with

the cellular responses to menthol and cold. PMCA4 is an example of a Ca^{2+} efflux pump, which can be inhibited by the peptide caloxin 1b1 with a proposed extracellular binding site. PMCA4 has many other biological regulators, including calmodulin and acidic phospholipids. NCX1 is an example of a NCX, with pharmacological modulators such as SN-6 capable of inhibiting the Ca^{2+} influx mode, and identified domains for regulators such as PIP_2 (phosphatidylinositol-4,5-bisphosphate). SERCA2a is an example of an SR/ER Ca^{2+} pump that sequesters Ca^{2+} into internal stores. Specific domains associated with the binding of the pharmacological inhibitor thapsigargin, and biological regulators such as phospholamban, have been identified. IP_3R is an example of an IP_3 -activated Ca^{2+} channel on the SR/ER Ca^{2+} stores. The domains associated with activation by the endogenous regulator IP_3 (generated after the activation of some G protein-coupled receptors) are shown. Endogenous regulators of IP_3 responsiveness include IRBIT, cytochrome c and calmodulin. (from ref. [9])



Cells manage external Ca^{2+} by activating various entry channels. The most widely known are voltage operated channels (VOCs). These channels are usually found in the PM of excitable cells. The permeability of channels is determined by the molecular characteristics of channel pore. They are activated by depolarizing membrane potentials. Another class of Ca^{2+} release channel is the receptor operated channels (ROCs). These channels open upon binding of an agonist to the channel. And lastly, store-operated channels (SOCs) which are believed to open in response to the emptying of the internal Ca^{2+} stores and their primary function is the replacement of internal Ca^{2+} stores after a steady flux of Ca^{2+} via these channels may itself serve as a biological signal.

In terms of Ca^{2+} release from internal stores, the two most important channels are RyR and IP_3R . These channels/receptors must bind Ca^{2+} and/or IP_3 in order to open and therefore may be considered as specialized forms of ROCs.

RyRs are ion channels responsible for the release of Ca^{2+} ions from the SR/ER. Ca^{2+} is a major physiological ligand that triggers opening of RyR. However, as Ca^{2+} level in the cytoplasm rises, Ca^{2+} can trigger closing of the RyR. This shows that there are multiple Ca^{2+} -binding sites with different affinities and binding kinetics [10,11]. There are three RyR subtypes that have been described which various cell types are known to express each. RyR1 is essential for excitation–contraction coupling in the skeletal muscle, while RyR2 is necessary in the cardiac muscle. RyR2 and RyR3 have roles in intracellular Ca^{2+} regulation in the brain [12,13]. Immunohistochemical studies and reverse transcription-PCR revealed the expression of all three types of RyR proteins in epidermal keratinocyte [11]. Recent study by Wang et al, emphasizes the role of RyR activation in mediating skin allergy [14].

IP_3R is a membrane glycoprotein complex acting as a Ca^{2+} channel activated by IP_3 . IP_3R is very diverse among organisms, and is necessary for control of cellular and physiological processes like cell adhesion, cell proliferation, apoptosis, and fertilization [15]. There is strong evidence suggesting that the IP_3R plays an important role in the conversion of external stimuli to intracellular Ca^{2+} signals characterized by complex patterns relative to both space and time. The basic property of the IP_3R is that they respond in a time-dependent manner to slopes of Ca^{2+} or IP_3 . Thus, in response to a step increase of IP_3 or Ca^{2+} the receptor opens, probability first opens to a peak and then declines to a lower plateau [16].

There are two principal ways in which Ca^{2+} ion can influence the concentration of IP_3 (Figure.1.3). Ca^{2+} can activate PLC, leading to an increase in the rate of production of IP_3 , and it can also increase the rate at which IP_3 is phosphorylated by the 3-kinase. The end product of phosphorylation by the

3-kinase, IP_4 , acts as a competitive inhibitor of dephosphorylation of IP_3 by the 5-phosphatase. Not all of these feedbacks are significant in every cell type.

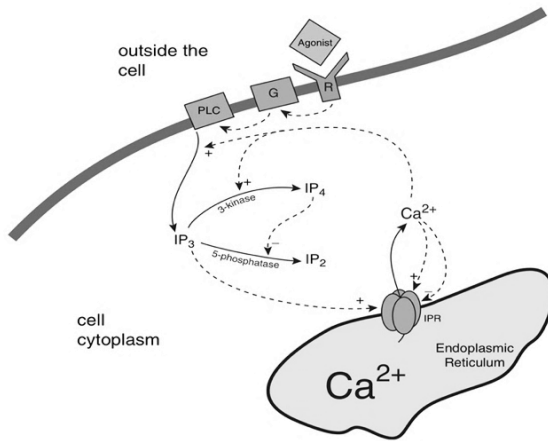


Figure 1.3 Schematic diagram of some of the interactions between Ca^{2+} and IP_3 dynamics. Ca^{2+} can activate PLC, leading to an increase in the rate of production of IP_3 , and it can also increase the rate at which IP_3 is phosphorylated by the 3-kinase. The end product of phosphorylation by the 3-kinase, IP_4 , acts as a competitive inhibitor of dephosphorylation of IP_3 by the 5-phosphatase. Not all of these feedbacks are significant in every cell type (from ref. [17]).

Another important receptor on PM is Ca^{2+} -sensing receptor (CaSR). The CaSR is a family C G protein-coupled receptors (GPCR) that is expressed on the cell surface as a dimer and signals via G proteins and β -arrestin. They have pivotal roles in neurotransmission, nutrient sensing and Ca^{2+} homeostasis [2]. X-ray crystallography studies have shown that the human CaSR has a glycosylated extracellular domain, which binds extracellular Ca^{2+} at three distinct sites within the Venus flytrap (VFT) module, and also at a site located between the VFT module and the cysteine-rich domain (CRD). The CaSR binds amino acids within the cleft of the VFT module, and the binding of both Ca^{2+} and amino acids might be required to fully activate the CaSR [2]. The binding of physiological ligands to G-protein or phosphotyrosine-coupled CaSR at the PM activates different isoforms of PLC, which most often initiates the primary route for Ca^{2+} mobilization. In turn, PLC hydrolyzes the PM lipid phosphatidylinositol 4,5-bisphosphate (PIP₂) to IP_3 and diacylglycerol (DAG). When IP_3 binds its receptor, Ca^{2+} is released into cytosol, thereby activating various Ca^{2+} regulated intracellular signal.

The CaSR has key physiological roles in calcitropic tissues (for instance, parathyroid glands, kidneys, bone and breast) and in noncalcitropic tissues (for example, brain, cardiovascular system, lungs, intestine, pancreas and skin). Altered CaSR activity in calcitropic tissues leads inherited diseases of Ca^{2+} homeostasis and contributes to the pathogenesis of both primary hyperparathyroidism and secondary hyperparathyroidism. By contrast, alterations in CaSR function or expression in noncalcitropic tissues are associated with many disease [2].

1.2 ATP as a signaling molecule

ATP is the source of energy for use and storage at the cellular level. Beside this, the breakdown of ATP through hydrolysis serves a broad range of cell functions, including intracellular signaling, DNA and RNA synthesis, purinergic signaling, synaptic signaling, active transport, and muscle contraction. The concept of purinergic signaling was accepted when in 1990's the receptor subtypes for purines and pyrimidines were cloned and characterized. Two families of purinergic receptors have been defined to date, namely P1 and P2 receptors. The P1 receptors belong to the superfamily of seven transmembrane receptors which are subdivided into four subtypes, namely A1, A2A, A2B and A3 receptor [18]. These receptors bind extracellular adenosine with different affinities [19]. The P2 receptor family is subdivided in two subfamilies, namely P2X and P2Y [20-22]. The P2X receptors are ligand-gated ion channels of which seven subtypes have been characterized (P2X1–7) [23,24]. The P2Y receptors are seven transmembrane receptors of which eight subtypes have been identified (P2Y1, 2, 4, 6, 11–14) [21, 25,26]. This trans-PM concentration gradient may cause large responses when ATP is released. Furthermore, ATP is water soluble which permits rapid diffusion through the aqueous tissue interstitium. Finally, ATP is quickly degraded by extracellular ecto-nucleotide enzymes that terminate its signaling action to prevent overstimulation. Thus, ATP molecules in the extracellular compartment are finely controlled by enzymes catalyzing their conversion. In particular, not only this molecule is crucial for peripheral and central nervous systems, but also it is a powerful extracellular messenger to non-neuronal cells, including: secretory, exocrine and endocrine, endothelial, immune, musculo-skeletal and inflammatory cells and is involved in various cellular pathways such as proliferation, differentiation, migration and death in development and regeneration [22,27,28]. Recently, the focus has been on the pathophysiology and therapeutic potential of both P1 and P2 receptors [29-37]. Studies focused on different pathophysiological aspects of purinergic receptors that are available, including inflammatory and immune disorders cancer, P2X7 receptors as therapeutic targets and pain [38-44].

ATP-mediate signaling and Ca^{2+} signaling are profoundly interconnected, and these two signaling pathways are essential for most of cellular responses and secretions. Cytosolic ATP concentration is generally between 1–10 mM, whereas the extracellular concentration does not exceed 1–10 nM [3]. ATP as an energy source is required to keep low the cytosolic Ca^{2+} concentration [45]. On the other hand, ATP molecules are often released by Ca^{2+} -regulated exocytosis to promote intercellular communication [46, 47]. ATP effects are mediated by the extended family of purinoceptors linked

to Ca^{2+} signaling. Generation of Ca^{2+} signals seems to be the general consequence of purinoceptors activation. All P2X receptors are permeable to Ca^{2+} and their activation leads to an enhancement in intracellular Ca^{2+} from extracellular sources [48,49]. P2Y receptors instead, may lead to elevation in intracellular Ca^{2+} from intracellular sources, depending on their subtype. Indeed, some of these receptors (P2Y1, P2Y2, P2Y4, P2Y11) are coupled, via G proteins, to PLC that produces IP_3 and DAG promoting Ca^{2+} release from the ER via IP_3 -gated receptors. The ATP-induced Ca^{2+} signaling mediated via the metabotropic route seems to be universal in non-excitabile cells such as immune cells, inner ear cell and epidermal keratinocytes cells [28,50-52]

1.3 Skin

The skin is the largest organ of the body which consists of epidermis and dermis (figure 1.4). The epidermis is the outer cellular layer of stratified squamous epithelium, that is avascular and takes on different thickness, while dermis is a dense bed of vascular connective tissue.

The different layers of epidermis are stratum basale, stratum spinosum, stratum granulosum, stratum lucidum, and stratum corneum. Stratum basale is the deepest layer and separated from dermis with the basement of membrane, and attached to it by hemidesmosome. Cells in stratum basale layer mitotically active stem cells which are constantly producing keratinocytes. Stratum spinosum

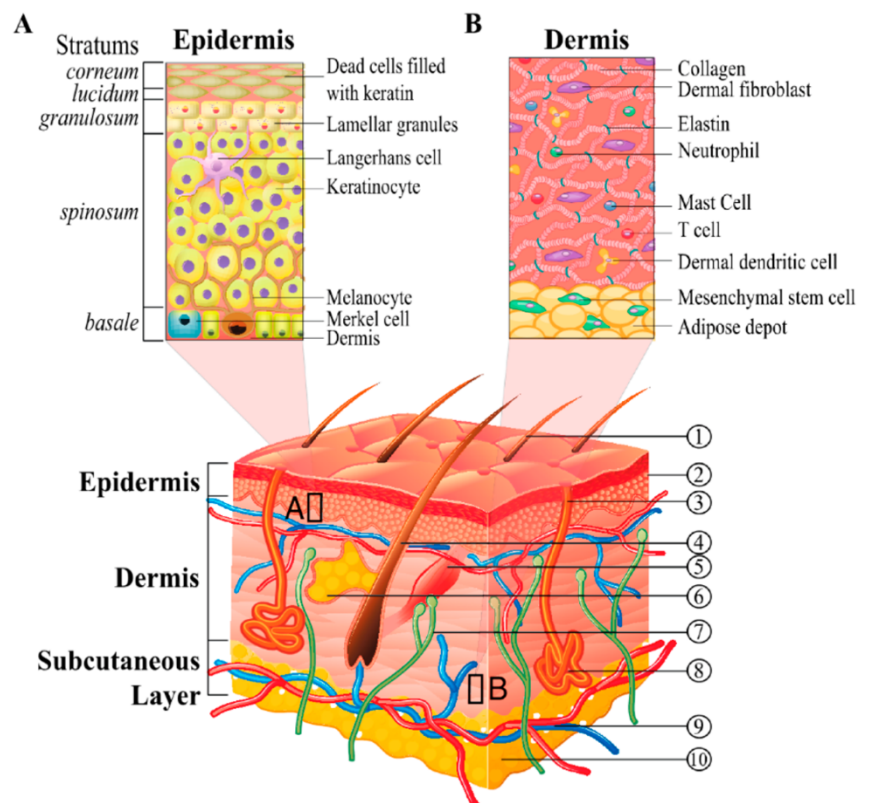


Figure 1.4 scheme of skin layers
 The references in the image point out: (1) hair shaft; (2) stratum corneum; (3) sweat-pore; (4) hair follicle; (5) arrector pili muscle; (6) sebaceous gland; (7) nerve; (8) eccrine sweat gland; (9) cutaneous vascular plexus; (10) adipose depot. Section (A) and (B) highlight a detailed structure of the epidermis and derma respectively. (from ref. [53])

(prickle cell layer), contains polyhedral cells with cytoplasmic processes which attach to neighboring cells by desmosome. Stratum granulosum contains diamond shaped cells with two types of granules, keratohyalin and lamellar, that contain keratin and glycolipid to form the bundles and keeping cell stuck together.

Stratum lucidum is thin clear layer composed of eleidin that is a transformation product of keratohyalin, and stratum corneum made of keratin and horny scales which is made of dead keratinocytes that is secrete defensins (part of first immune defense).

In terms of types of cell, epidermis has four types of cell, namely: keratinocytes, melanocytes, langerhans, and merkle's cell. The most abundant cell types in epidermis is keratinocytes that are located in basal layer, and by making and secreting lipids, they are responsible for formation of epidermal barrier. Melanocyte cells are highly differentiated cells that create pigment melanin inside melanosomes. With the process of differentiation these cells lose the proliferate potential. Langerhans cells are the first line defenders of skin and play a key role in antigen presentation. Merkle's cells are located above the basement membrane, and bounded to adjoining keratinocytes by desmosomes and contain intermediate keratin filaments.

The dermis layers are connected to epidermis and consist of two layers namely: papillary and reticular layer. The papillary layer is made of loose connective tissue and contacts epidermis, while reticular is composed of dense connective bundles of collagen fibers.

1.3.1 Keratinocytes differentiation

The process in which cellular maturation from the mitotic state to a differentiated state, that skin builds up a tough yet soft skin barrier to protect the body, occurs is called keratinocytes differentiation. Irreversibility of it, permits excessive keratinocytes' shedding, consequently, maintaining skin homeostasis and preventing different skin diseases [54].

Keratinocytes cells, as the predominant cells in skin, synthesize most structural components of epidermal barrier through the programmed process. They arise at innermost layer of the epidermis and follow cell division; some progeny stays in the basal layer as stem cell whereas other move to upper layer of epidermal. These migrating cells terminally differentiate to make the dead surface layer, however during this transition the cell changes both morphologically and biochemically. During the process, keratinocytes commences synthesize of important structural and catalytic dependent differentiation proteins including involucrin, keratin, filaggrin, and transglutaminase.

Ca^{2+} is the major regulator of keratinocytes differentiation both in vivo and in vitro. Signaling pathways involved with differentiation are regulated by Ca^{2+} and are including: the formation of desmosome, adhesion junction, and tight junctions. As keratinocytes move out from the basal layer and start to differentiate, desmogleins 2 and 3 (protein that binds with other cadherins to form desmosome), become the dominant desmosomal cadherins. An uneven distribution of integrins enables their attachment to basal lamina and adjacent cell, consequently helps to regulate their proliferation and subsequent differentiation. In epidermis, extracellular Ca^{2+} is provided by a Ca^{2+} gradient with peaking Ca^{2+} concentration in the granular layer and a significant decline in the stratum corneum. In basal layer, the concentration is low, however, that low Ca^{2+} keeps keratinocytes proliferating [55].

Keratinocytes in low Ca^{2+} concentration (0.03mM) proliferate but fail to differentiate into stratified layer [56]. Differentiation process is started as Ca^{2+} level is above 0.1mM. The response of keratinocytes to the Ca^{2+} switch (change in Ca^{2+} level) is multiphasic. The initial spike in intracellular Ca^{2+} concentration after an increase in extracellular Ca^{2+} indicates release from cell Ca^{2+} stores inside the cell and it's initiated by Ca^{2+} receptors [56]. Additionally, many of the specific proteins that are needed for keratinocyte differentiation are regulated in vitro by changes in Ca^{2+} at a transcriptional, and in some cases at a post-transcriptional level [57].

Skin by protecting from mechanical insults, microorganisms, chemicals, and allergens, functions as a barrier against environment. However, formation and maintenance of skin barrier integrity could be affected by genetic and also environmental factors that are involved in cell differentiation and proliferation, cell–cell adhesion, and skin lipids [58]. Regular keratinocytes differentiation is essential for the formation of an intact epidermal barrier and is triggered by release of Ca^{2+} from ER and influx from extracellular Ca^{2+} sources [55,58-59]. Ca^{2+} gradient disappears after disruption of barrier and reforms with barrier function recovery, stating that the epidermal barrier can inversely regulate the formation of the Ca^{2+} gradient [60]. Therefore, it is not completely obvious that whether disappearance of Ca^{2+} gradient or disruption of barrier is the primary phenomena under specific conditions. Ca^{2+} gradient is lost whether the barrier acutely or chronically disrupted, returning to normal as Ca^{2+} percolates into the epidermis from deeper layers of skin, aligned with normalization of barrier function. Conversely, the Ca^{2+} gradient appears in fetal skin in parallel to the appearance of an adequate permeability barrier. Denda et al study showed that when barrier state is modulated by constant exposure to either an increased or decreased external humidity, Ca^{2+} gradient varies [59]. Furthermore, skin diseases caused by an abnormal barrier such as experimental essential fatty acid deficiency and psoriasis, are associated with a loss of the Ca^{2+}

gradient [60-62]. The keratitis-ichthyosis-deafness (KID) syndrome, as one of the skin diseases, is caused by heterozygous dominant missense mutations in gap junction protein beta 2 (GJB2) and beta 6 (GJB6) genes, that are encoding Cx26 and Cx30, respectively. These mutations increase the release of ATP and Ca^{2+} influx, which perturb the epidermal Ca^{2+} gradient resulting defect of barrier [63]. Moreover, Rinnerthaler et al demonstrated the role for Ca^{2+} in skin aging which was based on the epidermal Ca^{2+} gradient collapse during the aging process [64].

The roles of Ca^{2+} channels, and calmodulin like skin protein in epidermal Ca^{2+} homeostasis have been studied and confirmed by many studies [65-68]. Transient receptor potential (TRP), one of the epidermal Ca^{2+} channels, can regulate skin barrier homeostasis with keratinocytes differentiation and proliferation. It has been revealed that blockade of specific TRP activation by physical and chemical stimuli, resulted in the disruption of epidermal barrier integrity and homeostasis in human keratinocytes [69]. STIM1 and ORAI1 are two proteins that have been identified as crucial components of store operated Ca^{2+} entry channel. Vanderberghe et al, reported that feedback repression of ORAI1 can reduce the Ca^{2+} -switch-induced Ca^{2+} response, resulting in impaired keratinocyte differentiation and epidermal barrier in human keratinocytes and in *Orai1*-knockout mice [70]. In another study, by Bikle et al, Ca^{2+} flux through the ORAI1 channel that controls epidermal proliferation was revealed. An evidence-based or potential association between epidermal Ca^{2+} gradients and the epidermal barrier is shown in figure (1.5).

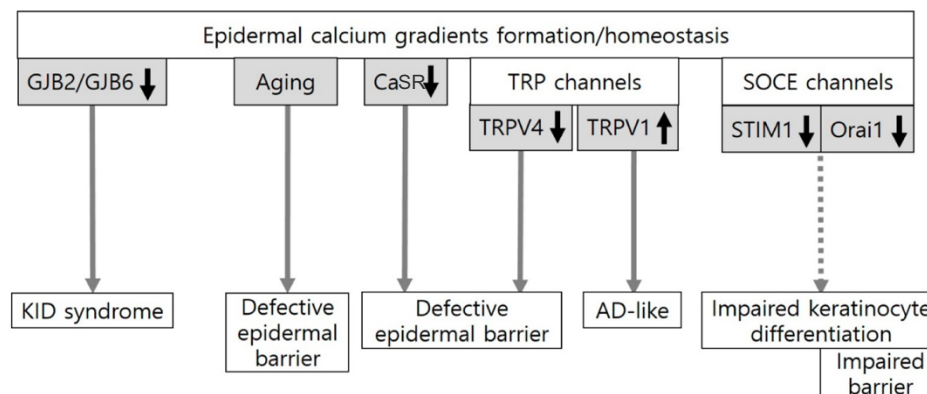


Figure 1.5 An evidence-based or potential association between epidermal Ca^{2+} gradients and the epidermal barrier. Epidermal Ca^{2+} gradients have been altered in KID syndrome induced by GJB2 or GJB6 missense mutations and in chronological skin aging. The formation and homeostasis of the epidermal Ca^{2+} gradients could be regulated by CaSR, TRP channels, and store-operated Ca^{2+} entry (SOCE) channels. Ca^{2+} receptor depletion, which inhibits Ca^{2+} influx impairs the epidermal barrier in mice. In TRP channels, TRP vanilloid 4 (TRPV4) activation which could be induced by heat ($>30^{\circ}\text{C}$) and hypo osmolarity, plays a crucial role in epidermal barrier formation and recovery in mice. On the other hand, the blockade of TRPV1 activation by physical and chemical stimuli such as heat (42°C) and capsaicin can suppress atopic dermatitis (AD)-like symptoms in mice. Two essential components of SOCE, STIM1 and *Orai1*, are activated by ER Ca^{2+} store depletion. Downregulation of *Orai1* can impair keratinocyte differentiation and barrier homeostasis in mice (from ref. [58])

The role for the CaSR in transducing the extracellular Ca^{2+} concentration signal during differentiation have been evaluated and confirmed by many experiments [71-73]. Keratinocytes produce two variants of the CaSR namely, the full-length CaSR and a smaller alternatively spliced variant lacking exon 5, CaSRalt. The amino acid residues from 460 to 536 in the extracellular domain are lost in the CaSRalt. Deglycosylation analyses revealed that the full length CaSR has two different N-glycosylated oligosaccharide chains whereas the CaSRalt has only high mannose type oligosaccharide chains [74]. The change of glycosylation pattern in the CaSRalt is attributed to the deletion of the 2 N-glycosylation sites within exon 5. When it is exogenously expressed in keratinocytes, only the full-length CaSR is able to mediate Ca^{2+} -stimulated inositol phosphate production and transcriptional activation of involucrin and TG1 genes [74]. The full-length CaSR and CaSRalt are expressed differentially during differentiation. Whereas the level of CaSRalt remains relatively unchanged, the level of full-length CaSR moderately decreases in the terminally differentiated keratinocytes [75]. This expression pattern of CaSR is consistent with the steady decline in intracellular Ca^{2+} concentration and inositol phosphate responses to extracellular Ca^{2+} concentration in differentiated cells but is different from the in vivo situation [74].

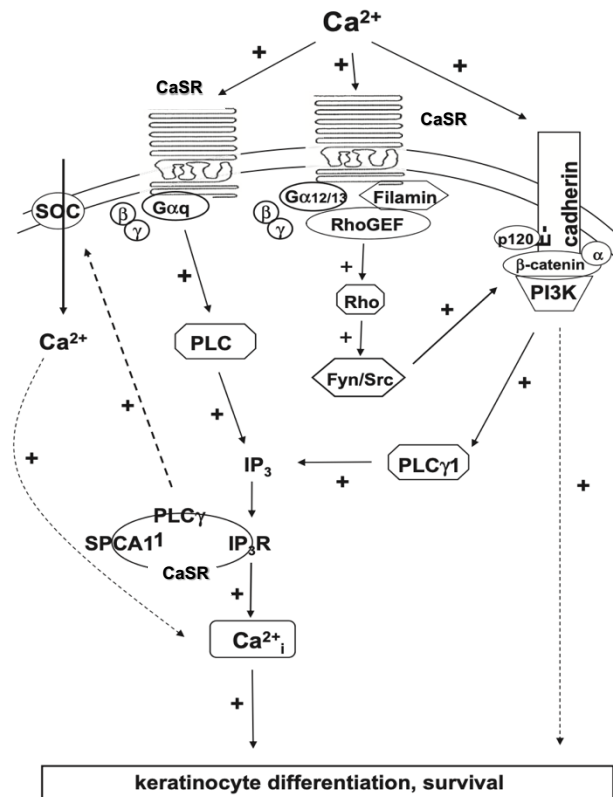
Aforementioned there are several mechanisms by which CaSR mediates extracellular Ca^{2+} concentration-induced increases in intracellular Ca^{2+} , thereby promoting differentiation. Inactivation of CaSR in keratinocytes by transfecting a full-length antisense CaSR cDNA construct greatly reduces Ca^{2+} release in response to elevated extracellular Ca^{2+} concentration [503, 506]. This is a consequence of a profound depletion of Ca^{2+} pools in cells lacking the CaSR, as indicated by the reduced amount of Ca^{2+} released by extracellular Ca^{2+} concentration, ionomycin, or thapsigargin [76]. Consistent with its effect to reduce intracellular Ca^{2+} stores, inhibition of CaSR expression also augments the SOC-mediated Ca^{2+} influx [76]. This result would be a mechanism addressing for the further loss of Ca^{2+} from internal stores. Additionally, CaSR null keratinocytes demonstrate increased Ca^{2+} accumulation by ER and Golgi due to their reduced Ca^{2+} stores and/or loss of regulation by CaSR. These are acute responses. The data were revealing increased SOC-mediated Ca^{2+} influx and accumulation by ER and Golgi in the absence of CaSR but overall loss of intracellular Ca^{2+} stores suggests that CaSR enables Ca^{2+} entry via channels which are important for the maintenance of the Ca^{2+} stores. Fluorescence immunostaining and co-immunoprecipitation studies revealed that CaSR co-localizes and forms a protein complex with several extracellular Ca^{2+} concentration modulators, i.e. PLC γ 1, IP₃R and SPCA1, in the trans-Golgi [76]. Since PLC γ 1 and IP₃R are crucial for initiating both Ca^{2+} release from stores and Ca^{2+} entry through

membrane channels, while SPCA1 is responsible for refilling the intracellular Ca^{2+} stores, the CaSR may serve as a coordinator of these signaling events because of its intrinsic ability to sense extracellular Ca^{2+} concentration and possibly the Ca^{2+} level in the lumen of intracellular stores [77-79].

Immunocytochemistry and in situ hybridization confirmed the expression of CaSR message and proteins in mammalian skin in the interfollicular suprabasal keratinocyte layers with little CaSR in the basal layer [80, 81]. The level of CaSR expression increases as cell differentiation continues across the epidermis, with the strongest expression in the cells of the upper stratum granulosum, whereas the corneocytes display weak staining [80]. Like the distribution of CaSR in cultured keratinocytes, most of the CaSR proteins in epidermal layers localize intracellularly [80]. Overall, the expression of CaSR closely parallels the Ca^{2+} gradient in the epidermis.

Extracellular Ca^{2+} concentration signaling regulates proliferation, differentiation and apoptosis in most, if not all, cell types including keratinocytes. Extracellular Ca^{2+} concentration stimulates the keratinocytes to differentiate in large part through the CaSR, which regulates cell survival and keratinocyte differentiation by two major pathways which is shown in (Figure. 1.6).

Figure 1.6 Extracellular Ca^{2+} concentration-stimulated signaling responses in keratinocytes. Membrane CaSR senses changes in extracellular Ca^{2+} concentration and activates two signaling pathways. One is mediated by the $\text{G}\alpha_q$ -activated PLC, which generates IP_3 to trigger Ca^{2+} release from internal stores including ER and Golgi via IP_3R . Depletion of Ca^{2+} stores stimulates Ca^{2+} influx through SOCs by an IP_3 - and $\text{PLC}\gamma 1$ -mediated mechanism to further raise intracellular Ca^{2+} concentration. The second involves activation of Rho through interaction with $\text{G}\alpha$ proteins, e.g. $\text{G}\alpha_q$ or $\text{G}\alpha_{12/13}$, filamin A, and RhoGEF to stimulate Fyn/Src kinases. Fyn/Src kinases phosphorylate catenins, promoting the formation of E-cadherin/catenin complex at the cell membrane and activation of PI3K. PI3K in turn activates $\text{PLC}\gamma 1$ to further increase intracellular Ca^{2+} concentration. The activation of PI3K downstream effectors and rise in intracellular Ca^{2+} concentration stimulate the expression of genes essential for differentiation and cell survival. Finally, the intracellular CaSR forms complexes with IP_3R , $\text{PLC}\gamma 1$, and SPCA1 in the Golgi and regulates Ca^{2+} uptake and release from intracellular Ca^{2+} stores, as well as Ca^{2+} entry via SOC. (from ref.[82])



1.3.2 Connexin HCs

Cx assemble as hexameric HCs that are transported to the PM where they can become functional channels by themselves, or move to regions of cell contact and find a partner HCs from an adjacent cell to complete gap junction (GJ) channel (GJC) formation allowing intercellular passage of ions, metabolites and other important signaling molecules of approximately 1 kDa [83-86].

The physiological roles of HCs and GJCs can be distinguished by their characteristic regulation. GJCs act as intercellular connections and are in a constitutively open state so that tissues function as syncytia, while HCs communicate with the extracellular space and by default are in a closed state [87-90]. Unopposed HCs become active under conditions of mechanical, or ischemic stress, and permit the extracellular release of molecules like ATP, glutamate, or Glutamate dehydrogenase, provoking various physiological responses (table. 1.2) [91,92]. In severe physiological conditions leading to cell death, HCs opening is widely associated with loss of ionic gradients and small metabolites, increased cell osmolarity and influx of Ca^{2+} . However, regulated HCs opening by specific signals results in defined roles for HCs in cell survival or development [93]. The schematic representation of the role of HCs in development, cell survival and death is depicted in (figure 1.7).

Table 1.2 Regulation of HCs activity. (from ref. [93])

Factors	Effect on HC
Mechanical stimulation	<ul style="list-style-type: none"> Increases surface expression and opens Cx43 HCs Opens PanX1 HCs
ATP bound purinergic receptors	<ul style="list-style-type: none"> Opens PanX1 HCs
pH	<ul style="list-style-type: none"> pH<6.5 closes Cx26 and Cx46 channels, and pH>7.6 opens Cx26 and Cx46
Ca^{2+}	<ul style="list-style-type: none"> Physiological and very high intracellular concentrations: Cx43 and Cx32 are closed Pannexin channels are open Low extracellular or pathologically high intracellular concentrations: Cx43 and Cx32 are open
Phosphorylation	<ul style="list-style-type: none"> Phosphorylated Cx43 generally from closed channels, and dephosphorylation during ischemia is associated with open channels
Nitrosylation	<ul style="list-style-type: none"> Activates Cx43 and Cx46 HCs opening
Bacterial infection	<ul style="list-style-type: none"> Increases Cx43 HC activity in endothelial cells

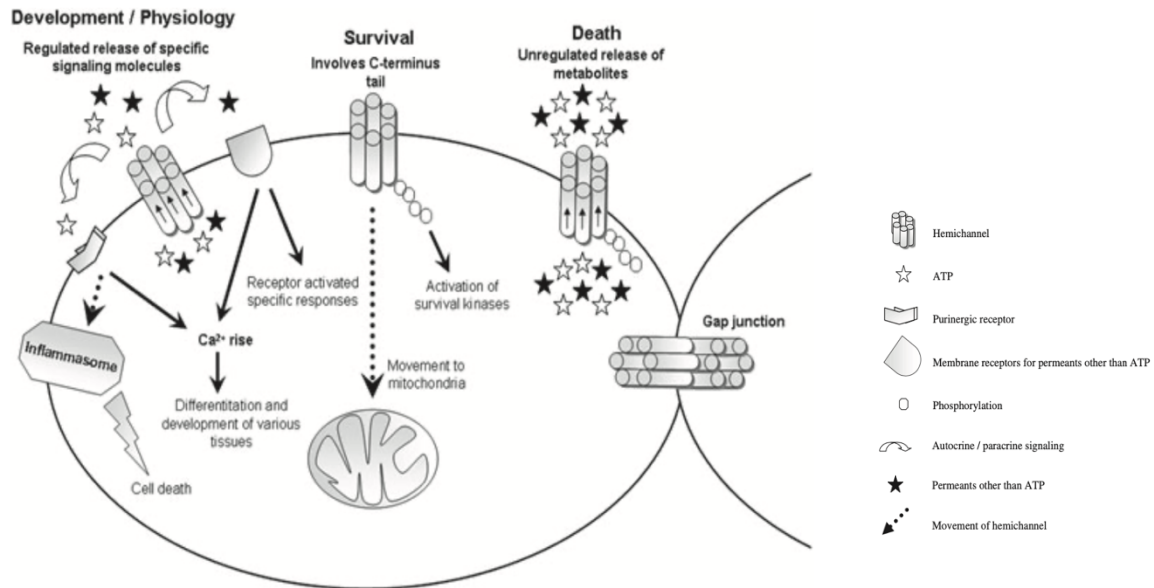


Figure 1.7 Schematic representation of the role of HCs in development, cell survival and death.

Regulated opening of HCs and, consequently, release of permeants is involved in several normal developmental and physiological roles. ATP binds to its receptor, which, in turn, facilitates most of the physiological phenomena leading to tissue development. The purinergic receptor also can bind to the inflammasome complex during immune response and cause regulated cell death. Other permeants such as PGE₂, Glutamate dehydrogenase and glutamate bind to their specific receptors, resulting to specific physiological outcomes. Cx43 tail plays a role in cell survival of osteoblasts by activation of growth kinases and also survival of cardiomyocytes upon pre-conditioning by moving to the mitochondria. Under conditions of trauma or tissue injury, HCs open for prolonged periods to result in unregulated release of permeants, which hastens cell death. (from ref. [93])

Structurally, Cxs are a 21-member family of integral membrane proteins with four transmembrane (TM) domains (M1–M4), connected two extracellular loops (E1 and E2), a cytoplasmic (CL). M2–M3 loop that play roles in the cell-cell recognition and docking processes, and cytoplasmic N- and C-terminal domains (NT and CT) that links the second and third TM domains (figure 1.8). The conducting pore region is composed of the amino acids from several domains. N-terminal, M1 and E1 domains participate in the formation of channel pore as revealed by substituted cysteine accessibility method and recent crystal structure data [94-96]. In general, the transmembrane domains are implicated in oligomerization, whereas the extracellular domains facilitate docking [97]. The intracellular regions play a role in regulation of the pore opening and interaction with other proteins [98,99].

Given that the formation and removal of GJs is a dynamic process, mechanistic details of how Cxs fold, oligomerize, traffic, dock, cluster, function, internalize and degrade have been mapped out. Several recent reviews indicated that most cells in the human body will completely renew their GJs in a remarkably short 24 hours period [100,101]. Cxs tend to follow a classical secretory pathway by co-translationally inserting into ER membranes where they proceed to undergo folding and

intramolecular disulfide bond formation [102,103]. While many Cxs oligomerize in the ER, others, like Cx43, appear to delay this process until reaching the trans Golgi network [104]. Reasons for this delay remain elusive but one argument suggests that this delay would avert any aberrant and premature opening of Cxs HCs or connexons in the ER membrane, which could destroy the integrity of the ER luminal compartment. Cxs frequently use the assistance of microtubules to traffic to the cell surface and may randomly appear at the cell surface or be directed via microtubule anchoring sites to the edges of pre-existing GJs [105, 106]. Docking of HCs is highly regulated and appears to occur quickly as most imaging technologies fail to detect a cohort of undocked HCs at the cell surface [107].

Even though Cxs share high homology, there are important differences in the sequence of amino acid of the intracellular loop and CT (figure 1.9). These segments contain motifs for regulatory kinases and cytoskeletal binding proteins [108,109].

Cxs have overlapping expression patterns, and many cells express more than one. For example, Cx26, Cx30, Cx30.3, Cx31, and Cx43 are all present in keratinocytes [110,111]. Co-expression of multiple Cxs within a cell influences the composition of the HCs and intercellular channels formed. HCs can be formed either from a single Cx, or from more than one type, resulting to the formation of either homomeric or heteromeric HCs, respectively. The formation of heteromeric HCs depends on the compatibility of the Cxs participating, because not all Cxs can interact with each other [112,113].

Inherited or acquired variations in the structure and function of Cx proteins have been associated with diseases. Undocked HCs can open and exchange substances or ions between the cytoplasm and the extracellular environment, which may employ signaling as well as pathophysiological functions [114].

Advances in understanding of functional role of Cxs in the skin, have been made by studying the diseases caused by mutation of Cxs (table 1.3). Cxs play a role in maintaining epidermal integrity and homeostasis [115]. At least ten different Cxs are expressed throughout the epidermis (figure 1.10), each representing a characteristic expression profile depend on the species and conditions. These Cxs profiles permit the formation of particular GJ communication compartments in different strata, while alternation of Cxs activity and compatibility may cause problems in keratinocyte differentiation.

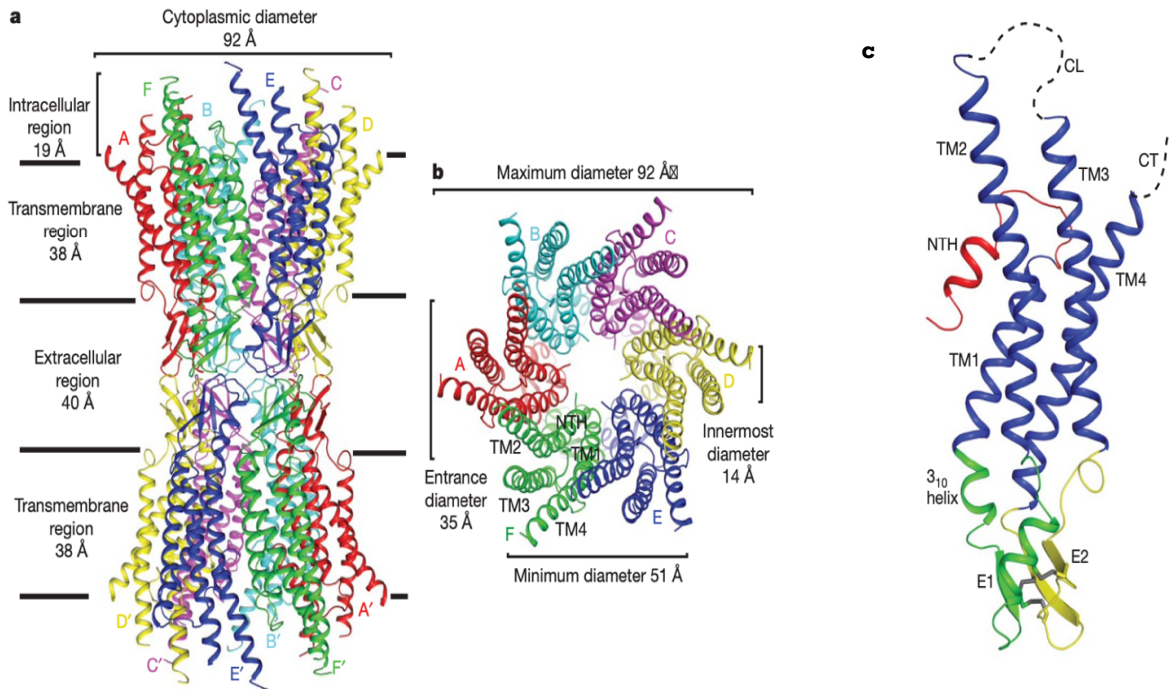


Figure 1.8 Overall structure of Cx26 GJ channel in ribbon representation.

The corresponding protomers in the two HCs, which are related by a two-fold axis, are shown in the same colour. (a), Side view of the Cx26 GJ channel. (b), Top view of the Cx26 GJ channel showing the arrangement of the transmembrane helices TM1 to TM4. The pore has an inner diameter of 35 Å at the cytoplasmic entrance, and the smallest diameter of the pore is 14 Å. (c) stereo view of the Cx26 protomer in ribbon representation. Color code: red, NTH; blue, TM1–TM4; green, E1; yellow, E2; grey, disulphide bonds; dashed lines, cytoplasmic loop (CL) and C terminus (CT). (from ref. [94])

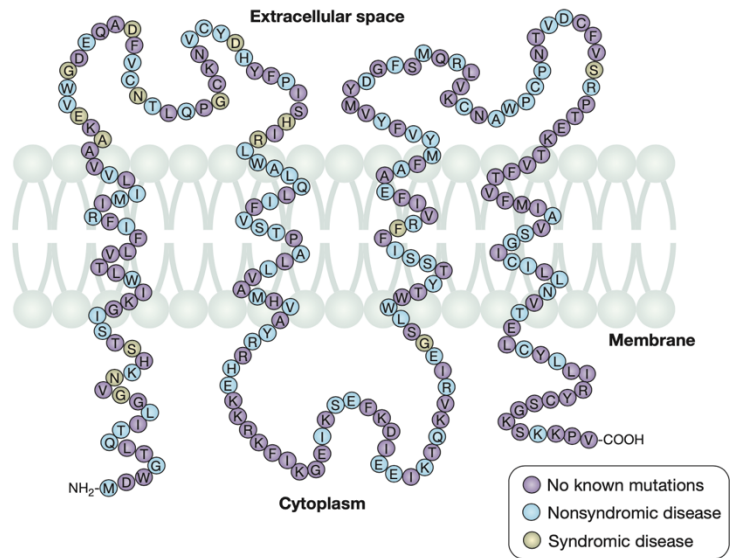


Figure 1.9 Cx26 topology and mutant residues.

This illustration displays the location of amino acid residues in Cx26 relative to the membrane. Purple residues are not mutated. Blue amino acids are mutated residues found in nonsyndromic deafness and brown amino acids are mutated residues in syndromic deafness which are generally found within the N-terminus and first extracellular loop. (from ref. [116])

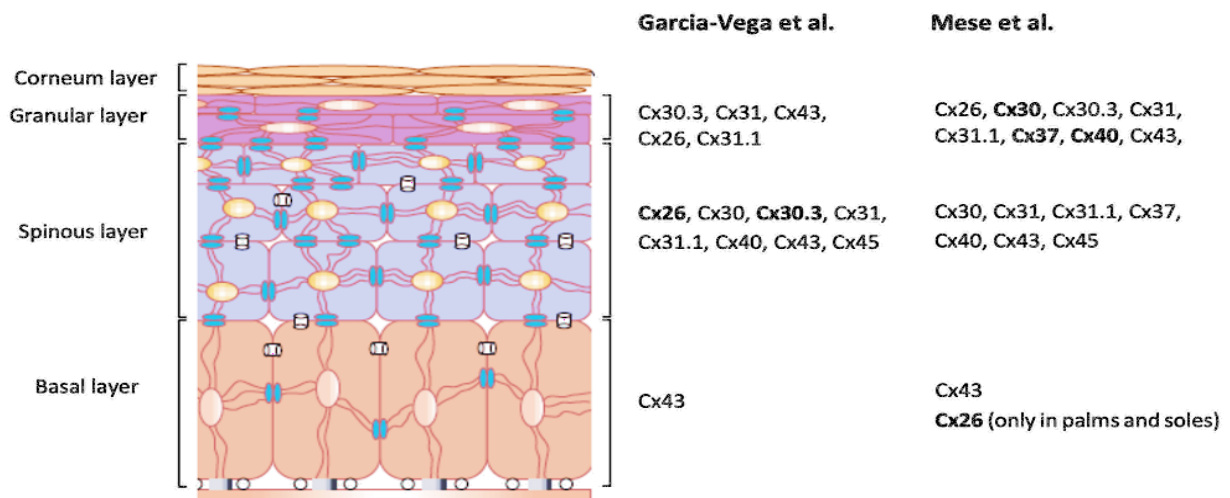


Figure 1.10 Cxs expression profiles through epidermis.
Structure of epidermis indicating Cxs expression profiles reported by Garcia-vega et al (from ref. [117]) and mese et al (from ref. [118]). differences highlighted in bold. Figure (from ref. [119])

As it mentioned earlier, Cx HCs opening may occur under physiological conditions and consequently the opening initiates the diffusive release of paracrine messengers, most importantly ATP [120-122]. The involvement of Cx HCs in the release of ATP was first suggested by Nedergaard and co-workers who observed that decreasing the extracellular Ca^{2+} concentration stimulated the uptake of the fluorescent probe propidium iodide in cells overexpressing human Cx32 or Cx43, as well as ATP release from the same cells [122].

Intracellularly, ATP enables energy-dependent processes releasing high-energy electrons by the hydrolyzation of its three phosphoanhydride bonds. Extracellular ATP (eATP) binds to specific P2 receptors, which are grouped into ionotropic P2X and metabotropic (G-protein-coupled) P2Y receptors [34,123]. After having bound eATP, P2X receptors undergo conformational change and facilitate the influx, and also efflux of mono- and divalent cations along their concentration gradient (particularly Na^+ , Ca^{2+} in and K^+ out) [124]. ATP release initiated by open HCs has been connected to a variety of pathophysiological responses in Cx- deficient mice, such as ischemia and epilepsy, deafness, skin disorder, and impaired activation of the immune system [125-131]. The results of research on Ca^{2+} signaling in the photodamaged skin by Donati and coworkers, also showed that Ca^{2+} wave propagation depended primarily on the release of ATP, a prime damage-associated molecular patterns, from the hit cell [132].

A major regulator of HCs activity under physiological conditions is extracellular Ca^{2+} , and reduction of extracellular Ca^{2+} increases the opening of most, if not all, unopposed Cxs HCs (i.e., Cx26, Cx32, Cx43, Cx46, Cx50) [133-136]. Unlike most other ion channels regulated by Ca^{2+} , Cx channels do not have a large semi-independent structural domain that binds Ca^{2+} and couples allosterically to the pore to control opening and closing. This type of Ca^{2+} -binding domain at the extracellular face of Cx HCs is not possible, because it would interfere with the formation of intercellular GJ channels. Most likely, Ca^{2+} sensing is mostly mediated by motifs that lie within or are exposed to the pore lumen [137]. Recent studies revealed that extracellular Ca^{2+} destabilizes the open state of HCs, at least in human Cx26 (hCx26) and hCx30, by disrupting a salt-bridge interaction between residues D50 and K61 located close to the extracellular entrance of the pore [138,139]. This open-state destabilization facilitates HCs closure. However, perturbation of this interaction does not seem to be a general mechanism for Ca^{2+} regulation of Cxs [94].

Proper control of HCs opening is crucial to sustain cell viability and is achieved by physiological levels of extracellular Ca^{2+} concentration, which significantly reduce HCs activity [140].

Cxs are linked to diseases or wound healing via several different mechanistic paradigms. First, Cx-mediated intercellular communication is often up- or down- regulated in response to cellular signals that in turn cause Cx gene expression, Cx assembly, or Cx turnover. This hypothesis has been widely studied in cancer prevention, onset and progression but likely influences the severity of other, less well examined disease processes [141, 142]. A second Cx-linked disease/injury paradigm is based on the concept that Cx expression acts a “brake” in wound healing and that a transient down regulation would function to facilitate the healing process [143,144]. An intriguing corollary to this elucidation is that a rapid spike in Cx expression or activity could stimulate healing of chronic wounds [145,146]. At the channel level, the community continues to interrogate the differential positive and negative roles of GJ intercellular communication and the Cxs HCs that may act as a pathological pore during wound healing, inflammation, and other diseases [147]. Third, Cxs as a core driver of disease was confirmed with the findings that Cx gene mutations lead to several developmental abnormalities and chronic disease conditions [100,148].

Cx mutations that disrupt HCs regulation by Ca²⁺ cause human pathologies due to aberrantly open HCs.

Table 1.3. Clinical phenotypes of Cx skin diseases (from ref.[149])

	gene	protein (mutation)	mode	palmoplantar keratoderma	other keratoderma	deafness	leukonychia	nail dystrophy	hypotrichosis	other skin findings	other findings
syndromic											
palmoplantar keratoderma with deafness (OMIM 148350)	<i>GJB2</i>	Cx26 (De42E, N54H, G59A, G59R, H73R, R75Q, R75W, G130V, S183F)	AD	diffuse> focal		sensori-neural					
Vohwinkel syndrome (OMIM 124500)	<i>GJB2</i>	Cx26 (D66H, G59S, G130V)	AD	diffuse	rarely	sensori-neural			rarely	pseudoainhum, starfish keratosis on knuckles	
Bart-Pumphrey syndrome (OMIM 149200)	<i>GJB2</i>	Cx26 (N54K, G59S)	AD	diffuse		sensori-neural	variable improves with age			knuckle pads	
keratitis ichthyosis-deafness syndrome (OMIM 148210)	<i>GJB2</i> > <i>GJB6</i>	Cx26 (G12R, N14K, N14Y, S17F, A40V, G45E, D50N, D50Y, A88V) > Cx30 (V37E)	AD	diffuse	areas of friction sometimes ulcerated	sensori-neural		variable	variable		vascular keratitis
hystrix-like ichthyosis deafness syndrome (OMIM 602540)	<i>GJB2</i>	Cx26 (D50N)	AD	Diffuse, milder than KID	more severe & extensive than KID	sensori-neural		variable	variable		absent to punctate keratitis
oculodentodigital dysplasia (OMIM 164200)	<i>GJA1</i>	Cx43 (Y17S, S18P, G21R, G22E, V96M, F52dup, R76S, L90V, Y98C, K102N, I130T, K134E, G138R, R202H, V216L, fs260)	AD	mild in rare cases		conductive		mild, some brittleness	variable		many, see [82]
non-syndromic											
porokeratotic eccrine ostial and dermal duct nevus	<i>GJB2</i>	Cx26 (N14Y, G12R, G45E, M93I)			Blaschkoid plaques						
erythrokeratoderma variabilis et progressiva (OMIM 133200)											
erythrokeratoderma variabilis	<i>GJB3</i> , <i>GJB4</i> > <i>GJA1</i>	Cx31 (G12R, G12D, L34P, R42P, C86S, L135V, F137L, L209F), Cx30.3 (R98C, T130M, F137L, M190L) > Cx43 (E227D, A44V)	AD> AR	variable	geographic plaques		prominent lunulae with GJA1 mutations			transient geographic pink patches (in childhood)	
progressive symmetric erythrokeratoderma	<i>GJB4</i>	Cx30.3 (G12D)	AD	variable	progressive symmetric plaques on extensors > trunk						
hidrotic ectodermal dysplasia (Clouston) (OMIM 129500)	<i>GJB6</i>	Cx30 (G11R, V37E, D50N, A88V)	AD	focal in areas of friction					total body worsens with age	pebbly plaques on dorsal fingers and toes	
keratoderma-hypotrichosis-leukonychia totalis syndrome (OMIM 104100)	<i>GJA1</i>	Cx43 (G8V)	AD	focal in areas of friction	plaques in areas of friction		all 20 nails		total body	keratosis pilaris	

Inherited diseases caused by Cx mutations are found in multiple organs and include hereditary deafness, congenital cataract, congenital heart diseases, hereditary skin diseases, and X-linked Charcot–Marie–Tooth disease (CMT1X). A large number of knockout and knock-in animal models have been used to study the pathology and pathogenesis of diseases of different organs. As the structures of different Cxs are highly homologous and the functions of GJ formed by these Cxs are

similar, Cx-related hereditary diseases may share the same pathogenic mechanism (figure 1.11) [150].

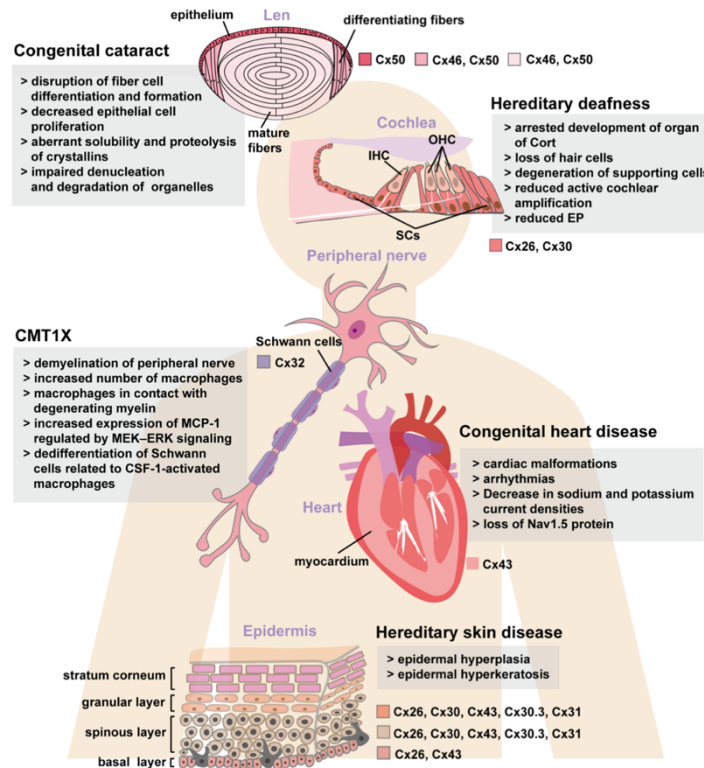


Figure 1.11. Main pathophysiological changes associated with human diseases. Main pathophysiological changes associated with human hereditary deafness, congenital cataract, congenital heart diseases, hereditary skin diseases, and CMT1X found in knock-in and knockout mouse models. EP: endolymphatic potential, OHC: outer hair cell, IHC: inner hair cell, SCs: knockout mouse models. EP: endolymphatic potential, OHC: outer hair cell, IHC: inner hair cell, SCs: supporting cells, MCP-1: monocyte chemoattractant protein-1, CSF-1: colony-stimulating factor 1. supporting cells, MCP-1: monocyte chemoattractant protein-1, CSF-1: colony-stimulating factor 1. (from ref. [150])

Studies of human and rodent epidermis have pinpointed GJ between keratinocytes residing in the basal, spinous, and granular layers, but not between cells in the cornified layers [151,152]. These data match with dye-transfer experiments that revealed junctional communication between keratinocytes populating the three inner epidermal layers of mouse and human skin [153,154]. These experiments suggested that epidermal keratinocytes were organized into communication compartments consisting of 20 – 25 cells, as dye transfer occurred between basal and supra basal keratinocytes within a compartment, but was reduced between keratinocytes in neighboring compartments. This communication compartment was hypothesized to correlate with the epidermal proliferative unit and suggested that GJ communication might help to mediate keratinocyte growth and differentiation [155]. Identified Cx genes, including that encoding Cx26 (GJB2), are expressed during keratinocyte differentiation, and they show overlapping spatial and temporal expression patterns [118, 156,157]. Dramatic alternations in Cx gene expression occur in the epidermis following changes in keratinocyte proliferation.

Studies revealed how changes in gating of HC and permeation resulting from KID mutations might contribute to the loss of epidermal homeostasis.

Although KID syndrome is rare, the cutaneous and extracutaneous manifestations of the disease are absolutely serious and refractory to treatment [158]. Patients with KID syndrome often present with severe skin involvement and are at high risk for cutaneous bacterial infection [159]. Almost half of patients with KID syndrome have chronic skin infection [160]. Skin tumors, particularly trichilemmal tumors and squamous cell carcinoma (SCC), are common during the disease course [143]. Indeed, near 15% of KID syndrome patients are reported to develop SCC of the skin and the oral mucosa [161]. Germline missense mutations in GJB2 encoding Cx26 have been found to be associated with KID syndrome. Many experiments have revealed that KID syndrome-causative GJB2 mutations result in the formation of Cx26 HCs with aberrant activity [162-168]. It has been shown that increased extracellular Ca^{2+} concentrations drive the HCs into their closed state [169]. Cysteine scanning of three mutants, Cx26-A40V, Cx26-G45E, and Cx26-D50N revealed that two of them, G45 and D50, lined the HC pore [149]. However, Sanchez et al reported that Cx26-G45E HCs has a markedly increased permeability to Ca^{2+} , whereas Cx26-D50N reduced the permeability [170,171]. Further support of these results was done by Mese et al, which they revealed that Cx26-G45E mice develop a severe lethal form of the disease, and also showed that significantly increased in activity of HCs is presented in primary keratinocytes derived from KID lesions [167,172]. The results of Taki et al. experiment suggested that both normal HCs of Cx26-WT and aberrant HCs of Cx26-D50N had similar activities under the Ca^{2+} -free conditions, but that aberrant HC activities were provoked under the condition of physiological Ca^{2+} concentration [173]. To further verify the formation of abnormal HCs in the PM, they performed dye uptake studies with the presence of HC blockers, carbenoxolone and 18α -Glycyrrhetic acid. Results showed that under the Ca^{2+} -free condition, the treatment of cells with blocker reduced the levels of dye uptake in both cells producing Cx26-WT and Cx26-D50N compared to counterpart without blocker. Additionally, under the condition of physiological Ca^{2+} concentration (1.2 mM) treatment of cells with blocker caused 40% reduction in the levels of dye uptake [173]. These findings suggested that the increase in the uptake of neurobiotin into cells was mediated by aberrant HCs consisting of Cx26-D50N.

1.3.3 Inhibitors of Cx HCs

Abnormal increase in HCs activity leads to cell damage in disorders such as cardiac infarct, stroke, deafness, cataracts, and skin diseases. For this reason, Cx HCs have emerged as a therapeutic target. Knowing the fact that small molecule HC inhibitors are not ideal, leads for the development of better drugs for clinical use because they are not specific or have toxic effects. Newer inhibitors are more selective and include Cx mimetic peptides, anti-Cx antibodies and drugs that reduce Cx expression such as antisense oligonucleotides [174]. Re-purposed drugs and their derivatives are also promising because of the significant experience with their clinical use. Specific inhibitors of Cx HCs equivalent to those available for ion-selective ion channels are not yet available. In principle, inhibition of HCs can be produced by reducing their number, open probability and/or intrinsic permeability [174]. Alterations in the number of HCs result from changes in synthesis, assembly, trafficking, degradation, and/or alterations in plaque formation and disassembly that favor HCs in GJ plaques vs. undocked HCs. Examples of inhibitors that reduce the number of HCs are antisense oligonucleotides and siRNAs [107]. The activity of HCs can also be reduced by decreasing their open probability. Increase in extracellular Ca^{2+} concentration and flufenamic acid are some examples of inhibitors that reduce HC open probability [139,140,174,175]. Finally, inhibition can also occur by reduction in intrinsic HC permeability. Examples include cyclodextrins and phosphorylation of Cx43 HCs by protein kinase C (PKC) and mitogen- activated protein kinase (MAPK) [140,176].

Aside from these inhibitors, monoclonal antibodies (mAbs) represent a rapidly growing pharmaceutical class of protein drugs that becomes an important part of the precision therapy. mAbs are characterized by their high specificity and affinity for the target antigen, which is mostly present on the cell surface. A human-derived single-chain fragment variable (scFv) fragment constant (Fc) antibody (scFv-Fc) named abEC1.1 was shown to inhibit both wild type and hyperactive pathological hCx26 HCs [177,178]. The crystal structure of the scFv domain was solved (Protein Data Base accession code 5WYM) and some of the residues that are critical for its binding to the extracellular domain of hCx26 HCs were identified [179]. Some other studies reported that monoclonal antibody could inhibit HCs formed by the Cx26-G45E mutation in vitro [178,180].

1.4 Aims and structure of this thesis work

Prof. Mammano and his group developed a novel all-optical assay based on fluorometric measurements of Ca^{2+} uptake with a Ca^{2+} -selective genetically encoded indicator (GCaMP6s) that permits the optical tracking of cytosolic Ca^{2+} concentration changes with high sensitivity. The choice was dictated by different considerations. First, the study of Ca^{2+} dynamics in cells expressing pathological HCs is of utmost importance, given that deregulated Ca^{2+} influx through HCs has been implicated in different disorders, as it mentioned previously. Second, fluorometric assays based on alternations of intracellular Ca^{2+} are industry standards widely used in drug screening for membrane channels and GPCRs. The assay provided a sensitive indication for the effect of HC inhibitors, considering that it allowed them to detect changes in the uptake of Ca^{2+} with as little as 0.1 nM of the abEC1.1h-IgG mAb in HaCaT-Cx26-GCaMP6s cells [181]. HaCaT cells, a spontaneously transformed human epithelial cell line from adult skin which maintains full epidermal differentiation capacity and nontumorigenic in vitro, are widely used for studying regulation of keratinization [182].

Knowing the fact that uncontrolled expression of leaky HCs causes toxicity and rapidly leads to cell death, they designed and produced lentiviruses (LVs) for Tet-on bicistronic expression of the Cxs of interest (Cx26 and Cx46) and the genetically encoded indicator GCaMP6s that permits optical tracking of cytosolic Ca^{2+} concentration changes with high sensitivity. In the experiments, GCaMP6s signals exhibited complex kinetics with an early peak in close temporal proximity to the CaCl_2 bolus application, followed by a delayed response that generated a second relative maximum with a delay of 2 to 3 min. The reason of the biphasic responses is not clear (figure 1.12).

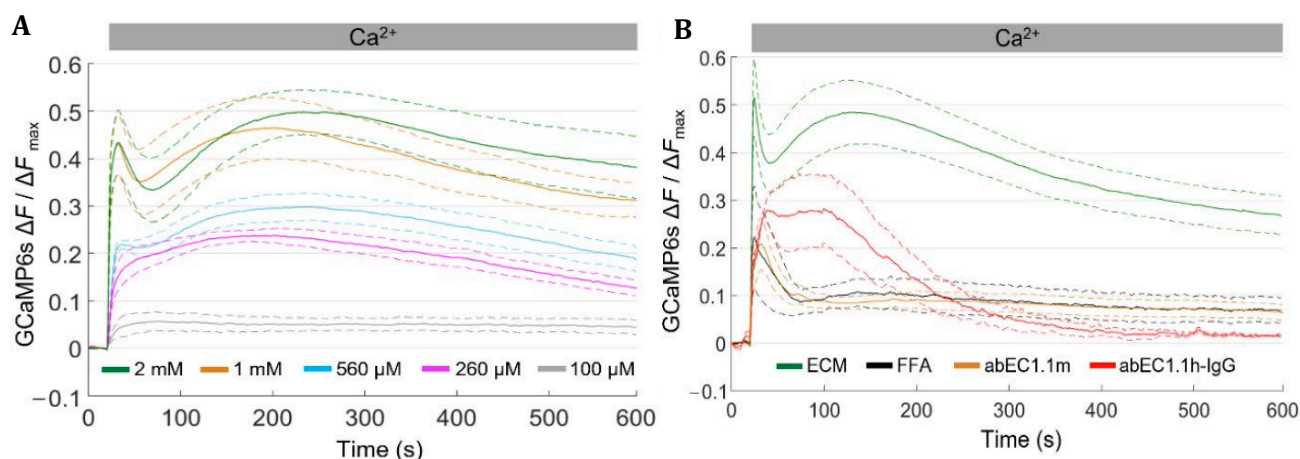


Figure 1.12 Experimental results of Ca^{2+} uptake in HaCaT-Cx26-GCaMP6s cells. (A) The mean Ca^{2+} uptake traces (solid line) \pm s.e.m (dashed line) obtained in HaCaT-Cx26-GCaMP6s cell cultures bathed in extracellular medium (ECM) and exposed to different CaCl_2 bolus concentration to reach the following final extracellular Ca^{2+} concentration: 2mM, 1mM, 560 μ M, 260 μ M, and 100 μ M. (B) The mean Ca^{2+} uptake responses (solid line) \pm s.e.m (dashed line) to a 1 M CaCl_2 bolus obtained from HaCaT-Cx26-GCaMP6s cell cultures bathed in following extracellular media: ECM (green), ECM+FFA (black), ECM+abEC1.1m (orange), ECM+abEC1.1h-IgG (red). (From ref.[181])

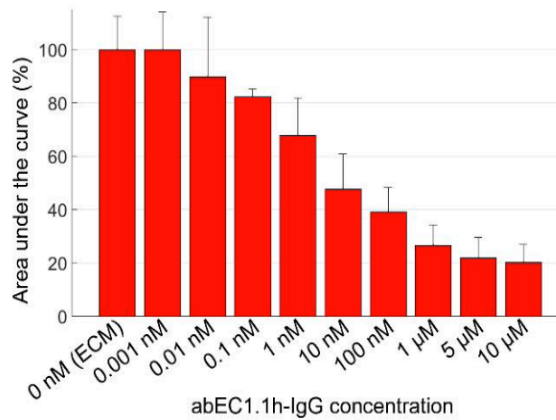


Figure 1.13 Dose-dependent effect of the abEC1.1h-IgG for concentration in the range 0.001nM- 10 μM (data are quoted as the mean± s.e.m for each condition) (from ref. [181])

The hypothesis for the first peak was that the sudden increase of extracellular Ca^{2+} concentration had the contrasting effect of initiating uptake of Ca^{2+} , due to the increased driving force for the cation, while also promoting HC closure. As for the second peak, considering that keratinocytes sense changes in extracellular Ca^{2+} concentration via G-protein coupled CaSR, (and consequent phenomena till production of IP_3 which then IP_3 mediates release of Ca^{2+} from ER by activating IP_3R), beside noting that IP_3R are regulated also by Ca^{2+} , they suggested that the amplitude of this delay, IP_3 -mediated response would depend strongly also on Ca^{2+} influx through HCs. In other words, the second peak that develops after addition of bolus of CaCl_2 can be seen as and IP_3 -dependent amplification mechanism for the signal generated by Ca^{2+} influx through HCs.

In order to find explanations for the biphasic responses which may validate the above hypothesis or not, the current thesis goal is to develop a mathematical model of Ca^{2+} dynamics with the aim of simulating the complex responses measured experimentally by fluorescence microscopy in HaCaT cells challenged by a sudden increase of the extracellular Ca^{2+} concentration. I use the set of previously derived differential equations that successfully modeled epidermal Ca^{2+} dynamics in vivo [51]. Then, by adapting these equations to the peculiar toolset of ion channels and transporters expressed in HaCaT cells, I will generate an original model variant that account quantitatively for the insurgence of a biphasic elevation of intracellular Ca^{2+} when the extracellular Ca^{2+} concentration overcomes a critical threshold. Additionally, this model aims to explain the observed damping effects caused by increasing concentrations of different HCs blockers, including monoclonal antibodies targeted at the HCs extracellular domain.

In the following technologies used to perform the experiment, and image processing results obtained for single cells are provided in chapter 2. The mathematical model of Ca^{2+} dynamic is

explained in details in chapter 3. Results of mathematical simulation and discussion on the results are reported in chapter 4.

1.5. References

1. Solomon, E. P., Berg, L. R., & Martin, D. W. Biology (6th ed). (2002) Brooks/Cole, Thomson Learning.
2. Hannan FM, Kallay E, Chang W, Brandi ML, Thakker RV. The calcium-sensing receptor in physiology and in calcitropic and noncalcitropic diseases. *Nat Rev Endocrinol*. 2018 Dec;15(1):33-51. doi: 10.1038/s41574-018-0115-0. PMID: 30443043; PMCID: PMC6535143.
3. Giorgi C, Danese A, Missiroli S, Patergnani S, Pinton P. Calcium Dynamics as a Machine for Decoding Signals. *Trends Cell Biol*. 2018 Apr;28(4):258-273. doi: 10.1016/j.tcb.2018.01.002. Epub 2018 Feb 3. PMID: 29409699.
4. Putney JW Jr, McKay RR. Capacitative calcium entry channels. *Bioessays*. 1999 Jan;21(1):38-46. doi: 10.1002/(SICI)1521-1878(199901)21:1<38::AID-BIES5>3.0.CO;2-S. PMID: 10070252.
5. Wang Q, Michalak M. Calsequestrin. Structure, function, and evolution. *Cell Calcium*. 2020 Sep;90:102242. doi: 10.1016/j.ceca.2020.102242. Epub 2020 Jun 20. PMID: 32574906.
6. Schwaller B. Calretinin: from a "simple" Ca(2+) buffer to a multifunctional protein implicated in many biological processes. *Front Neuroanat*. 2014 Feb 5;8:3. doi: 10.3389/fnana.2014.00003. PMID: 24550787; PMCID: PMC3913827.
7. Brini M, Bano D, Manni S, Rizzuto R, Carafoli E. Effects of PMCA and SERCA pump overexpression on the kinetics of cell Ca(2+) signalling. *EMBO J*. 2000 Sep 15;19(18):4926-35. doi: 10.1093/emboj/19.18.4926. PMID: 10990456; PMCID: PMC314231.
8. Periasamy M, Kalyanasundaram A. SERCA pump isoforms: their role in calcium transport and disease. *Muscle Nerve*. 2007 Apr;35(4):430-42. doi: 10.1002/mus.20745. PMID: 17286271.
9. Monteith GR, Prevarskaya N, Roberts-Thomson SJ. The calcium-cancer signalling nexus. *Nat Rev Cancer*. 2017 Jun;17(6):367-380. doi: 10.1038/nrc.2017.18. Epub 2017 Apr 7. PMID: 28386091.
10. Van Petegem F. Ryanodine receptors: structure and function. *J Biol Chem*. 2012 Sep 14;287(38):31624-32. doi: 10.1074/jbc.R112.349068. Epub 2012 Jul 20. PMID: 22822064; PMCID: PMC3442496.
11. Denda S, Kumamoto J, Takei K, Tsutsumi M, Aoki H, Denda M. Ryanodine receptors are expressed in epidermal keratinocytes and associated with keratinocyte differentiation and epidermal permeability barrier homeostasis. *J Invest Dermatol*. 2012 Jan;132(1):69-75. doi: 10.1038/jid.2011.256. Epub 2011 Sep 1. PMID: 21881589.
12. Zucchi R, Ronca-Testoni S. The sarcoplasmic reticulum Ca²⁺ channel/ryanodine receptor: modulation by endogenous effectors, drugs and disease states. *Pharmacol Rev*. 1997 Mar;49(1):1-51. PMID: 9085308.
13. Kushnir A, Betzenhauser MJ, Marks AR. Ryanodine receptor studies using genetically engineered mice. *FEBS Lett*. 2010 May 17;584(10):1956-65. doi: 10.1016/j.febslet.2010.03.005. Epub 2010 Mar 7. PMID: 20214899; PMCID: PMC3690514.
14. Wang Z, Zhao X, Zhou H, Che D, Du X, Ye D, Zeng W, Geng S. Activation of ryanodine-sensitive calcium store drives pseudo-allergic dermatitis *via* Mas-related G protein-coupled receptor X2 in mast cells. *Front Immunol*. 2023 Jun 19;14:1207249. doi: 10.3389/fimmu.2023.1207249. PMID: 37404822; PMCID: PMC10315577.

15. Foskett JK, Daniel Mak DO. Regulation of IP(3)R Channel Gating by Ca(2+) and Ca(2+) Binding Proteins. *Curr Top Membr.* 2010;66:235-72. doi: 10.1016/S1063-5823(10)66011-5. Epub 2010 Jul 25. PMID: 22353483; PMCID: PMC6707373.
16. Bertram R, Greenstein JL, Hinch R, Pate E, Reisert J, Sanderson MJ, Shannon TR, Sneyd J, Winslow RL. *Tutorials in mathematical biosciences II: Mathematical modeling of calcium dynamics and signal transduction.* Springer Science & Business Media; 2005 Jun 22.
17. Bertram R, Greenstein JL, Hinch R, Pate E, Reisert J, Sanderson MJ, Shannon TR, Sneyd J, Winslow RL. *Tutorials in mathematical biosciences II: Mathematical modeling of calcium dynamics and signal transduction.* Springer Science & Business Media; 2005 Jun 22.
18. Ralevic V, Burnstock G. Receptors for purines and pyrimidines. *Pharmacol Rev.* 1998 Sep;50(3):413-92. PMID: 9755289.
19. Bours MJ, Swennen EL, Di Virgilio F, Cronstein BN, Dagnelie PC. Adenosine 5'-triphosphate and adenosine as endogenous signaling molecules in immunity and inflammation. *Pharmacol Ther.* 2006 Nov;112(2):358-404. doi: 10.1016/j.pharmthera.2005.04.013. Epub 2006 Jun 19. PMID: 16784779.
20. Abbracchio MP, Burnstock G. Purinoceptors: are there families of P2X and P2Y purinoceptors? *Pharmacol Ther.* 1994;64(3):445-75. doi: 10.1016/0163-7258(94)00048-4. PMID: 7724657.
21. Jacobson KA, Jarvis MF, Williams M. Purine and pyrimidine (P2) receptors as drug targets. *J Med Chem.* 2002 Sep 12;45(19):4057-93. doi: 10.1021/jm020046y. PMID: 12213051.
22. Burnstock G, Knight GE. Cellular distribution and functions of P2 receptor subtypes in different systems. *Int Rev Cytol.* 2004;240:31-304. doi: 10.1016/S0074-7696(04)40002-3. PMID: 15548415.
23. Khakh BS, Burnstock G, Kennedy C, King BF, North RA, Séguéla P, Voigt M, Humphrey PP. International union of pharmacology. XXIV. Current status of the nomenclature and properties of P2X receptors and their subunits. *Pharmacol Rev.* 2001 Mar;53(1):107-18. PMID: 11171941.
24. North RA. Molecular physiology of P2X receptors. *Physiol Rev.* 2002 Oct;82(4):1013-67. doi: 10.1152/physrev.00015.2002. PMID: 12270951.
25. von Kügelgen I, Wetter A. Molecular pharmacology of P2Y-receptors. *Naunyn Schmiedebergs Arch Pharmacol.* 2000 Nov;362(4-5):310-23. doi: 10.1007/s002100000310. PMID: 11111826.
26. Boeynaems, Jean-Marie & Wilkin, Françoise & Marteau, Frédéric & Duhant, Xavier & Savi, Pierre & Suarez Gonzalez, Nathalie & Robaye, Bernard & Communi, Didier. (2003). P2Y receptors: New subtypes, new functions. *Drug Development Research.* 59. 30 - 35. 10.1002/ddr.10199.
27. Fields RD, Burnstock G. Purinergic signalling in neuron-glia interactions. *Nat Rev Neurosci.* 2006 Jun;7(6):423-36. doi: 10.1038/nrn1928. PMID: 16715052; PMCID: PMC2062484.
28. Burnstock G. Short- and long-term (trophic) purinergic signalling. *Philos Trans R Soc Lond B Biol Sci.* 2016 Aug 5;371(1700):20150422. doi: 10.1098/rstb.2015.0422. PMID: 27377731; PMCID: PMC4938022.
29. Chen JF, Eltzschig HK, Fredholm BB. Adenosine receptors as drug targets--what are the challenges? *Nat Rev Drug Discov.* 2013 Apr;12(4):265-86. doi: 10.1038/nrd3955. PMID: 23535933; PMCID: PMC3930074.
30. de Lera Ruiz M, Lim YH, Zheng J. Adenosine A2A receptor as a drug discovery target. *J Med Chem.* 2014 May 8;57(9):3623-50. doi: 10.1021/jm4011669. Epub 2013 Nov 15. PMID: 24164628.

31. Layland J, Carrick D, Lee M, Oldroyd K, Berry C. Adenosine: physiology, pharmacology, and clinical applications. *JACC Cardiovasc Interv.* 2014 Jun;7(6):581-91. doi: 10.1016/j.jcin.2014.02.009. Epub 2014 May 14. PMID: 24835328.
32. Liu H, Xia Y. Beneficial and detrimental role of adenosine signaling in diseases and therapy. *J Appl Physiol (1985).* 2015 Nov 15;119(10):1173-82. doi: 10.1152/jappphysiol.00350.2015. Epub 2015 Aug 27. PMID: 26316513; PMCID: PMC4839494.
33. Borea PA, Gessi S, Merighi S, Varani K. Adenosine as a Multi-Signalling Guardian Angel in Human Diseases: When, Where and How Does it Exert its Protective Effects? *Trends Pharmacol Sci.* 2016 Jun;37(6):419-434. doi: 10.1016/j.tips.2016.02.006. Epub 2016 Mar 2. PMID: 26944097.
34. Burnstock G. Purinergic Signalling: Therapeutic Developments. *Front Pharmacol.* 2017 Sep 25;8:661. doi: 10.3389/fphar.2017.00661. PMID: 28993732; PMCID: PMC5622197.
35. Burnstock G, Kennedy C. P2X receptors in health and disease. *Adv Pharmacol.* 2011;61:333-72. doi: 10.1016/B978-0-12-385526-8.00011-4. PMID: 21586364.
36. Bartlett R, Stokes L, Sluyter R. The P2X7 receptor channel: recent developments and the use of P2X7 antagonists in models of disease. *Pharmacol Rev.* 2014 Jul;66(3):638-75. doi: 10.1124/pr.113.008003. PMID: 24928329.
37. Ford AP, Udem BJ, Birder LA, Grundy D, Pijacka W, Paton JF. P2X3 receptors and sensitization of autonomic reflexes. *Auton Neurosci.* 2015 Sep;191:16-24. doi: 10.1016/j.autneu.2015.04.005. Epub 2015 Apr 25. PMID: 25956567.
38. Arulkumaran N, Unwin RJ, Tam FW. A potential therapeutic role for P2X7 receptor (P2X7R) antagonists in the treatment of inflammatory diseases. *Expert Opin Investig Drugs.* 2011 Jul;20(7):897-915. doi: 10.1517/13543784.2011.578068. Epub 2011 Apr 21. PMID: 21510825; PMCID: PMC3114873.
39. Junger WG. Immune cell regulation by autocrine purinergic signalling. *Nat Rev Immunol.* 2011 Mar;11(3):201-12. doi: 10.1038/nri2938. Epub 2011 Feb 18. PMID: 21331080; PMCID: PMC4209705.
40. Hansson E, Werner T, Björklund U, Skiöldebrand E. Therapeutic innovation: Inflammatory-reactive astrocytes as targets of inflammation. *IBRO Rep.* 2016 Jun 23;1:1-9. doi: 10.1016/j.ibror.2016.06.001. PMID: 30135924; PMCID: PMC6084881.
41. Burnstock G, Di Virgilio F. Purinergic signalling and cancer. *Purinergic Signal.* 2013 Dec;9(4):491-540. doi: 10.1007/s11302-013-9372-5. PMID: 23797685; PMCID: PMC3889385.
42. Di Virgilio F, Adinolfi E. Extracellular purines, purinergic receptors and tumor growth. *Oncogene.* 2017 Jan 19;36(3):293-303. doi: 10.1038/onc.2016.206. Epub 2016 Jun 20. PMID: 27321181; PMCID: PMC5269532.
43. Romagnoli R, Baraldi PG, Cruz-Lopez O, Lopez-Cara C, Preti D, Borea PA, Gessi S. The P2X7 receptor as a therapeutic target. *Expert Opin Ther Targets.* 2008 May;12(5):647-61. doi: 10.1517/14728222.12.5.647. PMID: 18410246.
44. Sawynok J. Adenosine receptor targets for pain. *Neuroscience.* 2016 Dec 3;338:1-18. doi: 10.1016/j.neuroscience.2015.10.031. Epub 2015 Oct 21. PMID: 26500181.
45. Clapham DE. Calcium signaling. *Cell.* 2007 Dec 14;131(6):1047-58. doi: 10.1016/j.cell.2007.11.028. PMID: 18083096.
46. Rettig J, Neher E. Emerging roles of presynaptic proteins in Ca⁺⁺-triggered exocytosis. *Science.* 2002 Oct 25;298(5594):781-5. doi: 10.1126/science.1075375. Erratum in: *Science* 2002 Nov 15;298(5597):1336. PMID: 12399579.

47. Zhang X, Kim-Miller MJ, Fukuda M, Kowalchuk JA, Martin TF. Ca²⁺-dependent synaptotagmin binding to SNAP-25 is essential for Ca²⁺-triggered exocytosis. *Neuron*. 2002 May 16;34(4):599-611. doi: 10.1016/s0896-6273(02)00671-2. PMID: 12062043.
48. White SM, Imig JD, Kim TT, Hauschild BC, Inscho EW. Calcium signaling pathways utilized by P2X receptors in freshly isolated preglomerular MVSMC. *Am J Physiol Renal Physiol*. 2001 Jun;280(6):F1054-61. doi: 10.1152/ajprenal.2001.280.6.F1054. PMID: 11352845.
49. Surprenant A, North RA. Signaling at purinergic P2X receptors. *Annu Rev Physiol*. 2009;71:333-59. doi: 10.1146/annurev.physiol.70.113006.100630. PMID: 18851707.
50. Burnstock G, Boeynaems JM. Purinergic signalling and immune cells. *Purinergic Signal*. 2014 Dec;10(4):529-64. doi: 10.1007/s11302-014-9427-2. Epub 2014 Oct 29. PMID: 25352330; PMCID: PMC4272370.
51. Ceriani F, Pozzan T, Mammano F. Critical role of ATP-induced ATP release for Ca²⁺ signaling in nonsensory cell networks of the developing cochlea. *Proc Natl Acad Sci U S A*. 2016 Nov 15;113(46):E7194-E7201. doi: 10.1073/pnas.1616061113. Epub 2016 Nov 2. PMID: 27807138; PMCID: PMC5135323.
52. Mammano F. ATP-dependent intercellular Ca²⁺ signaling in the developing cochlea: facts, fantasies and perspectives. *Semin Cell Dev Biol*. 2013 Jan;24(1):31-9. doi: 10.1016/j.semdb.2012.09.004. Epub 2012 Sep 28. PMID: 23022499.
53. Massella D, Argenziano M, Ferri A, Guan J, Giraud S, Cavalli R, Barresi AA, Salaün F. Bio-Functional Textiles: Combining Pharmaceutical Nanocarriers with Fibrous Materials for Innovative Dermatological Therapies. *Pharmaceutics*. 2019 Aug 11;11(8):403. doi: 10.3390/pharmaceutics11080403. PMID: 31405229; PMCID: PMC6723157.
54. Liu B, Zhu F, Xia X, Park E, Hu Y. A tale of terminal differentiation: IKK α , the master keratinocyte regulator. *Cell Cycle*. 2009 Feb 15;8(4):527-31. doi: 10.4161/cc.8.4.7598. Epub 2009 Feb 10. PMID: 19197157; PMCID: PMC7243803.
55. Elsholz F, Harteneck C, Muller W, Friedland K. Calcium--a central regulator of keratinocyte differentiation in health and disease. *Eur J Dermatol*. 2014 Nov-Dec;24(6):650-61. doi: 10.1684/ejd.2014.2452. PMID: 25514792.
56. Bikle DD, Xie Z, Tu CL. Calcium regulation of keratinocyte differentiation. *Expert Rev Endocrinol Metab*. 2012 Jul;7(4):461-472. doi: 10.1586/eem.12.34. PMID: 23144648; PMCID: PMC3491811.
57. Elias P, Ahn S, Brown B, Crumrine D, Feingold KR. Origin of the epidermal calcium gradient: regulation by barrier status and role of active vs passive mechanisms. *J Invest Dermatol*. 2002 Dec;119(6):1269-74. doi: 10.1046/j.1523-1747.2002.19622.x. PMID: 12485427.
58. Lee AY. Molecular Mechanism of Epidermal Barrier Dysfunction as Primary Abnormalities. *Int J Mol Sci*. 2020 Feb 11;21(4):1194. doi: 10.3390/ijms21041194. PMID: 32054030; PMCID: PMC7072774.
59. Denda M, Sato J, Masuda Y, Tsuchiya T, Koyama J, Kuramoto M, Elias PM, Feingold KR. Exposure to a dry environment enhances epidermal permeability barrier function. *J Invest Dermatol*. 1998 Nov;111(5):858-63. doi: 10.1046/j.1523-1747.1998.00333.x. PMID: 9804350.
60. Elias PM, Menon GK. Structural and lipid biochemical correlates of the epidermal permeability barrier. *Adv Lipid Res*. 1991;24:1-26. doi: 10.1016/b978-0-12-024924-4.50005-5. PMID: 1763710.
61. Menon GK, Elias PM, Feingold KR. Integrity of the permeability barrier is crucial for maintenance of the epidermal calcium gradient. *Br J Dermatol*. 1994 Feb;130(2):139-47. doi: 10.1111/j.1365-2133.1994.tb02892.x. PMID: 8123567.

62. Pallon J, Malmqvist KG, Werner-Linde Y, Forslind B. Pixe analysis of pathological skin with special reference to psoriasis and atopic dry skin. *Cell Mol Biol (Noisy-le-grand)*. 1996 Feb;42(1):111-8. PMID: 8833672.
63. García IE, Bosen F, Mujica P, Pupo A, Flores-Muñoz C, Jara O, González C, Willecke K, Martínez AD. From Hyperactive Connexin26 Hemichannels to Impairments in Epidermal Calcium Gradient and Permeability Barrier in the Keratitis-Ichthyosis-Deafness Syndrome. *J Invest Dermatol*. 2016 Mar;136(3):574-583. doi: 10.1016/j.jid.2015.11.017. Epub 2016 Jan 8. PMID: 26777423.
64. Rinnerthaler M, Richter K. The Influence of Calcium on the Skin pH and Epidermal Barrier During Aging. *Curr Probl Dermatol*. 2018;54:79-86. doi: 10.1159/000489521. Epub 2018 Aug 21. PMID: 30130776.
65. Hwang J, Kalinin A, Hwang M, Anderson DE, Kim MJ, Stojadinovic O, Tomic-Canic M, Lee SH, Morasso MI. Role of Scarf and its binding target proteins in epidermal calcium homeostasis. *J Biol Chem*. 2007 Jun 22;282(25):18645-18653. doi: 10.1074/jbc.M702035200. Epub 2007 Apr 30. PMID: 17470426.
66. Donovan M, Ambach A, Thomas-Collignon A, Prado C, Bernard D, Jammayrac O, Gollnick H, de Lacharriere O. Calmodulin-like skin protein level increases in the differentiated epidermal layers in atopic dermatitis. *Exp Dermatol*. 2013 Dec;22(12):836-7. doi: 10.1111/exd.12274. PMID: 24279918.
67. Lee SE, Lee SH. Skin Barrier and Calcium. *Ann Dermatol*. 2018 Jun;30(3):265-275. doi: 10.5021/ad.2018.30.3.265. Epub 2018 Apr 23. PMID: 29853739; PMCID: PMC5929942.
68. Méhul B, Bernard D, Schmidt R. Calmodulin-like skin protein: a new marker of keratinocyte differentiation. *J Invest Dermatol*. 2001 Jun;116(6):905-9. doi: 10.1046/j.0022-202x.2001.01376.x. PMID: 11407979.
69. Sokabe T, Tominaga M. The TRPV4 cation channel: A molecule linking skin temperature and barrier function. *Commun Integr Biol*. 2010 Nov;3(6):619-21. doi: 10.4161/cib.3.6.13461. Epub 2010 Nov 1. PMID: 21331258; PMCID: PMC3038082.
70. Vandenberghe M, Raphaël M, Lehen'kyi V, Gordienko D, Hastie R, Oddos T, Rao A, Hogan PG, Skryma R, Prevarskaya N. ORAI1 calcium channel orchestrates skin homeostasis. *Proc Natl Acad Sci U S A*. 2013 Dec 10;110(50):E4839-48. doi: 10.1073/pnas.1310394110. Epub 2013 Nov 25. PMID: 24277812; PMCID: PMC3864283.
71. Brown EM, MacLeod RJ. Extracellular calcium sensing and extracellular calcium signaling. *Physiol Rev*. 2001 Jan;81(1):239-297. doi: 10.1152/physrev.2001.81.1.239. PMID: 11152759.
72. Tu CL, Oda Y, Bikle DD. Effects of a calcium receptor activator on the cellular response to calcium in human keratinocytes. *J Invest Dermatol*. 1999 Sep;113(3):340-5. doi: 10.1046/j.1523-1747.1999.00698.x. PMID: 10469331.
73. Tu CL, Chang W, Bikle DD. The extracellular calcium-sensing receptor is required for calcium-induced differentiation in human keratinocytes. *J Biol Chem*. 2001 Nov 2;276(44):41079-85. doi: 10.1074/jbc.M107122200. Epub 2001 Aug 10. PMID: 11500521.
74. Oda Y, Tu CL, Pillai S, Bikle DD. The calcium sensing receptor and its alternatively spliced form in keratinocyte differentiation. *J Biol Chem*. 1998 Sep 4;273(36):23344-52. doi: 10.1074/jbc.273.36.23344. PMID: 9722568.
75. Tu CL, Oda Y, Komuves L, Bikle DD. The role of the calcium-sensing receptor in epidermal differentiation. *Cell Calcium*. 2004 Mar;35(3):265-73. doi: 10.1016/j.ceca.2003.10.019. PMID: 15200150.

76. Tu CL, Chang W, Bikle DD. The role of the calcium sensing receptor in regulating intracellular calcium handling in human epidermal keratinocytes. *J Invest Dermatol.* 2007 May;127(5):1074-83. doi: 10.1038/sj.jid.5700633. Epub 2006 Nov 23. PMID: 17124506.
77. Tu CL, Chang W, Bikle DD. Phospholipase cgamma 1 is required for activation of store-operated channels in human keratinocytes. *J Invest Dermatol.* 2005 Jan;124(1):187-97. doi: 10.1111/j.0022-202X.2004.23544.x. PMID: 15654973.
78. Boulay G, Brown DM, Qin N, Jiang M, Dietrich A, Zhu MX, Chen Z, Birnbaumer M, Mikoshiba K, Birnbaumer L. Modulation of Ca(2+) entry by polypeptides of the inositol 1,4, 5-trisphosphate receptor (IP3R) that bind transient receptor potential (TRP): evidence for roles of TRP and IP3R in store depletion-activated Ca(2+) entry. *Proc Natl Acad Sci U S A.* 1999 Dec 21;96(26):14955-60. doi: 10.1073/pnas.96.26.14955. PMID: 10611319; PMCID: PMC24754.
79. Behne MJ, Tu CL, Aronchik I, Epstein E, Bench G, Bikle DD, Pozzan T, Mauro TM. Human keratinocyte ATP2C1 localizes to the Golgi and controls Golgi Ca2+ stores. *J Invest Dermatol.* 2003 Oct;121(4):688-94. doi: 10.1046/j.1523-1747.2003.12528.x. PMID: 14632183.
80. Komuves L, Oda Y, Tu CL, Chang WH, Ho-Pao CL, Mauro T, Bikle DD. Epidermal expression of the full-length extracellular calcium-sensing receptor is required for normal keratinocyte differentiation. *J Cell Physiol.* 2002 Jul;192(1):45-54. doi: 10.1002/jcp.10107. PMID: 12115735.
81. Oda Y, Tu CL, Chang W, Crumrine D, Kömüves L, Mauro T, Elias PM, Bikle DD. The calcium sensing receptor and its alternatively spliced form in murine epidermal differentiation. *J Biol Chem.* 2000 Jan 14;275(2):1183-90. doi: 10.1074/jbc.275.2.1183. PMID: 10625662.
82. Tu CL, Bikle DD. Role of the calcium-sensing receptor in calcium regulation of epidermal differentiation and function. *Best Pract Res Clin Endocrinol Metab.* 2013 Jun;27(3):415-27. doi: 10.1016/j.beem.2013.03.002. Epub 2013 Apr 12. PMID: 23856269; PMCID: PMC3713412
83. Bruzzone R, White TW, Paul DL. Connections with connexins: the molecular basis of direct intercellular signaling. *Eur J Biochem.* 1996 May 15;238(1):1-27. doi: 10.1111/j.1432-1033.1996.0001q.x. PMID: 8665925./
84. Vinken M. Introduction: connexins, pannexins and their channels as gatekeepers of organ physiology. *Cell Mol Life Sci.* 2015 Aug;72(15):2775-8. doi: 10.1007/s00018-015-1958-3. Epub 2015 Jun 18. PMID: 26084871; PMCID: PMC4562364.].
85. Loewenstein WR. Junctional intercellular communication: the cell-to-cell membrane channel. *Physiol Rev.* 1981 Oct;61(4):829-913. doi: 10.1152/physrev.1981.61.4.829. PMID: 6270711.
86. Yeager M, Unger VM, Falk MM. Synthesis, assembly and structure of gap junction intercellular channels. *Curr Opin Struct Biol.* 1998 Aug;8(4):517-24. doi: 10.1016/s0959-440x(98)80131-0. Erratum in: *Curr Opin Struct Biol* 1998 Dec;8(6):810-1. PMID: 9729745.
87. Sanchez HA, Bienkowski R, Slavi N, Srinivas M, Verselis VK. Altered inhibition of Cx26 hemichannels by pH and Zn2+ in the A40V mutation associated with keratitis-ichthyosis-deafness syndrome. *J Biol Chem.* 2014 Aug 1;289(31):21519-32. doi: 10.1074/jbc.M114.578757. Epub 2014 Jun 17. PMID: 24939841; PMCID: PMC4118113.
88. Abrams CK, Islam M, Mahmoud R, Kwon T, Bargiello TA, Freidin MM. Functional requirement for a highly conserved charged residue at position 75 in the gap junction protein connexin 32. *J Biol Chem.* 2013 Feb 1;288(5):3609-19. doi: 10.1074/jbc.M112.392670. Epub 2012 Dec 3. PMID: 23209285; PMCID: PMC3561579.
89. Ambrosi C, Walker AE, Depriest AD, Cone AC, Lu C, Badger J, Skerrett IM, Sosinsky GE. Analysis of trafficking, stability and function of human connexin 26 gap junction channels with deafness-causing mutations in the fourth transmembrane helix. *PLoS One.* 2013 Aug 15;8(8):e70916. doi: 10.1371/journal.pone.0070916. PMID: 23967136; PMCID: PMC3744544.

90. Harris AL. Emerging issues of connexin channels: biophysics fills the gap. *Q Rev Biophys.* 2001 Aug;34(3):325-472. doi: 10.1017/s0033583501003705. Erratum in: *Q Rev Biophys* 2002 Feb;35(1):109. PMID: 11838236.
91. Evans WH, De Vuyst E, Leybaert L. The gap junction cellular internet: connexin hemichannels enter the signalling limelight. *Biochem J.* 2006 Jul 1;397(1):1-14. doi: 10.1042/BJ20060175. PMID: 16761954; PMCID: PMC1479757
92. Retamal MA, Reyes EP, García IE, Pinto B, Martínez AD, González C. Diseases associated with leaky hemichannels. *Front Cell Neurosci.* 2015 Jul 27;9:267. doi: 10.3389/fncel.2015.00267. PMID: 26283912; PMCID: PMC4515567
93. Chandrasekhar A, Bera AK. Hemichannels: permeants and their effect on development, physiology and death. *Cell Biochem Funct.* 2012 Mar;30(2):89-100. doi: 10.1002/cbf.2794. Epub 2012 Jan 4. PMID: 22392438.
94. Maeda S, Nakagawa S, Suga M, Yamashita E, Oshima A, Fujiyoshi Y, Tsukihara T. Structure of the connexin 26 gap junction channel at 3.5 Å resolution. *Nature.* 2009 Apr 2;458(7238):597-602. doi: 10.1038/nature07869. PMID: 19340074.
95. Zhou XW, Pfahnl A, Werner R, Hudder A, Llanes A, Luebke A, Dahl G. Identification of a pore lining segment in gap junction hemichannels. *Biophys J.* 1997 May;72(5):1946-53. doi: 10.1016/S0006-3495(97)78840-4. PMID: 9129799; PMCID: PMC1184391.
96. Kronengold J, Trexler EB, Bukauskas FF, Bargiello TA, Verselis VK. Single-channel SCAM identifies pore-lining residues in the first extracellular loop and first transmembrane domains of Cx46 hemichannels. *J Gen Physiol.* 2003 Oct;122(4):389-405. doi: 10.1085/jgp.200308861. Epub 2003 Sep 15. PMID: 12975451; PMCID: PMC2233777.
97. Foote CI, Zhou L, Zhu X, Nicholson BJ. The pattern of disulfide linkages in the extracellular loop regions of connexin 32 suggests a model for the docking interface of gap junctions. *J Cell Biol.* 1998 Mar 9;140(5):1187-97. doi: 10.1083/jcb.140.5.1187. PMID: 9490731; PMCID: PMC2132700.
98. Morley GE, Taffet SM, Delmar M. Intramolecular interactions mediate pH regulation of connexin43 channels. *Biophys J.* 1996 Mar;70(3):1294-302. doi: 10.1016/S0006-3495(96)79686-8. PMID: 8785285; PMCID: PMC1225055.
99. Giepmans BN. Gap junctions and connexin-interacting proteins. *Cardiovasc Res.* 2004 May 1;62(2):233-45. doi: 10.1016/j.cardiores.2003.12.009. PMID: 15094344.
100. Laird DW, Naus CC, Lampe PD. SnapShot: Connexins and Disease. *Cell.* 2017 Sep 7;170(6):1260-1260.e1. doi: 10.1016/j.cell.2017.08.034. PMID: 28886388.
101. Laird DW. Closing the gap on autosomal dominant connexin-26 and connexin-43 mutants linked to human disease. *J Biol Chem.* 2008 Feb 8;283(6):2997-3001. doi: 10.1074/jbc.R700041200. Epub 2007 Dec 18. PMID: 18089569.
102. Koval M. Pathways and control of connexin oligomerization. *Trends Cell Biol.* 2006 Mar;16(3):159-66. doi: 10.1016/j.tcb.2006.01.006. Epub 2006 Feb 21. PMID: 16490353; PMCID: PMC7119061.
103. Koval M, Molina SA, Burt JM. Mix and match: investigating heteromeric and heterotypic gap junction channels in model systems and native tissues. *FEBS Lett.* 2014 Apr 17;588(8):1193-204. doi: 10.1016/j.febslet.2014.02.025. Epub 2014 Feb 20. PMID: 24561196; PMCID: PMC3992227.
104. Musil LS3 Goodenough DA. Multisubunit assembly of an integral plasma membrane channel protein, gap junction connexin43, occurs after exit from the ER. *Cell.* 1993 Sep 24;74(6):1065-77. doi: 10.1016/0092-8674(93)90728-9. PMID: 7691412.

105. Shaw RM, Fay AJ, Puthenveedu MA, von Zastrow M, Jan YN, Jan LY. Microtubule plus-end-tracking proteins target gap junctions directly from the cell interior to adherens junctions. *Cell*. 2007 Feb 9;128(3):547-60. doi: 10.1016/j.cell.2006.12.037. Erratum in: *Cell*. 2008 Apr 18;133(2):376. PMID: 17289573; PMCID: PMC1955433.
106. Giepmans BN, Verlaan I, Hengeveld T, Janssen H, Calafat J, Falk MM, Moolenaar WH. Gap junction protein connexin-43 interacts directly with microtubules. *Curr Biol*. 2001 Sep 4;11(17):1364-8. doi: 10.1016/s0960-9822(01)00424-9. PMID: 11553331.
107. Laird DW, Lampe PD. Therapeutic strategies targeting connexins. *Nat Rev Drug Discov*. 2018 Dec;17(12):905-921. doi: 10.1038/nrd.2018.138. Epub 2018 Oct 12. PMID: 30310236; PMCID: PMC6461534.
108. Laird DW, Castillo M, Kasprzak L. Gap junction turnover, intracellular trafficking, and phosphorylation of connexin43 in brefeldin A-treated rat mammary tumor cells. *J Cell Biol*. 1995 Dec;131(5):1193-203. doi: 10.1083/jcb.131.5.1193. PMID: 8522583; PMCID: PMC2120642.
109. Lampe PD, Lau AF. Regulation of gap junctions by phosphorylation of connexins. *Arch Biochem Biophys*. 2000 Dec 15;384(2):205-15. doi: 10.1006/abbi.2000.2131. PMID: 11368307.
110. Kretz M, Euwens C, Hombach S, Eckardt D, Teubner B, Traub O, Willecke K, Ott T. Altered connexin expression and wound healing in the epidermis of connexin-deficient mice. *J Cell Sci*. 2003 Aug 15;116(Pt 16):3443-52. doi: 10.1242/jcs.00638. Epub 2003 Jul 2. PMID: 12840073.
111. Wiszniewski L, Limat A, Saurat JH, Meda P, Salomon D. Differential expression of connexins during stratification of human keratinocytes. *J Invest Dermatol*. 2000 Aug;115(2):278-85. doi: 10.1046/j.1523-1747.2000.00043.x. PMID: 10951247.
112. Segretain D, Falk MM. Regulation of connexin biosynthesis, assembly, gap junction formation, and removal. *Biochim Biophys Acta*. 2004 Mar 23;1662(1-2):3-21. doi: 10.1016/j.bbamem.2004.01.007. PMID: 15033576.
113. Bai D, Wang AH. Extracellular domains play different roles in gap junction formation and docking compatibility. *Biochem J*. 2014 Feb 15;458(1):1-10. doi: 10.1042/BJ20131162. PMID: 24438327.
114. Nielsen MS, Axelsen LN, Sorgen PL, Verma V, Delmar M, Holstein-Rathlou NH. Gap junctions. *Compr Physiol*. 2012 Jul;2(3):1981-2035. doi: 10.1002/cphy.c110051. PMID: 23723031; PMCID: PMC3821273
115. Martin PE, Easton JA, Hodgins MB, Wright CS. Connexins: sensors of epidermal integrity that are therapeutic targets. *FEBS Lett*. 2014 Apr 17;588(8):1304-14. doi: 10.1016/j.febslet.2014.02.048. Epub 2014 Mar 4. PMID: 24607543
116. Lee JR, White TW. Connexin-26 mutations in deafness and skin disease. *Expert Rev Mol Med*. 2009 Nov 19;11:e35. doi: 10.1017/S1462399409001276. PMID: 19939300.
117. Braun J, Abney JR, Owicki JC. How a gap junction maintains its structure. *Nature*. 1984 Jul 26-Aug 1;310(5975):316-8. doi: 10.1038/310316a0. PMID: 6462217.
118. Meşe G, Richard G, White TW. Gap junctions: basic structure and function. *J Invest Dermatol*. 2007 Nov;127(11):2516-24. doi: 10.1038/sj.jid.5700770. PMID: 17934503.
119. McGrath, J.A., R.A.J. Eady, and F.M. Pope, *Anatomy and Organization of Human Skin*. Rook's Textbook of Dermatology, 2004
120. Toma I, Bansal E, Meer EJ, Kang JJ, Vargas SL, Peti-Peterdi J. Connexin 40 and ATP-dependent intercellular calcium wave in renal glomerular endothelial cells. *Am J Physiol Regul Integr Comp Physiol*. 2008 Jun;294(6):R1769-76. doi: 10.1152/ajpregu.00489.2007. Epub 2008 Apr 9. PMID: 18401004; PMCID: PMC2440586.

121. Pearson RA, Dale N, Llaudet E, Mobbs P. ATP released via gap junction hemichannels from the pigment epithelium regulates neural retinal progenitor proliferation. *Neuron*. 2005 Jun 2;46(5):731-44. doi: 10.1016/j.neuron.2005.04.024. PMID: 15924860.
122. Cotrina ML, Lin JH, Alves-Rodrigues A, Liu S, Li J, Azmi-Ghadimi H, Kang J, Naus CC, Nedergaard M. Connexins regulate calcium signaling by controlling ATP release. *Proc Natl Acad Sci U S A*. 1998 Dec 22;95(26):15735-40. doi: 10.1073/pnas.95.26.15735. PMID: 9861039; PMCID: PMC28113.
123. Antonio LS, Stewart AP, Xu XJ, Varanda WA, Murrell-Lagnado RD, Edwardson JM. P2X4 receptors interact with both P2X2 and P2X7 receptors in the form of homotrimers. *Br J Pharmacol*. 2011 Jul;163(5):1069-77. doi: 10.1111/j.1476-5381.2011.01303.x. PMID: 21385174; PMCID: PMC3130952.
124. Spari D, Beldi G. Extracellular ATP as an Inter-Kingdom Signaling Molecule: Release Mechanisms by Bacteria and Its Implication on the Host. *Int J Mol Sci*. 2020 Aug 4;21(15):5590. doi: 10.3390/ijms21155590. PMID: 32759857; PMCID: PMC7432876.].
125. Dale N, Frenguelli BG. Release of adenosine and ATP during ischemia and epilepsy. *Curr Neuropharmacol*. 2009 Sep;7(3):160-79. doi: 10.2174/157015909789152146. PMID: 20190959; PMCID: PMC2769001.
126. Huckstepp RT, id Bihi R, Eason R, Spyer KM, Dicke N, Willecke K, Marina N, Gourine AV, Dale N. Connexin hemichannel-mediated CO₂-dependent release of ATP in the medulla oblongata contributes to central respiratory chemosensitivity. *J Physiol*. 2010 Oct 15;588(Pt 20):3901-20. doi: 10.1113/jphysiol.2010.192088. Epub 2010 Aug 24. PMID: 20736421; PMCID: PMC3000581.
127. Anselmi F, Hernandez VH, Crispino G, Seydel A, Ortolano S, Roper SD, Kessar N, Richardson W, Rickheit G, Filippov MA, Monyer H, Mammano F. ATP release through connexin hemichannels and gap junction transfer of second messengers propagate Ca²⁺ signals across the inner ear. *Proc Natl Acad Sci U S A*. 2008 Dec 2;105(48):18770-5. doi: 10.1073/pnas.0800793105. Epub 2008 Dec 1. PMID: 19047635; PMCID: PMC2596208.
128. Rodriguez L, Simeonato E, Scimemi P, Anselmi F, Calì B, Crispino G, Ciubotaru CD, Bortolozzi M, Ramirez FG, Majumder P, Arslan E, De Camilli P, Pozzan T, Mammano F. Reduced phosphatidylinositol 4,5-bisphosphate synthesis impairs inner ear Ca²⁺ signaling and high-frequency hearing acquisition. *Proc Natl Acad Sci U S A*. 2012 Aug 28;109(35):14013-8. doi: 10.1073/pnas.1211869109. Epub 2012 Aug 13. PMID: 22891314; PMCID: PMC3435166.
129. García IE, Bosen F, Mujica P, Pupo A, Flores-Muñoz C, Jara O, González C, Willecke K, Martínez AD. From Hyperactive Connexin26 Hemichannels to Impairments in Epidermal Calcium Gradient and Permeability Barrier in the Keratitis-Ichthyosis-Deafness Syndrome. *J Invest Dermatol*. 2016 Mar;136(3):574-583. doi: 10.1016/j.jid.2015.11.017. Epub 2016 Jan 8. PMID: 26777423.
130. Eltzschig HK, Eckle T, Mager A, Küper N, Karcher C, Weissmüller T, Boengler K, Schulz R, Robson SC, Colgan SP. ATP release from activated neutrophils occurs via connexin 43 and modulates adenosine-dependent endothelial cell function. *Circ Res*. 2006 Nov 10;99(10):1100-8. doi: 10.1161/01.RES.0000250174.31269.70. Epub 2006 Oct 12. PMID: 17038639.
131. Chen Y, Yao Y, Sumi Y, Li A, To UK, Elkhail A, Inoue Y, Woehrle T, Zhang Q, Hauser C, Junger WG. Purinergic signaling: a fundamental mechanism in neutrophil activation. *Sci Signal*. 2010 Jun 8;3(125):ra45. doi: 10.1126/scisignal.2000549. PMID: 20530802; PMCID: PMC4209711.
132. Donati V, Peres C, Nardin C, Scavizzi F, Raspa M, Ciubotaru CD, Bortolozzi M, Pedersen MG, Mammano F. Calcium Signaling in the Photodamaged Skin: In Vivo Experiments and

- Mathematical Modeling. *Function (Oxf)*. 2021 Dec 1;3(1):zqab064. doi: 10.1093/function/zqab064. Erratum in: *Function (Oxf)*. 2022 Feb 15;3(2):zqac003. PMID: 35330924; PMCID: PMC8788836.
133. Beahm DL, Hall JE. Hemichannel and junctional properties of connexin 50. *Biophys J*. 2002 Apr;82(4):2016-31. doi: 10.1016/S0006-3495(02)75550-1. PMID: 11916859; PMCID: PMC1301997.
 134. Gómez-Hernández JM, de Miguel M, Larrosa B, González D, Barrio LC. Molecular basis of calcium regulation in connexin-32 hemichannels. *Proc Natl Acad Sci U S A*. 2003 Dec 23;100(26):16030-5. doi: 10.1073/pnas.2530348100. Epub 2003 Dec 8. PMID: 14663144; PMCID: PMC307687.
 135. Zampighi GA, Loo DD, Kreman M, Eskandari S, Wright EM. Functional and morphological correlates of connexin50 expressed in *Xenopus laevis* oocytes. *J Gen Physiol*. 1999 Apr;113(4):507-24. doi: 10.1085/jgp.113.4.507. PMID: 10102933; PMCID: PMC2217170.
 136. Valiunas V, Weingart R. Electrical properties of gap junction hemichannels identified in transfected HeLa cells. *Pflugers Arch*. 2000 Jul;440(3):366-79. doi: 10.1007/s004240000294. PMID: 10954323.
 137. Bennett BC, Purdy MD, Baker KA, Acharya C, McIntire WE, Stevens RC, Zhang Q, Harris AL, Abagyan R, Yeager M. An electrostatic mechanism for Ca(2+)-mediated regulation of gap junction channels. *Nat Commun*. 2016 Jan 12;7:8770. doi: 10.1038/ncomms9770. PMID: 26753910; PMCID: PMC4730032.
 138. Lopez W, Gonzalez J, Liu Y, Harris AL, Contreras JE. Insights on the mechanisms of Ca(2+) regulation of connexin26 hemichannels revealed by human pathogenic mutations (D50N/Y). *J Gen Physiol*. 2013 Jul;142(1):23-35. doi: 10.1085/jgp.201210893. PMID: 23797420; PMCID: PMC3691447.
 139. Lopez W, Liu Y, Harris AL, Contreras JE. Divalent regulation and intersubunit interactions of human connexin26 (Cx26) hemichannels. *Channels (Austin)*. 2014;8(1):1-4. doi: 10.4161/chan.26789. Epub 2013 Oct 14. PMID: 24126106; PMCID: PMC4048337
 140. Lopez W, Ramachandran J, Alsamarah A, Luo Y, Harris AL, Contreras JE. Mechanism of gating by calcium in connexin hemichannels. *Proc Natl Acad Sci U S A*. 2016 Dec 6;113(49):E7986-E7995. doi: 10.1073/pnas.1609378113. Epub 2016 Nov 21. PMID: 27872296; PMCID: PMC5150374.
 141. Aasen T, Mesnil M, Naus CC, Lampe PD, Laird DW. Gap junctions and cancer: communicating for 50 years. *Nat Rev Cancer*. 2016 Dec;16(12):775-788. doi: 10.1038/nrc.2016.105. Epub 2016 Oct 21. Erratum in: *Nat Rev Cancer*. 2017 Jan;17 (1):74. PMID: 27782134; PMCID: PMC5279857.
 142. Naus CC, Laird DW. Implications and challenges of connexin connections to cancer. *Nat Rev Cancer*. 2010 Jun;10(6):435-41. doi: 10.1038/nrc2841. PMID: 20495577
 143. Zhang X, He Y, Zhou H, Luo Q, Li C. Severe ichthyosis-related disorders in children: response to acitretin. *J Dermatolog Treat*. 2007;18(2):118-22. doi: 10.1080/09546630601156348. PMID: 17520471.
 144. Becker DL, Phillips AR, Duft BJ, Kim Y, Green CR. Translating connexin biology into therapeutics. *Semin Cell Dev Biol*. 2016 Feb;50:49-58. doi: 10.1016/j.semcdb.2015.12.009. Epub 2015 Dec 10. PMID: 26688335.
 145. Ghatnekar GS, O'Quinn MP, Jourdan LJ, Gurjarpadhye AA, Draughn RL, Gourdie RG. Connexin43 carboxyl-terminal peptides reduce scar progenitor and promote regenerative healing

- following skin wounding. *Regen Med.* 2009 Mar;4(2):205-23. doi: 10.2217/17460751.4.2.205. PMID: 19317641; PMCID: PMC2720252.
146. Gourdie RG, Ghatnekar GS, O'Quinn M, Rhatt MJ, Barker RJ, Zhu C, Jourdan J, Hunter AW. The unstoppable connexin43 carboxyl-terminus: new roles in gap junction organization and wound healing. *Ann N Y Acad Sci.* 2006 Oct;1080:49-62. doi: 10.1196/annals.1380.005. PMID: 17132774.
 147. Willebrords J, Crespo Yanguas S, Maes M, Decrock E, Wang N, Leybaert L, Kwak BR, Green CR, Cogliati B, Vinken M. Connexins and their channels in inflammation. *Crit Rev Biochem Mol Biol.* 2016 Nov/Dec;51(6):413-439. doi: 10.1080/10409238.2016.1204980. Epub 2016 Jul 7. PMID: 27387655; PMCID: PMC5584657.
 148. Srinivas M, Verselis VK, White TW. Human diseases associated with connexin mutations. *Biochim Biophys Acta Biomembr.* 2018 Jan;1860(1):192-201. doi: 10.1016/j.bbamem.2017.04.024. Epub 2017 Apr 27. PMID: 28457858; PMCID: PMC5659969.
 149. Lilly E, Sellitto C, Milstone LM, White TW. Connexin channels in congenital skin disorders. *Semin Cell Dev Biol.* 2016 Feb;50:4-12. doi: 10.1016/j.semdb.2015.11.018. Epub 2016 Jan 13. PMID: 26775130; PMCID: PMC4779425.
 150. Qiu Y, Zheng J, Chen S, Sun Y. Connexin Mutations and Hereditary Diseases. *Int J Mol Sci.* 2022 Apr 12;23(8):4255. doi: 10.3390/ijms23084255. PMID: 35457072; PMCID: PMC9027513.
 151. Caputo R, Peluchetti D. The junctions of normal human epidermis. A freeze-fracture study. *J Ultrastruct Res.* 1977 Oct;61(1):44-61. doi: 10.1016/s0022-5320(77)90005-3. PMID: 915975.
 152. Risek B, Klier FG, Gilula NB. Multiple gap junction genes are utilized during rat skin and hair development. *Development.* 1992 Nov;116(3):639-51. doi: 10.1242/dev.116.3.639. PMID: 1289057.
 153. Kam E, Melville L, Pitts JD. Patterns of junctional communication in skin. *J Invest Dermatol.* 1986 Dec;87(6):748-53. doi: 10.1111/1523-1747.ep12456937. PMID: 3537149.
 154. Salomon D, Saurat JH, Meda P. Cell-to-cell communication within intact human skin. *J Clin Invest.* 1988 Jul;82(1):248-54. doi: 10.1172/JCI113578. PMID: 2455735; PMCID: PMC303501.
 155. Potten CS. Cell replacement in epidermis (keratopoiesis) via discrete units of proliferation. *Int Rev Cytol.* 1981;69:271-318. doi: 10.1016/s0074-7696(08)62326-8. PMID: 6163744.
 156. Kelsell DP, Wilgoss AL, Richard G, Stevens HP, Munro CS, Leigh IM. Connexin mutations associated with palmoplantar keratoderma and profound deafness in a single family. *Eur J Hum Genet.* 2000 Feb;8(2):141-4. doi: 10.1038/sj.ejhg.5200407. Corrected and republished in: *Eur J Hum Genet.* 2000 Jun;8(6):469-72. PMID: 10757647.
 157. Di WL, Common JE, Kelsell DP. Connexin 26 expression and mutation analysis in epidermal disease. *Cell Commun Adhes.* 2001;8(4-6):415-8. doi: 10.3109/15419060109080763. PMID: 12064628.
 158. Caceres-Rios H, Tamayo-Sanchez L, Duran-Mckinster C, de la Luz Orozco M, Ruiz-Maldonado R. Keratitis, ichthyosis, and deafness (KID syndrome): review of the literature and proposal of a new terminology. *Pediatr Dermatol.* 1996 Mar-Apr;13(2):105-13. doi: 10.1111/j.1525-1470.1996.tb01414.x. PMID: 9122065.
 159. Gilliam A, Williams ML. Fatal septicemia in an infant with keratitis, ichthyosis, and deafness (KID) syndrome. *Pediatr Dermatol.* 2002 May-Jun;19(3):232-6. doi: 10.1046/j.1525-1470.2002.00075.x. PMID: 12047643.
 160. Miteva L. Keratitis, ichthyosis, and deafness (KID) syndrome. *Pediatr Dermatol.* 2002 Nov-Dec;19(6):513-6. doi: 10.1046/j.1525-1470.2002.00222.x. PMID: 12437553.

161. Coggshall K, Farsani T, Ruben B, McCalmont TH, Berger TG, Fox LP, Shinkai K. Keratitis, ichthyosis, and deafness syndrome: a review of infectious and neoplastic complications. *J Am Acad Dermatol.* 2013 Jul;69(1):127-34. doi: 10.1016/j.jaad.2012.12.965. Epub 2013 Feb 4. PMID: 23384797.
162. Ogawa Y, Takeichi T, Kono M, Hamajima N, Yamamoto T, Sugiura K, Akiyama M. Revertant mutation releases confined lethal mutation, opening Pandora's box: a novel genetic pathogenesis. *PLoS Genet.* 2014 May 1;10(5):e1004276. doi: 10.1371/journal.pgen.1004276. PMID: 24785414; PMCID: PMC4006701.
163. Aypek H, Bay V, Meşe G. Altered cellular localization and hemichannel activities of KID syndrome associated connexin26 I30N and D50Y mutations. *BMC Cell Biol.* 2016 Feb 2;17:5. doi: 10.1186/s12860-016-0081-0. PMID: 26831144; PMCID: PMC4736630.
164. García IE, Maripillán J, Jara O, Ceriani R, Palacios-Muñoz A, Ramachandran J, Olivero P, Perez-Acle T, González C, Sáez JC, Contreras JE, Martínez AD. Keratitis-ichthyosis-deafness syndrome-associated Cx26 mutants produce nonfunctional gap junctions but hyperactive hemichannels when co-expressed with wild type Cx43. *J Invest Dermatol.* 2015 May;135(5):1338-1347. doi: 10.1038/jid.2015.20. Epub 2015 Jan 27. PMID: 25625422; PMCID: PMC4801018.
165. Press ER, Shao Q, Kelly JJ, Chin K, Alaga A, Laird DW. Induction of cell death and gain-of-function properties of connexin26 mutants predict severity of skin disorders and hearing loss. *J Biol Chem.* 2017 Jun 9;292(23):9721-9732. doi: 10.1074/jbc.M116.770917. Epub 2017 Apr 20. PMID: 28428247; PMCID: PMC5465495.
166. Donnelly S, English G, de Zwart-Storm EA, Lang S, van Steensel MA, Martin PE. Differential susceptibility of Cx26 mutations associated with epidermal dysplasias to peptidoglycan derived from *Staphylococcus aureus* and *Staphylococcus epidermidis*. *Exp Dermatol.* 2012 Aug;21(8):592-8. doi: 10.1111/j.1600-0625.2012.01521.x. Epub 2012 May 30. PMID: 22643125.
167. Mese G, Sellitto C, Li L, Wang HZ, Valiunas V, Richard G, Brink PR, White TW. The Cx26-G45E mutation displays increased hemichannel activity in a mouse model of the lethal form of keratitis-ichthyosis-deafness syndrome. *Mol Biol Cell.* 2011 Dec;22(24):4776-86. doi: 10.1091/mbc.E11-09-0778. Epub 2011 Oct 26. PMID: 22031297; PMCID: PMC3237621.
168. Jara O, Acuña R, García IE, Maripillán J, Figueroa V, Sáez JC, Araya-Secchi R, Lagos CF, Pérez-Acle T, Berthoud VM, Beyer EC, Martínez AD. Critical role of the first transmembrane domain of Cx26 in regulating oligomerization and function. *Mol Biol Cell.* 2012 Sep;23(17):3299-311. doi: 10.1091/mbc.E11-12-1058. Epub 2012 Jul 11. PMID: 22787277; PMCID: PMC3431943.
169. Müller DJ, Hand GM, Engel A, Sosinsky GE. Conformational changes in surface structures of isolated connexin 26 gap junctions. *EMBO J.* 2002 Jul 15;21(14):3598-607. doi: 10.1093/emboj/cdf365. PMID: 12110573; PMCID: PMC126111.
170. Sánchez HA, Mese G, Srinivas M, White TW, Verselis VK. Differentially altered Ca²⁺ regulation and Ca²⁺ permeability in Cx26 hemichannels formed by the A40V and G45E mutations that cause keratitis ichthyosis deafness syndrome. *J Gen Physiol.* 2010 Jul;136(1):47-62. doi: 10.1085/jgp.201010433. PMID: 20584891; PMCID: PMC2894548.
171. Sanchez HA, Villone K, Srinivas M, Verselis VK. The D50N mutation and syndromic deafness: altered Cx26 hemichannel properties caused by effects on the pore and intersubunit interactions. *J Gen Physiol.* 2013 Jul;142(1):3-22. doi: 10.1085/jgp.201310962. PMID: 23797419; PMCID: PMC3691445.

172. Schütz M, Auth T, Gehrt A, Bosen F, Körber I, Strenzke N, Moser T, Willecke K. The connexin26 S17F mouse mutant represents a model for the human hereditary keratitis-ichthyosis-deafness syndrome. *Hum Mol Genet.* 2011 Jan 1;20(1):28-39. doi: 10.1093/hmg/ddq429. Epub 2010 Oct 6. PMID: 20926451.
173. Taki T, Takeichi T, Sugiura K, Akiyama M. Roles of aberrant hemichannel activities due to mutant connexin26 in the pathogenesis of KID syndrome. *Sci Rep.* 2018 Aug 27;8(1):12824. doi: 10.1038/s41598-018-30757-3. PMID: 30150638; PMCID: PMC6110719.
174. Natha CM, Vemulapalli V, Fiori MC, Chang CT, Altenberg GA. Connexin hemichannel inhibitors with a focus on aminoglycosides. *Biochim Biophys Acta Mol Basis Dis.* 2021 Jun 1;1867(6):166115. doi: 10.1016/j.bbadis.2021.166115. Epub 2021 Mar 9. PMID: 33711451.
175. Eskandari S, Zampighi GA, Leung DW, Wright EM, Loo DD. Inhibition of gap junction hemichannels by chloride channel blockers. *J Membr Biol.* 2002 Jan 15;185(2):93-102. doi: 10.1007/s00232-001-0115-0. Epub 2002 Feb 5. PMID: 11891568.
176. Locke D, Koren IV, Liu JY, Harris AL. Reversible pore block of connexin channels by cyclodextrins. *J Biol Chem.* 2004 May 28;279(22):22883-92. doi: 10.1074/jbc.M401980200. Epub 2004 Mar 23. PMID: 15044473.
177. Qu Z., Yang G., Mammano F., Zonta F. (2017). Fully human antibody specifically inhibiting connexin 26. International Patent Application No. PCT/CN2016/109847. Available at: <https://patentscope.wipo.int/search/en/detail.jsf?docId=WO2017128880>
178. Xu L, Carrer A, Zonta F, Qu Z, Ma P, Li S, Ceriani F, Buratto D, Crispino G, Zorzi V, Ziraldo G, Bruno F, Nardin C, Peres C, Mazzarda F, Salvatore AM, Raspa M, Scavizzi F, Chu Y, Xie S, Yang X, Liao J, Liu X, Wang W, Wang S, Yang G, Lerner RA, Mammano F. Design and Characterization of a Human Monoclonal Antibody that Modulates Mutant Connexin 26 Hemichannels Implicated in Deafness and Skin Disorders. *Front Mol Neurosci.* 2017 Sep 22;10:298. doi: 10.3389/fnmol.2017.00298. PMID: 29018324; PMCID: PMC5615210.
179. Ziraldo G, Buratto D, Kuang Y, Xu L, Carrer A, Nardin C, Chiani F, Salvatore AM, Paludetti G, Lerner RA, Yang G, Zonta F, Mammano F. A Human-Derived Monoclonal Antibody Targeting Extracellular Connexin Domain Selectively Modulates Hemichannel Function. *Front Physiol.* 2019 Jun 11;10:392. doi: 10.3389/fphys.2019.00392. PMID: 31263420; PMCID: PMC6584803.
180. Bruzzone R, White TW. Connexin hemichannel inhibition improves skin pathology in Clouston syndrome mice. *EBioMedicine.* 2020 Jul;57:102856. doi: 10.1016/j.ebiom.2020.102856. Epub 2020 Jul 3. PMID: 32629388; PMCID: PMC7334806.
181. Nardin C, Tettey-Matey A, Donati V, Marazziti D, Di Pietro C, Peres C, Raspa M, Zonta F, Yang G, Gorelik M, Singh S, Cardarelli L, Sidhu SS, Mammano F. A Quantitative Assay for Ca²⁺Uptake through Normal and Pathological Hemichannels. *Int J Mol Sci.* 2022 Jun 30;23(13):7337. doi: 10.3390/ijms23137337. PMID: 35806342; PMCID: PMC9266989.
182. Boukamp P, Petrussevska RT, Breitkreutz D, Hornung J, Markham A, Fusenig NE. Normal keratinization in a spontaneously immortalized aneuploid human keratinocyte cell line. *J Cell Biol.* 1988 Mar;106(3):761-71. doi: 10.1083/jcb.106.3.761. PMID: 2450098; PMCID: PMC2115116.

(This page is intentionally left blank)

2 MATERIALS AND METHODS

2.1 A Short review of the experimental work

Uncontrolled expression of leaky HCs leads to toxicity and consequently results in cell death [1-6]. In the experimental work that preceded this thesis, Nardin et al, designed and produced lentiviruses for Tet-on bicistronic expression of Cx26 [7]. Additionally, they were used the genetically encoded indicator GCaMP6s that permits optical tracking of changes in cytosolic concentration of Ca^{2+} . The Cx coding sequence upstream of an internal ribosome entry site sequence were added, which then followed by the Cx coding sequence of GCaMP6s. Afterward, by puromycin selection of virally transduced cells, stable cell pools expressing human Cx26 (referred to as HaCaT-Cx26-GCaMP6s cells) or the lethal KID-related mutant Cx26G45E that generates leaky HCs were obtained. To confirm that functional HCs were present in the plasma membrane of live HaCaT- Cx26-GCaMP6s cells, 4',6- diamidino-2-phenylindole (DAPI) that is a non-fluorescent in the medium but becomes fluorescent as penetrating into the cell and binding to nucleic acids was used. Analyses of HaCaT-Cx26-GCaMP6s cells was done by live microscopy. A kind of custom-built spinning disk confocal fluoresce microscope to monitor Ca^{2+} uptake experiments in confluent cultures of HaCaT-Cx26-GCaMP6s cells were used. With a suitable objective lens, a wide field of view with a diameter of 630 μm was achieved, which permitted to collect and average images of GCaMP6s fluorescence emission from more than 100 cells per culture was achieved. For the experiments with HaCaT-Cx26-GCaMP6s pool, both before and after 5 minutes incubation with DAPI solution, coverslip with plated cell were imaged using the two-photon microscope. Afterward, fluorescence images of cells, previously incubated in extracellular medium containing a low Ca^{2+} concentration (60 μM), at 1 frame/s for 20 s of baseline was recorded during excitation of GCaMP6s by 488 nm laser. A bolus of CaCl_2 (2 μL) to the medium was added in the recording chamber (1 mL volume) at different concentrations for different experiments, aiming to achieve final estimated extracellular Ca^{2+} of 100 μM , 260 μM , 560 μM , 1 mM and 2 mM.

After adding CaCl_2 the images were recorded for next 10 min. By the end of each recording interval, bolus of the Ca^{2+} ionophore ionomycin was used to confirm that GCaMP6s signals were not saturated. For each of these experiments, fluorescence emission of GCaMP6s was quantified pixel-by-pixel and for each frame. Additionally, these experiments were also done in the presence

of HC blocker, flufenamic acid (FFA), as well as an antibody used for different Cx HCs, called abEC1.1m and abEC1.1h [8].

2.2 Calcium imaging overview

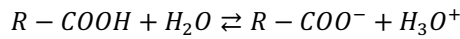
Calcium imaging is a microscopy technique to optically measure the Ca^{2+} status of a cell, group of cells, tissue or medium. Calcium imaging takes advantage of Ca^{2+} indicators, namely fluorescent molecules that respond to the binding of Ca^{2+} ions by fluorescence properties. Regardless of type of indicators, the imaging procedure is very similar. A quantitative assess of ion concentrations can be obtained from measurements of fluorescence indicator, however several important experimental conditions need to be considered [9,10]. For instance, the ion-sensitive indicator has to be chemically uniform and smoothly distributed in the cytosol, and indicator binding and properties of fluorescence should be similar to those measured in isolated systems. Additionally, there should be a linear estimate of fluorescence emission between the imaging and measurement, and finally, the free ion concentration should fall within the indicator's useful dynamic rang [11].

2.2.1 Optical measurement of ion concentration

The patch-clamp technique as a versatile electrophysiological tool can detect ion fluxes across membrane with high temporal resolution ($<1\text{ms}$), however, fails to track spatial resolution. In contrast, optical measurement of concentration of ion species and dynamic of them under super advance microscopes via use of indicators provides access to the three-dimensional volume of a cell and can be used to monitor cell behavior in vivo.

Many indicators have been developed in order to study the physiology and function of cell. Several molecular probes, called fluorescent dyes, capable of monitoring the local ion concentration with high selectivity have been produced over the last decades. The two main classes of Ca^{2+} indicator are chemical indicators and genetically encoded Ca^{2+} indicators (GECI).

Chemical indicators are small molecules based on BAPTA (1,2-bis (o-amino phenoxy) ethane- N,N,N',N' -tetra acetic acid), a highly selective Ca^{2+} chelating reagent (figure 2.1). The ability to attach and chelate Ca^{2+} depends on acetic acid which is the carboxylic acids consist of a $\text{C}=\text{O}$ pair with OH element bounded to the same carbon. The carboxylic acid ($\text{R}-\text{COOH}$) will be dissociated if the pH of the solution is higher than the pK of the acid.



$$K_a = \frac{[R - CO_2^-][H_3O^+]}{[R - CO_2H]}$$

$$pH = -\log([H_3O^+])$$

$$pK_a = -\log K_a$$

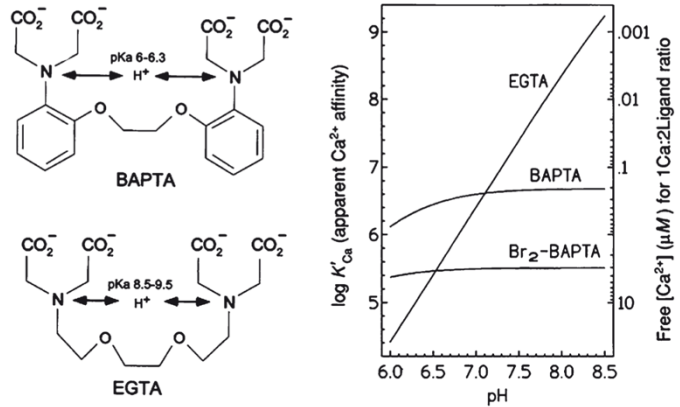


Figure 2.1 Chemical structure and pH dependence of Ca^{2+} affinity of BAPTA and EGTA. BAPTA is a pH-sensitive evolution of the widely use Ca^{2+} -selective chelator ethylene glycol tetra acetic acid (EGTA), which is in turn related to EGTA, but with the much higher affinity for Ca^{2+} than for Mg^{2+} . (From ref. [26])

BAPTA is a fluorescent dye with wavelength emission and excitation of 363nm and 251nm, respectively. However, these wavelengths are in the UV region and incompatible with most of instrumentation and with cell survival. The chemical indicators are including fura-2, indo-1, fluo-3, fluo-4, Ca Green-1, each has different affinities for Ca^{2+} and excitation/emission wavelengths [12,13]. Some of the has been chemically modified by adding covalent of fluorescein derivatives, resulting the spectral characteristics appropriate for live cell imaging.

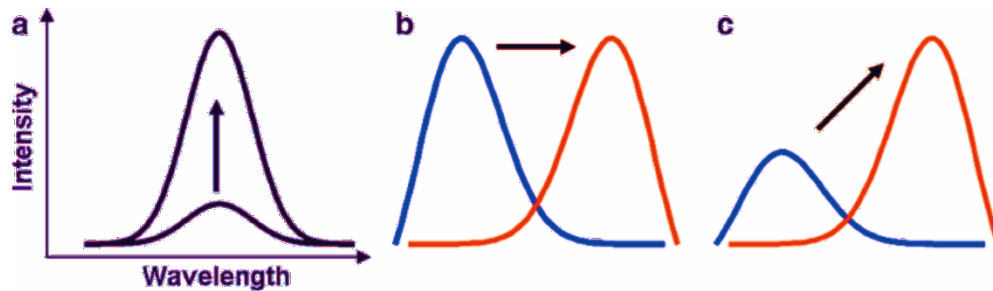


Figure 2.2: Spectral properties that can be used to measure Ca^{2+} concentration. a) a change in fluorescent yield, b) a shift in the excitation or emission spectrum, c) combination of a and c. (from ref.[26])

In general, when fluorescent dyes bind to the specific ligand, the molecular state of the fluorescent element changes, therefore modulating the fluorescent readout. A change in fluorescent yield represents a change in the local free ion concentration (figure 2.1).

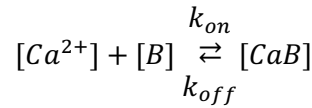
The Ca^{2+} -selective genetically encoded indicator are used to study Ca^{2+} transients in distinct cell types or in subcellular organelles. These indicators are including green fluorescent protein variants using Förster resonance energy transfer (FRET) pairs or circularly permuted green fluorescent mutants [14-17]. GCaMPs are green fluorescent protein (GFP)-based genetically encoded

indicators which consist of circular permuted GFP, calmodulin, and a calmodulin binding motif derived from skeletal muscle myosin light chain kinase [14,18]. These indicators undergo conformational changes, as they bound to Ca^{2+} , causes increases in intensity of fluorescence. The most recent derivative of GCaMP are GCaMP6s, 6m and 6f (indicating slow, medium and fast kinetics) [19,20]. GCaMP6s has higher sensitivity and brighter fluorescent among them, and used in detecting small changes in Ca^{2+} [21]. Overall, genetically encoded Ca^{2+} indicators would facilitate monitoring of intracellular Ca^{2+} over long-term imaging.

As it mentioned in section 2.1, a specific dye, DAPI, was used to validate the functional channel on plasma membrane. DAPI, is a fluorescent stain that tightly binds to adenine–thymine-rich sequence of DNA [22]. Furthermore, it forms nonfluorescent intercalative complexes with double-stranded nucleic acids. It is used commonly in fluorescence microscopy. As it can pass through an intact cell membrane, it is used to stain both live and fixed cells. DAPI maximum absorption wavelength is at 358 nm (UV) and its emission maximum is at 461 nm (blue).

2.2.2 Linking fluorescent to ion concentration

Bonding of Ca^{2+} by a buffer B to form a complex CaB is described by the reaction:



, and corresponding kinetic equation, based on differential rate law for first order reaction, is written as:

$$\frac{d[\text{CaB}]}{dt} = k_{on}[\text{Ca}^{2+}][\text{B}] - k_{off}[\text{CaB}] \quad (2.1)$$

where k_{on} and k_{off} are rate constants for Ca^{2+} binding to B and Ca^{2+} dissociation, respectively. the squared bracket used to represent concentrations. At the equilibrium, left side of equation is equal to zero, consequently we have:

$$\frac{k_{off}}{k_{on}} \equiv K_d = \frac{[\text{Ca}^{2+}][\text{B}]}{[\text{CaB}]} \quad (2.2)$$

where K_d is called dissociation constant.

In general, the concentration of free and Ca^{2+} bound indicator differs with respect to quantum yield or absorption cross section. Hence, for a given wavelength, they will show different contributions to the overall intensity of fluorescent, F :

$$F = S_b[\text{CaB}] + S_f[B] \quad (2.3)$$

All factors regarding to indicators properties and experimental setup combine in the constants, S_b , S_f . let us, consider total amount of indicator as:

$$c_T \equiv [B] + [\text{CaB}] \quad (2.4)$$

and then define, $[\text{Ca}^{2+}]$ at saturating as

$$F_{max} \equiv S_b c_T \quad (2.5)$$

and at zero

$$F_{min} \equiv S_f c_T \quad (2.6)$$

Hence, we can substitute equations (2.5) and (2.6), separately in equation (2.3), which we obtain:

$$F_{max} - F = (S_b - S_f)[B] \quad (2.7)$$

$$F - F_{min} = (S_b - S_f)[\text{CaB}] \quad (2.8)$$

, respectively.

Now, dividing equation (2.8) by (2.7), and then combining with equation (2.2), resulting in:

$$[\text{Ca}^{2+}] = K_d \frac{F - F_{min}}{F_{max} - F} \quad (2.9)$$

However, there are a number of caveats and problems with the practical use of this equation. Firstly, F , F_{max} and F_{min} change rapidly over time due to photobleaching, which is the dye photochemical damage due to continuous illumination. Secondly, small fluctuations in the estimate of F_{max} and F (e.g., due to instrumental noise) may cause large fluctuations in the estimate of $[\text{Ca}^{2+}]$ as F/F_{max} approaches one (to unreliable zone) (figure 2.3).

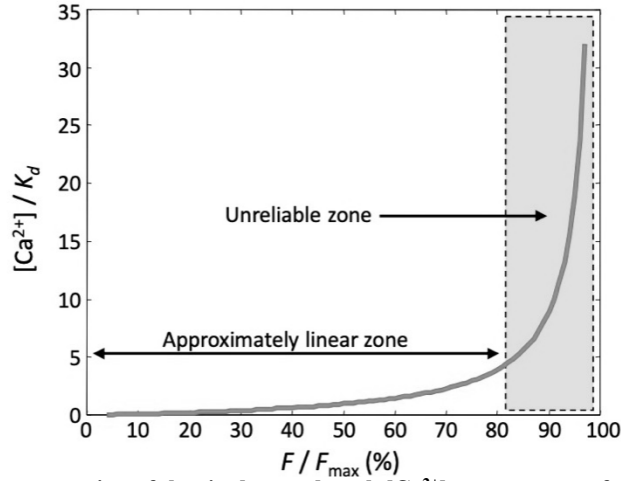


Figure 2.3 Graphical representation of the single wavelength $[Ca^{2+}]$ -measurement formula. (from ref. [26])

To address the issue, it is useful to consider the first order Taylor's expansion of equation (2.9) around F_0 , the fluorescence signal correspondent to the pre-stimulus (resting) Ca^{2+} concentration $[Ca^{2+}]$, which yields:

$$\Delta[Ca^{2+}] = [Ca^{2+}] - [Ca^{2+}]_0 \cong K_d \frac{F_{max} - F_{min}}{(F_{max} - F_0)^2} (F - F_0) \quad (2.10)$$

By substituting

$$\Delta F = F - F_0 \quad (2.11)$$

and

$$K = F_0 K_d \frac{F_{max} - F_{min}}{(F_{max} - F_0)^2} \quad (2.12)$$

in equation (2.10), we obtain:

$$\Delta[Ca^{2+}] \cong K \frac{\Delta F}{F_0} \quad (2.13)$$

Estimation of Ca^{2+} variations $\Delta F/F_0$ instead of absolute Ca^{2+} values is a practical method used in biology to compare Ca^{2+} events in a single cell or a population of cells. The computation of $\Delta F/F_0$ is performed point-by-point in the experimental movie and averaged over regions of interest which correspondent to subcellular domains or groups of cells.

As it mentioned earlier, dye photobleaching occurs due to continuous illumination. To compensate this effect in the measurement of F , F_{max} and F_{min} , utilizing ratiometric (or dual wavelength) Ca^{2+} dyes such as Fura-2 and Fura-Red, or mag-Fura-2, Fura-2FF, and BTC is useful. The ratio of the

emissions at their wavelengths is directly related to the amount of intracellular Ca^{2+} . The most notable feature of these dyes is the existence of a spectral shift due to Ca^{2+} binding and the existence of an isosbestic point (at 360nm) for which fluorescence is independent of concentration of the Ca^{2+} [1] (figure 2.4). The shift can occur in the excitation or in the emission spectrum. As a result, the amplitudes of spectral increase as Ca^{2+} concentration increasing to the left of the isosbestic point and decrease to the right.

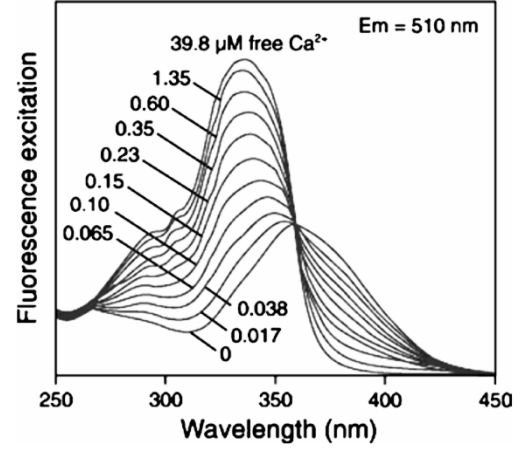


Figure 2.4 Excitation spectra of fura-2 for the indicated values of the free Ca^{2+} concentration (from ref. [26])

In order to derive the equation to quantify Ca^{2+} concentration at equilibrium in term of ratio signal, we start from the fact that, two wavelengths and two indicator dyes (free and bound) require four proportionality constants. We can write:

$$F_1 = S_{f1}[B] + S_{b1} [CaB],$$

$$F_2 = S_{f2}[B] + S_{b2} [CaB] \quad (2.14)$$

then, using equation (2.2), and defining the fluorescence ratio as:

$$R \equiv \frac{F_1(x,y,t)}{F_2(x,y,t)} \quad (2.15)$$

we obtain:

$$R = \frac{S_{f1} + S_{b1}[Ca^{2+}]/K_d}{S_{f2} + S_{b2}[Ca^{2+}]/K_d} \quad (2.16)$$

Now, defining minimum value of R that can attain at zero $[\text{Ca}^{2+}]$ as $R_{min} \equiv S_{f1}/S_{f2}$, and maximum at saturating $[\text{Ca}^{2+}]$ as $R_{max} \equiv S_{b1}/S_{b2}$, we can conclude that:

$$[Ca^{2+}] = K_d \left(\frac{S_{f2}}{S_{b2}} \right) \left(\frac{R - R_{min}}{R_{max} - R} \right) \quad (2.17)$$

2.2.3 Confocal microscopy

In light microscopy, illuminating light pass through the sample evenly over widefield resulting in lack of contrast and axial blurring. In contrast, confocal microscope provides point by point illumination of sample with finely focused spot. Depending of the objective numerical aperture (NA), the size of the illumination point can be varied between 0.2 and 0.8 μm in diameter and 0.5 to 1.5 μm along axial axis. Furthermore, point wise detection through pinhole could improve contrast and reduce axial blurring by preventing out of focus light reaching the detector. A significant advantage of this kind of microscope is the optical sectioning provided, through which three-dimensional reconstruction of a sample from high-resolution stacks of images is achievable [23]. Basic components of confocal microscope are including: the pinholes, the objective lenses, and low-noise detectors, scanning mirror, filters, and laser illumination. (figure 2.5).

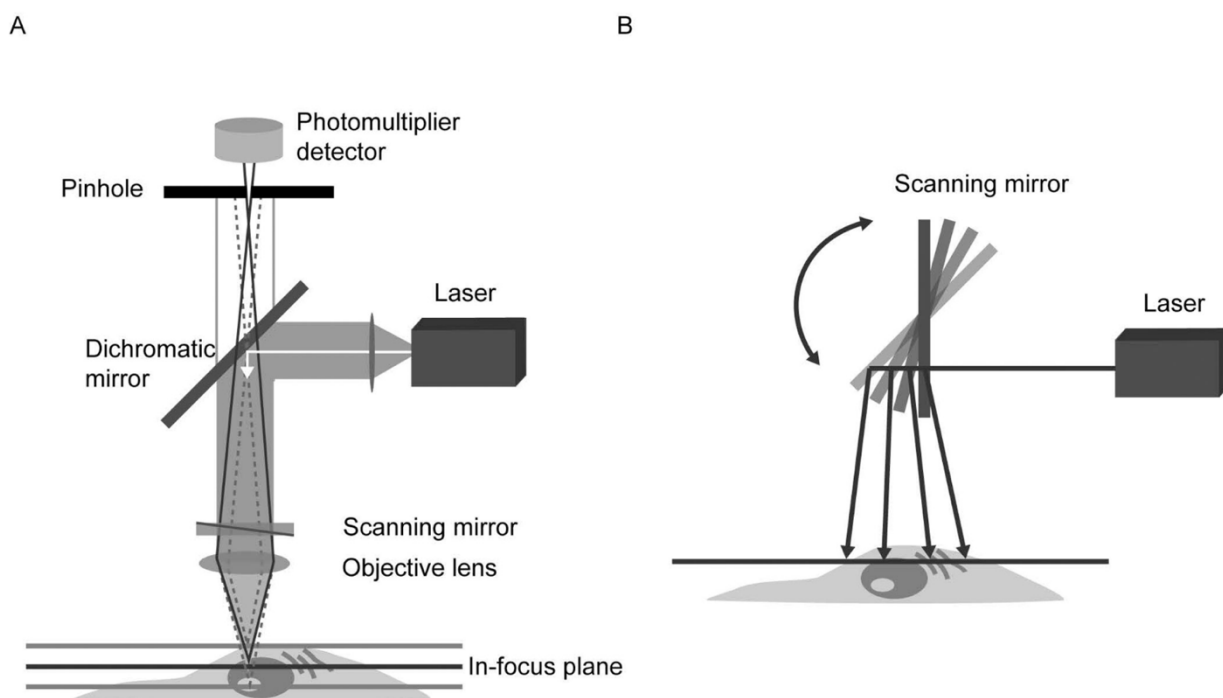


Figure 2.5 Components of a confocal microscope. A. Light from a laser source is passed through collimating optics to a variable dichromatic mirror or acousto-optical beamsplitter (AOBS) and reflected to the objective lens which focuses the beam on a point in the sample. Scanning mirrors sweep the excitation beam over the sample point by point to build the image. Emitted fluorescence passes back through the objective lens, the dichromatic mirror or AOBS, and is detected by the PMT(s). A pinhole placed in the conjugate image plane to the focal point in the sample serves to reject out-of-focus light, which does not get picked up by the detector. In this epifluorescence configuration, the illumination and emission light both pass through the same lens, thus requiring only the detector-side pinhole. Varying the size of the pinhole changes the amount of light collected and the optical section thickness. Spectral imaging can be achieved with an array of PMTs and a diffraction grating, or prism, placed in the emission light path. B. A schematic of the scanning mirrors employed by confocal microscopes to sweep the excitation light across the sample (from ref.[23])

In light microscopy, the resolution is determined by NA, refractive index and wavelength of light. Lateral resolution of a microscope, in imaging self-illuminous object is determined by lateral extent of its intensity point spread function. In Confocal microscope, the lateral extent is 30% narrower than the conventional. The equations used to determine lateral and axial resolution are:

$$R_{lateral} = \frac{0.4 \lambda_0}{NA} \quad (2.18)$$

$$R_{axial} = \frac{1.4 \lambda_0 n}{(NA)^2} \quad (2.19)$$

where λ_0 is wavelength of emission light, and n is the refractive index in the object space.

Different types of confocal microscope depending on their scanning methods are existed. The main classes of scanning confocal microscope are including: laser scanning confocal microscope, spinning disc confocal microscope, and hybrid scanning confocal microscope.

In a laser scanning confocal microscope (LSCM), the image of an extended specimen is generated by scanning the focused beam across a defined area in a raster pattern controlled by two high speed oscillating mirrors. One of the mirrors moves the beam from left to right along the x axis, while the other translates the beam in the y -direction. Consequently, the fluorescence emission is collected by the objective and passed back through the confocal optical system. The main advantages of the LSCM are the optical sectioning competence, resolution, and adaptability with three-dimensional imaging.

A spinning disc confocal microscope corresponds to the point- by-point illumination and detection processes, in which light from the excitation source is distributed over multiple foci and the image is created over a two-dimensional sensor instead of a single photomultiplier tube (PMT). Typically, a rotating disc is located in a plane that is optically conjugated with that of the specimen. In the Nipkow disc configuration, the surface consists of fixed-width holes arranged in outwardly spiraling tracks. These holes were positioned in such a way that all part of the image was scanned as the disk turned [23,24]. The fluorescent signal from the molecule then passed through the objective lens and the disc, then it is projected through a relay lens onto a charge-coupled device (CCD) or a scientific complementary metal–oxide–semiconductor (sCMOS) camera sensor instead of PMT. Therefore, the overall speed of image acquisition is constrained by camera sensitivity and maximal frame rate.

The highly configurable spinning disk confocal microscope used for the experimental part of this thesis by Nardin et al, is suitable to perform imaging and electrophysiological recordings

simultaneously (described in ref. [24]) (figure 2.6). The variety of specialization have been developed to enhance the quality of images, and they are grouped in the hybrid scanning confocal microscopy. As an example, swept field confocal microscope are used in a pinhole in such a way that the apertures stay immobile while galvanometer and piezo-controlled mirrors sweep the image of the illuminated apertures across the sample. The main dominances of the microscope are including increase in light collection efficiency, speed, and reduction in artifact from moving the apertures.

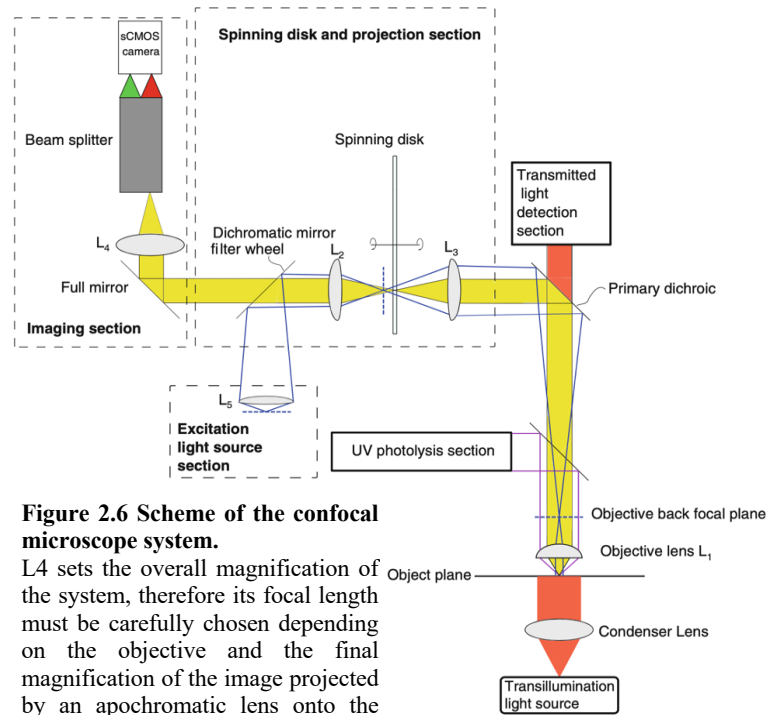


Figure 2.6 Scheme of the confocal microscope system.

L4 sets the overall magnification of the system, therefore its focal length must be carefully chosen depending on the objective and the final magnification of the image projected by an apochromatic lens onto the camera sensor. (from ref. [24])

2.2.4 Two photons microscopy

Towards solution of scattering problem which results in out of focused and lose of signal generation, as well as exponential decrease in excitation depth, two photons excitation method was defined. In this approach, two photons can be simultaneously absorbed by combining their energies in order to initiate the electronic transition of fluorophores to the excited state. As the photon energy is inversely related to wavelength, the resulting photon has twice a single photon wavelength. Therefore, the fluorescent that previously excited by UV illumination, now can be excited by the infrared. The requirement for two-photon excitation is that the photons are absorbed at the same time (approximately 10^{-18} sec). To achieve this goal, a much higher photon flux is required ($\sim 10^6$ times more) compared to one-photon excitation. Therefore, a high laser power is required. To further increase the likelihood of the incident, the illumination focusing via using a high NA objective which creates a spatial concentration of photon flux is used [25]. Overall, in comparison with confocal microscopy, in two photons microscopy, no absorption and fluorescence (consequently, compensate photobleaching and phototoxicity) above and below the plane of focus occurs.

2.3 Image processing

Image processing and data analysis were used to relate Ca^{2+} concentration fluctuations to GCaMp6s fluorescence emission. For these purposes, open source ImageJ software, the MATLAB programming environment (version R2021a, The MathWorks, Inc., MA, USA) and Vimmaging, a custom-made software developed under the MATLAB environment by Catalin D. Ciubotrau and Fabio Mammano, were used.

ImageJ can display multiple spatially or temporally related images in a single window. To derive traces for each cell from the provided movies of experiments (different total Ca^{2+} concentrations), cells are selected by drawing region of interests (ROIs) around each. Before selecting each cell, background subtraction was done by drawing a ROI. The value derived, which was the average intensity in that region, and then subtracted for all frames. Cells were selected based on their appearance. Those cells that were brighter than others, round shaped ones, as well as cells that started to show bubbles after the addition of ionomycin or did not respond to it, were discarded. Then selected ROIs were saved and uploaded to Vimmaging software. For visualization of the data, first the conversion of pixel to micrometer was done. Consequently, information (intensity) of each ROI was extracted by taking the average of grey value of the first 20 frame (fluo reference frame), and then subtracted that value from the average grey value of the selected ROIs, in each frame, through all the recorded time.

Traces of the experiments starting from a low Ca^{2+} concentration, in which the fluorescence signal should be at its basal level, then adding the bolus of CaCl_2 , it enters HC and, consequently there is an increase in fluorescence intensity. In principle, the fluorescence shouldn't go below zero, because it means that the Ca^{2+} concentration inside the cell is lower than the basal concentration of Ca^{2+} .

Even though the imaging setup was designed to diminish the photobleaching, there existed a minor effect. In order to compensate for it, all traces were corrected by drawing the fit on the first part (20sec) of the trace and subtracted with an exponential function (figure 2.7). The reason for considering the first 20 seconds to draw the fit is that after adding bolus of CaCl_2 it is not possible to decide whether the decrease is related to decrease in Ca^{2+} or to photobleaching.

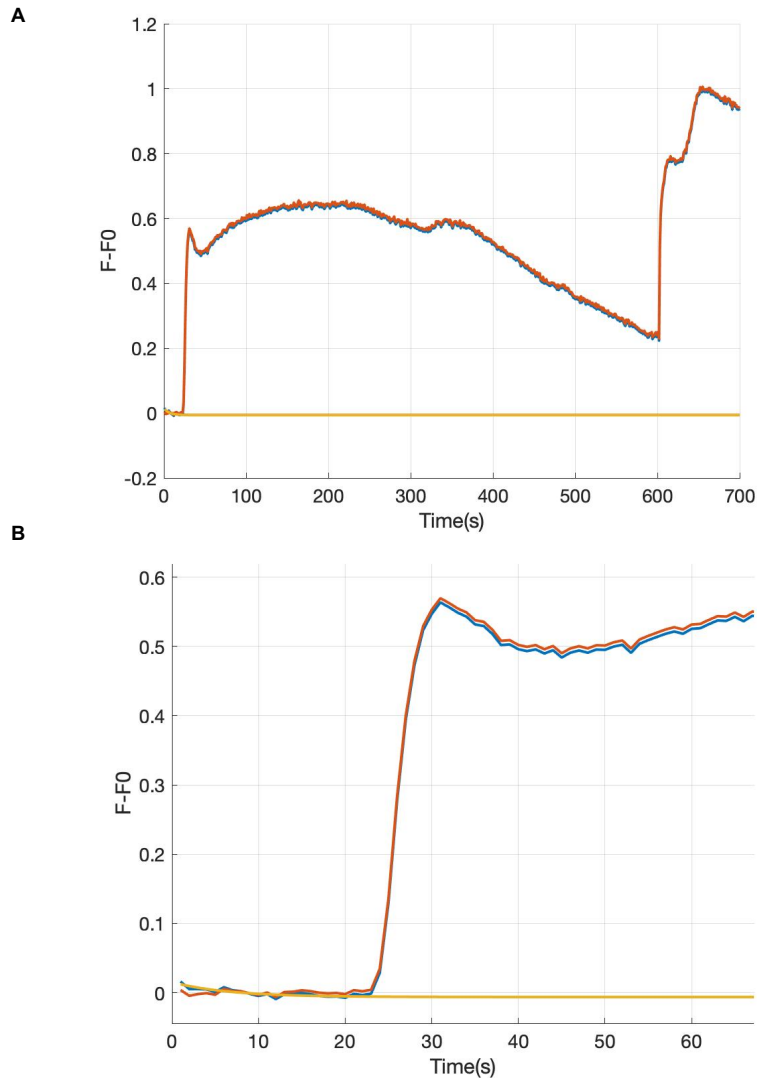


Figure 2.7 Photobleaching correction for an individual cell exposed to CaCl_2 to reach 2mM final Ca^{2+} concentration. Input trace shown in blue, the exponential fit in orange color, and corrected trace in red color. (A) An example of photobleaching correction for a single cell (B) zoom of first 70 seconds of (A).

As it was mentioned earlier the bolus of CaCl_2 and ionomycin were added during the experiments, however since this procedure was done manually by the experimenters, the time wasn't exactly the same for all experiments. To address this issue, traces further corrected. Subsequently, they were sorted based on the maximum of the first peak at 20s (the time bolus of CaCl_2 were added). Furthermore, the mean and standard error of mean Ca^{2+} uptake traces were derived, which consequently used as references for writing the mathematical model. Final outputs are shown in figure (2.8).

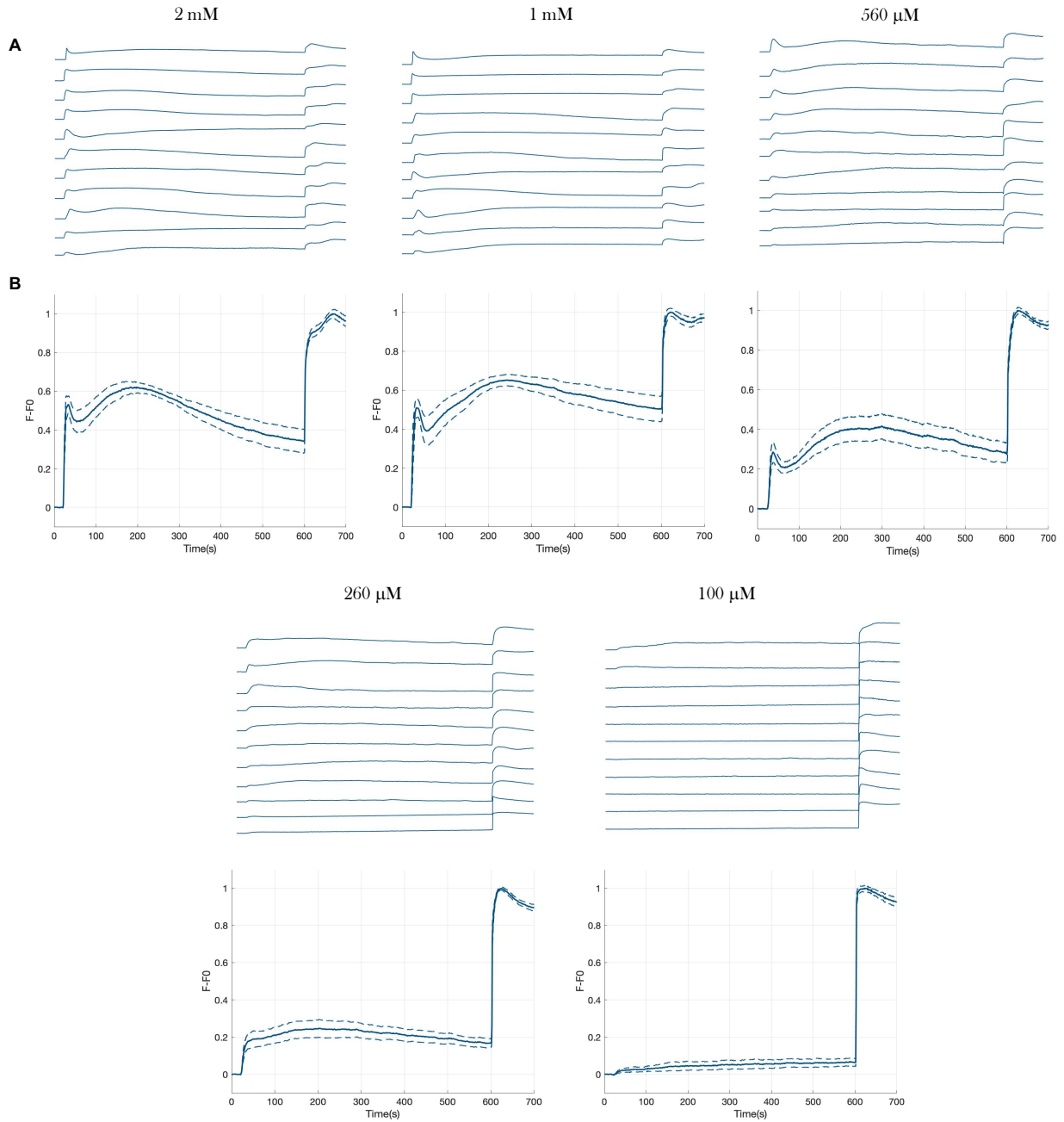


Figure 2.8 Ca^{2+} uptake of HaCaT-Cx26-GCaMP6s cells exposed CaCl_2 bolus concentration to reach different final Ca^{2+} concentrations A) single cell traces sorted by first high peak at 20s shown in one figure (B)Output of mean Ca^{2+} uptake traces (solid line) \pm s.e.m (dashed line).

2.4 References

1. Lu Y, Zhang R, Wang Z, Zhou S, Song Y, Chen L, Chen N, Liu W, Ji C, Wu W, Zhang L. Mechanistic effect of the human GJB6 gene and its mutations in HaCaT cell proliferation and apoptosis. *Braz J Med Biol Res.* 2018 Jul 23;51(9):e7560. doi: 10.1590/1414-431X20187560. PMID: 30043857; PMCID: PMC6065815.
2. Essenfelder GM, Bruzzone R, Lamartine J, Charollais A, Blanchet-Bardon C, Barbe MT, Meda P, Waksman G. Connexin30 mutations responsible for hidrotic ectodermal dysplasia cause abnormal hemichannel activity. *Hum Mol Genet.* 2004 Aug 15;13(16):1703-14. doi: 10.1093/hmg/ddh191. Epub 2004 Jun 22. PMID: 15213106.
3. Helmuth A. Sánchez, Gülistan Meşe, Miduturu Srinivas, Thomas W. White, Vytas K. Verselis; Differentially altered Ca²⁺ regulation and Ca²⁺ permeability in Cx26 hemichannels formed by the A40V and G45E mutations that cause keratitis ichthyosis deafness syndrome. *J Gen Physiol* 1 July 2010; 136 (1): 47–62. doi: <https://doi.org/10.1085/jgp.201010433>
4. Terrinoni A, Codispoti A, Serra V, Bruno E, Didona B, Paradisi M, Nisticò S, Campione E, Napolitano B, Diluvio L, Melino G. Connexin 26 (GJB2) mutations as a cause of the KID syndrome with hearing loss. *Biochem Biophys Res Commun.* 2010 Apr 23;395(1):25-30. doi: 10.1016/j.bbrc.2010.03.098. Epub 2010 Mar 20. PMID: 20307501.
5. Berger AC, Kelly JJ, Lajoie P, Shao Q, Laird DW. Mutations in Cx30 that are linked to skin disease and non-syndromic hearing loss exhibit several distinct cellular pathologies. *J Cell Sci.* 2014 Apr 15;127(Pt 8):1751-64. doi: 10.1242/jcs.138230. Epub 2014 Feb 12. PMID: 24522190.
6. Stong, B.C., Chang, Q., Ahmad, S. and Lin, X. (2006), A Novel Mechanism for Connexin 26 Mutation Linked Deafness: Cell Death Caused by Leaky Gap Junction Hemichannels. *The Laryngoscope*, 116: 2205-2210.
7. Nardin C, Tettey-Matey A, Donati V, Marazziti D, Di Pietro C, Peres C, Raspa M, Zonta F, Yang G, Gorelik M, Singh S, Cardarelli L, Sidhu SS, Mammano F. A Quantitative Assay for Ca²⁺Uptake through Normal and Pathological Hemichannels. *Int J Mol Sci.* 2022 Jun 30;23(13):7337. doi: 10.3390/ijms23137337. PMID: 35806342; PMCID: PMC9266989.
8. Sellitto C, Li L, White TW. Connexin hemichannel inhibition ameliorates epidermal pathology in a mouse model of keratitis ichthyosis deafness syndrome. *Sci Rep.* 2021 Dec 16;11(1):24118. doi: 10.1038/s41598-021-03627-8. PMID: 34916582; PMCID: PMC8677806.
9. Takahashi A, Camacho P, Lechleiter JD, Herman B. Measurement of intracellular calcium. *Physiol Rev.* 1999 Oct;79(4):1089-125. doi: 10.1152/physrev.1999.79.4.1089. PMID: 10508230.
10. Moore ED, Becker PL, Fogarty KE, Williams DA, Fay FS. Ca²⁺ imaging in single living cells: theoretical and practical issues. *Cell Calcium.* 1990 Feb-Mar;11(2-3):157-79. doi: 10.1016/0143-4160(90)90068-6. PMID: 2191780.
11. Hyrc KL, Rzeszotnik Z, Kennedy BR, Goldberg MP. Determining calcium concentration in heterogeneous model systems using multiple indicators. *Cell Calcium.* 2007 Dec;42(6):576-89. doi: 10.1016/j.ceca.2007.02.002. Epub 2007 Mar 21. PMID: 17376527; PMCID: PMC7343377.
12. Grynkiewicz G, Poenie M, Tsien RY. A new generation of Ca²⁺ indicators with greatly improved fluorescence properties. *J Biol Chem.* 1985 Mar 25;260(6):3440-50. PMID: 3838314.
13. Bootman MD, Rietdorf K, Collins T, Walker S, Sanderson M. Ca²⁺-sensitive fluorescent dyes and intracellular Ca²⁺ imaging. *Cold Spring Harb Protoc.* 2013 Feb 1;2013(2):83-99. doi: 10.1101/pdb.top066050. PMID: 23378644.
14. Nakai J, Ohkura M, Imoto K. A high signal-to-noise Ca(2+) probe composed of a single green fluorescent protein. *Nat Biotechnol.* 2001 Feb;19(2):137-41. doi: 10.1038/84397. PMID: 11175727.

15. Nagai T, Sawano A, Park ES, Miyawaki A. Circularly permuted green fluorescent proteins engineered to sense Ca²⁺. *Proc Natl Acad Sci U S A*. 2001 Mar 13;98(6):3197-202. doi: 10.1073/pnas.051636098. Epub 2001 Mar 6. PMID: 11248055; PMCID: PMC30630.
16. Baird GS, Zacharias DA, Tsien RY. Circular permutation and receptor insertion within green fluorescent proteins. *Proc Natl Acad Sci U S A*. 1999 Sep 28;96(20):11241-6. doi: 10.1073/pnas.96.20.11241. PMID: 10500161; PMCID: PMC18018.
17. Miyawaki A, Llopis J, Heim R, McCaffery JM, Adams JA, Ikura M, Tsien RY. Fluorescent indicators for Ca²⁺ based on green fluorescent proteins and calmodulin. *Nature*. 1997 Aug 28;388(6645):882-7. doi: 10.1038/42264. PMID: 9278050.
18. Bayley PM, Findlay WA, Martin SR. Target recognition by calmodulin: dissecting the kinetics and affinity of interaction using short peptide sequences. *Protein Sci*. 1996 Jul;5(7):1215-28. doi: 10.1002/pro.5560050701. PMID: 8819155; PMCID: PMC2143466.
19. Chen TW, Wardill TJ, Sun Y, Pulver SR, Renninger SL, Baohan A, Schreiter ER, Kerr RA, Orger MB, Jayaraman V, Looger LL, Svoboda K, Kim DS. Ultrasensitive fluorescent proteins for imaging neuronal activity. *Nature*. 2013 Jul 18;499(7458):295-300. doi: 10.1038/nature12354. PMID: 23868258; PMCID: PMC3777791.
20. Ohkura M, Sasaki T, Sadakari J, Gengyo-Ando K, Kagawa-Nagamura Y, Kobayashi C, Ikegaya Y, Nakai J. Genetically encoded green fluorescent Ca²⁺ indicators with improved detectability for neuronal Ca²⁺ signals. *PLoS One*. 2012;7(12):e51286. doi: 10.1371/journal.pone.0051286. Epub 2012 Dec 11. PMID: 23240011; PMCID: PMC3519846.
21. Boehning D, Patterson RL, Sedaghat L, Glebova NO, Kurosaki T, Snyder SH. Cytochrome c binds to inositol (1,4,5) trisphosphate receptors, amplifying calcium-dependent apoptosis. *Nat Cell Biol*. 2003 Dec;5(12):1051-61. doi: 10.1038/ncb1063. Epub 2003 Nov 9. Erratum in: *Nat Cell Biol*. 2004 Jan;6(1):77. PMID: 14608362.
22. Kapuscinski J. DAPI: a DNA-specific fluorescent probe. *Biotech Histochem*. 1995 Sep;70(5):220-33. doi: 10.3109/10520299509108199. PMID: 8580206.
23. Elliott AD. Confocal Microscopy: Principles and Modern Practices. *Curr Protoc Cytom*. 2020 Mar;92(1):e68. doi: 10.1002/cpcy.68. PMID: 31876974; PMCID: PMC6961134.
24. Ceriani, F.; Ciubotaru, C.D.; Bortolozzi, M.; Mammano, F. Design and Construction of a Cost-Effective Spinning Disk System for Live Imaging of Inner Ear Tissue. *Methods Mol. Biol*. 2016, 1427, 223–241
25. Benninger RKP, Piston DW. Two-photon excitation microscopy for the study of living cells and tissues. *Curr Protoc Cell Biol*. 2013 Jun;Chapter 4:4.11.1-4.11.24. doi: 10.1002/0471143030.cb0411s59. PMID: 23728746; PMCID: PMC4004770.
26. Mammano, Fabio & Bortolozzi, Mario. (2009). Ca²⁺ Imaging: Principles of Analysis and Enhancement. 10.1007/978-1-60761-476-0_3.

(This page is intentionally left blank)

3 MATHEMATICAL MODEL

3.1 Introduction

Cellular dynamics refers to any process or observable that changes over time. Living cells are inherently dynamic. Indeed, to sustain the characteristic features of life, cells must continually extract energy from their surroundings. This requires that cells function thermodynamically as open systems that are far from static thermal equilibrium. Much energy is used by cells in the maintenance of gradient of ions. These processes are dynamic due to the continuous movement of ionic and molecular species across the cell membrane [1]. In the physical sciences, theoretical methods in combination with experimental measurements have provided rich insights into dynamical phenomena.

As it mentioned in chapter 1, intracellular Ca^{2+} levels can be modulated by a large variety of mechanisms, which include Ca^{2+} influx from the extracellular space or release from various intracellular stores [2-5].

In this chapter, based on experimental results we obtain for individual cell for all different experiments, a mathematical model of Ca^{2+} dynamics to show and explain that complex responses were developed [6].

3.2 Regulation of cytosolic Ca^{2+}

The cell is described as compartments with different concentrations of important constituents using ordinary differential equations. The spatial distribution of these constituents inside each compartment is assumed to be uniform at all times [7-9]. Considering that a realistic model of cytosolic Ca^{2+} dynamics (figure 3.1) should involve several actors influencing intracellular Ca^{2+} concentration in time and space, e.g. pumps, channels and receptors, the continuity equation for cytosolic Ca^{2+} was written by:

$$\frac{d[\text{Ca}^{2+}]}{dt} = f(J_{IP3R} + J_{leak} - J_{SERCA} - J_{PMCA} + J_{HC} + m) \quad (3.1)$$

where f stands for fraction of free Ca^{2+} . Since most of Ca^{2+} inside the cell are bound (buffer or proteins), this value is a small number. In above equation, J_s represent fluxes for:

- J_{IP3R} IP_3 – dependent Ca^{2+} flux from ER to cytosol through IP_3R
- J_{leak} IP_3 -independent Ca^{2+} flux from ER to cytosol

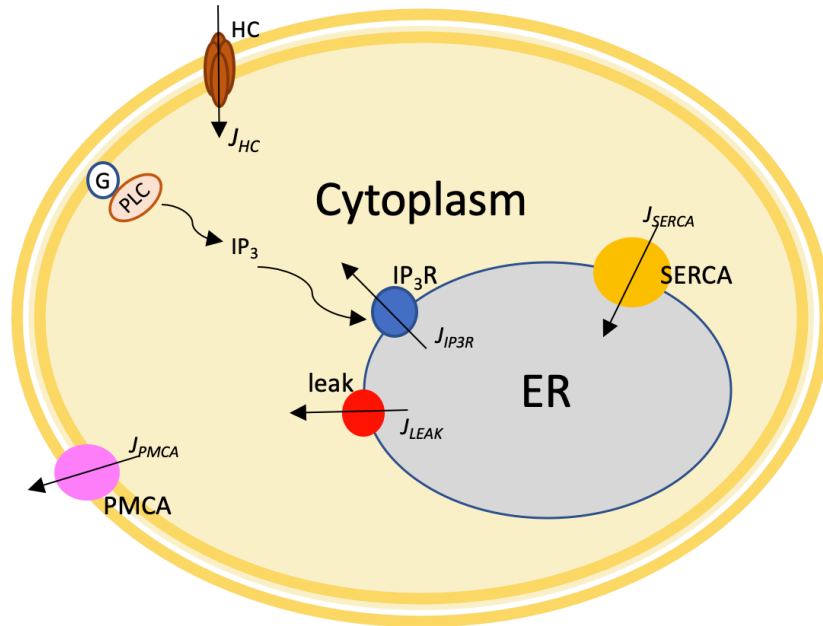


Figure 3.1 Components of computational model. Letter Js indicate fluxes. Other components are ER (endoplasmic reticulum), PLC (phospholipase C), HC (hemichannel), PMCA (plasma membrane Ca^{2+} ATPase), SERCA (sarco-/endoplasmic reticulum), and IP_3R (IP_3 receptor).

- J_{SERCA} is flux from cytosol to ER due to uptake by SERCA
- J_{PMCA} is the Ca^{2+} flux from cytosol to extracellular milieu due to PMCA pump
- J_{HC} flux of Ca^{2+} through the HC
- m influx of Ca^{2+} (non-modelled fluxes/ leakage) from outside of the cell (it is assumed to be constant because the extracellular Ca^{2+} concentration is much larger than outside compared to inside the cell).

In many cells, increases in cytosolic Ca^{2+} concentration can be due to, at least in part, the release of Ca^{2+} from internal stores such as ER. Associated with this membrane network are pumps for Ca^{2+} uptake, Ca^{2+} binding proteins for Ca^{2+} storage and channels for Ca^{2+} release [9]. In our model dynamic of Ca^{2+} concentration in ER was expressed as:

$$\frac{d[Ca^{2+}]_{ER}}{dt} = \alpha (J_{SERCA} - J_{IP3R} - J_{Leak}) \quad (3.2)$$

in which $[Ca^{2+}]_{ER}$ stands for Ca^{2+} concentration in ER, and α is for ratio between cytosolic and ER volumes [11,12].

A basic property of IP_3R is they respond in a time-dependent manner to the changes of Ca^{2+} or IP_3 . To consider this, change of concentration of IP_3 in cell was described by:

$$\frac{d[IP_3]}{dt} = \frac{V_{max} [Ca^{2+}]_{ex}}{[Ca^{2+}]_{ex} + k_m} - (k_{IP_3} \times IP_3) \quad (3.3)$$

where V_{max} is the maximal rate of PLC production, k_m is ATP value for the production of PLC, and k_{IP_3} for IP_3 degradation rate. $[Ca^{2+}]_{ex}$ stands for extracellular Ca^{2+} concentration, described by:

$$[Ca^{2+}]_{ex} = \sigma + [Ca^{2+}]_f * H(t - 2000) \quad (3.4)$$

in which σ is concentration of Ca^{2+} at steady level (at the start of the experiment which was $60\mu M$), and $[Ca^{2+}]_f$ is final Ca^{2+} concentration which was aimed to achieve by adding the bolus. $H(x)$ is Heaviside function which is zero for $x < 0$, and equal to unity for $x > 0$. We ran the simulation for 2000s to get steady state of Ca^{2+} which then it was used as the start point for rest of simulation.

The Ca^{2+} outflow from ER to cytosol through IP_3R channels, so, for J_{IP_3R} following expression was used:

$$J_{IP_3R} = k_{IP_3R} \left(\frac{[IP_3]}{[IP_3] + k_i} \right)^3 \left(\frac{[Ca^{2+}]}{[Ca^{2+}] + k_a} \right)^3 h^3 ([Ca^{2+}]_{ER} - [Ca^{2+}]) \quad (3.5)$$

where k_{IP_3R} is maximal IP_3R release rate, k_i and k_a are for Li-Rinzel model parameter for IP_3 receptor activation by IP_3 and Ca^{2+} , respectively [13]. The second and third term in above formula indicate the probability of activated subunits [14]. In fact, IP_3 is not the only regulator of IP_3R function; Ca^{2+} itself is an allosteric modulator of the IP_3R and plays a critical role in shaping the IP_3R -evoked Ca^{2+} response. In general, this regulation follows a biphasic bell-shaped curve for all subtypes, such that low Ca^{2+} concentrations (< 300 nM) activate the channel and increase its open probability, whereas high Ca^{2+} concentrations inhibit channel opening [15,16]. In above formula, inactivation of IP_3R , indicated by h , and is expressed by:

$$\frac{dh}{dt} = \eta (k_d - ([Ca^{2+}] + k_a) h) \quad (3.6)$$

where k_d and η are Li-Rinzel model parameters for IP₃R inactivation by IP₃ and Ca²⁺, respectively. In whole cell model we generally use empirical, Hill-type formula for pump rate. SERCA pumps transport Ca²⁺ into ER, so the flux from cytosol to ER was defined as:

$$J_{SERCA} = \frac{V_{SERCA} [Ca^{2+}]^2}{[Ca^{2+}]^2 + k_{SERCA}^2} \quad (3.7)$$

The maximal pump rate V_{SERCA} is proportional to the total number of SERCA and to the rate of a single pump, and is typically expressed here in $\mu\text{M/s}$.

The presence of the ER leak channel is inferred from the passive release of ER Ca²⁺ upon blocking the counterbalancing SERCA pumps with compounds such as thapsigargin or cyclopiazonic acid (CPA) [17-20]. Ca²⁺ leaks from the ER are driven by concentration gradients between the ER and cytosol. The leak flux from ER to cytosol is given by:

$$J_{Leak} = L \cdot ([Ca^{2+}]_{ER} - [Ca^{2+}]) \quad (3.8)$$

where L shows leak rate, and thermodynamic driving force for a symmetric channel is representing by variables in the parenthesis. As we see from this equation, there is no contribution of membrane potential to ER driving force. It is generally, though not universally, believed that there is no significant ER membrane potential because of counterions that balance the fluxes of Ca²⁺.

PMCA functions to pump out Ca²⁺ from cytosol to extracellular milieu, so, J_{PMCA} was written as

$$J_{PMCA} = \frac{V_{PMCA} [Ca^{2+}]}{[Ca^{2+}] + k_{PMCA}} \quad (3.9)$$

where V_{PMCA} is the maximum PMCA current, and k_{PMCA} is the Ca²⁺ concentration for the half activation of PMCA channels.

To make model results more similar to experimental one, we used

$$Fluo = f_{max} \frac{[Ca^{2+}]}{k_f + [Ca^{2+}]} \quad (3.10)$$

for fluorescent signal as a non-linear function of Ca²⁺.

3.3 Hemichannel model

To account for the experimentally determined bell-shaped dependence of probability of HC on cytosolic free Ca^{2+} concentration, we formulated the four-state model described in figure 3.2 [21,22]. Each subunit, activating binding sites and an inhibitory site were indicated by $i=0,1$ and $j=0,1$. The rate of Ca^{2+} binding to the activation site was assumed to be independent of Ca^{2+} at the inactivating site, and vice versa: the channel is open if Ca^{2+} is bound to the activating site and not to the inactivating site (state $S_{1,0}$).

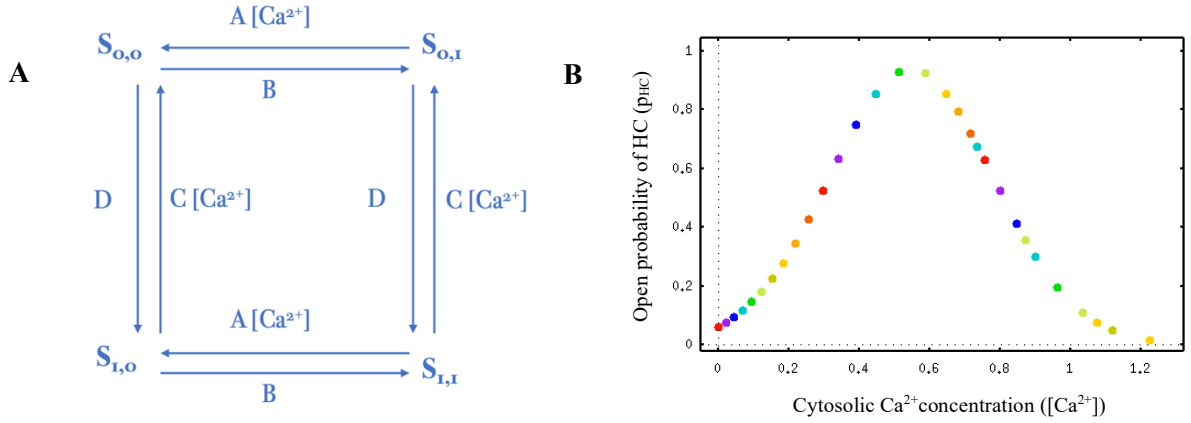


Figure 3.2 HC model (A) Four-states model of a Cx HC (B) HC open probability as a function of $[Ca^{2+}]$

Consequently, denoting the fraction of channel subunits with x_{ij} in the state $S_{i,j}$, the equivalent set of equations are:

$$\frac{dx_{0,0}}{dt} = -(A \cdot [Ca^{2+}] \cdot x_{0,0}) + (B \cdot x_{0,1}) - (C \cdot [Ca^{2+}] \cdot x_{0,0}) + (D \cdot x_{1,0}) \quad (3.11)$$

$$\frac{dx_{1,0}}{dt} = -(A \cdot [Ca^{2+}] \cdot x_{1,0}) + (B \cdot x_{1,1}) + (C \cdot [Ca^{2+}] \cdot x_{0,0}) - (D \cdot x_{1,0}) \quad (3.12)$$

$$\frac{dx_{0,1}}{dt} = (A \cdot [Ca^{2+}] \cdot x_{0,0}) - (B \cdot x_{0,1}) - (C \cdot [Ca^{2+}] \cdot x_{0,1}) + (D \cdot x_{1,1}) \quad (3.13)$$

$$x_{1,1} = 1 - (x_{0,0} + x_{1,0} + x_{0,1}) \quad (3.14)$$

and the open probability is given by

$$p_{HC} = \beta \cdot (x_{1,0})^y \quad (3.15)$$

where β is a normalization constant, and γ is a constant of the HC model. Using above formula, we expressed flux of Ca^{2+} through HC by

$$J_{HC} = p_{HC} \cdot ([\text{Ca}^{2+}]_{ex} - [\text{Ca}^{2+}]) \quad (3.16)$$

The model is compartmental and uses ordinary differential equations. The tools used in constructing this model were XPPAUT. Model parameter were used are listed in table 3.1 and 3.2.

Table 3.1 Cytosolic Ca^{2+} model parameters

Parameter	Unit	Value	Description	Source
f	-	0.0009	Fraction of free Ca^{2+}	simulation
V_{max}	$\mu\text{M} \cdot \text{s}^{-1}$	0.02	Maximal rate of PLC production	simulation
k_m	μM	5000.05	ATP value for PLC production	simulation
k_{IP_3}	s^{-1}	0.003	IP_3 degradation rate	simulation
η	$\mu\text{M}^{-1} \cdot \text{s}^{-1}$	0.02	Li-Rinzel model parameters for IP_3R inactivation by Ca^{2+}	simulation
k_d	μM	0.02	Li-Rinzel model parameters for IP_3R inactivation by IP_3	simulation
k_{IP_3R}	$\mu\text{M} \cdot \text{s}^{-1}$	3000	Maximal IP_3R release rate	simulation
k_i	μM	0.1	Li-Rinzel model parameter for IP_3R activation by IP_3	simulation
k_a	μM	0.4	Li-Rinzel model parameter for IP_3R activation by Ca^{2+}	Ref.[23]
L	s^{-1}	0.01	Leak rate	simulation
V_{SERCA}	$\mu\text{M} \cdot \text{s}^{-1}$	60	Maximal SERCA pump rate	simulation
k_{SERCA}	μM	0.2	Ca^{2+} affinity of SERCA pumps	Ref.[23]
α	-	0.47	Ratio between cytosolic and ER volumes	simulation
V_{PMCA}	$\mu\text{M} \cdot \text{s}^{-1}$	35	Maximum PMCA current	simulation
k_{PMCA}	μM	0.25	Affinity of PMCA pumps	simulation
m	$\mu\text{M} \cdot \text{s}^{-1}$	7	Ca^{2+} flux from outside of the cell	simulation
σ	μM	60	Ca^{2+} concentration at equilibrium	Ref.[6]
f_{max}	-	0.97	Maximal fluorescence signal	simulation
k_f	-	0.65	Affinity constant	simulation

Table 3.2 HC model parameters

Parameter	Unit	Value	Description	Source
β	-	23E8	Normalization constant	simulation
γ	-	9	Constant of HC model	Ref.[22]
A	$\mu\text{M}^{-1} \cdot \text{s}^{-1}$	1.08	HC model parameter	simulation
B	s^{-1}	0.11	HC model parameter	simulation
C	$\mu\text{M}^{-1} \cdot \text{s}^{-1}$	0.014	HC model parameter	simulation
D	s^{-1}	0.011	HC model parameter	simulation

3.4 References

1. Christopher P. Fall, Eric S. Marland, John M. Wagner, John J. Tyson. Computational cell biology, Springer New York, NY, ISBN 978-0-387-95369-4 Published: 09 July 2002
2. Alonso MT, Manjarrés IM, García-Sancho J. Modulation of calcium signalling by intracellular organelles seen with targeted aequorins. *Acta Physiol (Oxf)*. 2009 Jan;195(1):37-49. doi: 10.1111/j.1748-1716.2008.01920.x. Epub 2008 Oct 28. PMID: 18983457.
3. Papp B, Launay S, Gélébart P, Arbabian A, Enyedi A, Brouland JP, Carosella ED, Adle-Biassette H. Endoplasmic Reticulum Calcium Pumps and Tumor Cell Differentiation. *Int J Mol Sci*. 2020 May 9;21(9):3351. doi: 10.3390/ijms21093351. PMID: 32397400; PMCID: PMC7247589.
4. Sharma, A.; Ramena, G.T.; Elble, R.C. Advances in Intracellular Calcium Signaling Reveal Untapped Targets for Cancer Therapy. *Biomedicines* 2021, 9, 1077. <https://doi.org/10.3390/biomedicines9091077>
5. Putney JW Jr.. Ca²⁺ Stores and Ca²⁺ Pools. In: Siegel GJ, Agranoff BW, Albers RW, et al., editors. *Basic Neurochemistry: Molecular, Cellular and Medical Aspects*. 6th edition. Philadelphia: Lippincott-Raven; 1999.
6. Nardin C, Tettey-Matey A, Donati V, Marazziti D, Di Pietro C, Peres C, Raspa M, Zonta F, Yang G, Gorelik M, Singh S, Cardarelli L, Sidhu SS, Mammano F. A Quantitative Assay for Ca²⁺ Uptake through Normal and Pathological Hemichannels. *Int J Mol Sci*. 2022 Jun 30;23(13):7337. doi: 10.3390/ijms23137337. PMID: 35806342; PMCID: PMC9266989.
7. Martin Falcke. Reading the patterns in living cells —the physics of ca²⁺ signaling, *Advances in Physics*. 2004, 53:3, 255-440
8. Baker HL, Errington RJ, Davies SC, Campbell AK. A mathematical model predicts that calreticulin interacts with the endoplasmic reticulum Ca(2+)-ATPase. *Biophys J*. 2002 Feb;82(2):582-90. doi: 10.1016/S0006-3495(02)75423-4. PMID: 11806903; PMCID: PMC1301870.
9. K. Hallé n, M. Huss, P. Kettunen, A. El Manira, J. Hellgren Kotaleski, mGluR-mediated calcium oscillations in the lamprey: a computational model, *Neurocomputing* 58–60 (2004) 431.
10. Meldolesi J, Pozzan T. The endoplasmic reticulum Ca²⁺ store: a view from the lumen. *Trends Biochem Sci*. 1998 Jan;23(1):10-4. doi: 10.1016/s0968-0004(97)01143-2. PMID: 9478128.
11. Solovyova N, Veselovsky N, Toescu EC, Verkhratsky A. Ca(2+) dynamics in the lumen of the endoplasmic reticulum in sensory neurons: direct visualization of Ca(2+)-induced Ca(2+) release triggered by physiological Ca(2+) entry. *EMBO J*. 2002 Feb 15;21(4):622-30. doi: 10.1093/emboj/21.4.622. PMID: 11847110; PMCID: PMC125857.
12. Stutzmann GE, Mattson MP. Endoplasmic reticulum Ca(2+) handling in excitable cells in health and disease. *Pharmacol Rev*. 2011 Sep;63(3):700-27. doi: 10.1124/pr.110.003814. Epub 2011 Jul 7. PMID: 21737534; PMCID: PMC3141879.
13. Li YX, Rinzel J. Equations for InsP3 receptor-mediated [Ca²⁺]_i oscillations derived from a detailed kinetic model: a Hodgkin-Huxley like formalism. *J Theor Biol*. 1994 Feb 21;166(4):461-73. doi: 10.1006/jtbi.1994.1041. PMID: 8176949.
14. Sun, M.; Li, Y.; Yao, W. A Dynamic Model of Cytosolic Calcium Concentration Oscillations in Mast Cells. *Mathematics* 2021, 9, 2322.
15. Thrower EC, Hagar RE, Ehrlich BE. Regulation of Ins(1,4,5)P3 receptor isoforms by endogenous modulators. *Trends Pharmacol Sci*. 2001 Nov;22(11):580-6. doi: 10.1016/s0165-6147(00)01809-5. PMID: 11698102.

16. Foskett JK, White C, Cheung KH, Mak DO. Inositol trisphosphate receptor Ca²⁺ release channels. *Physiol Rev.* 2007 Apr;87(2):593-658. doi: 10.1152/physrev.00035.2006. PMID: 17429043; PMCID: PMC2901638.
17. Flourakis M, Van Coppenolle F, Lehen'kyi V, Beck B, Skryma R, Prevarskaya N. Passive calcium leak via translocon is a first step for iPLA₂-pathway regulated store operated channels activation. *FASEB J.* 2006 Jun;20(8):1215-7. doi: 10.1096/fj.05-5254fje. Epub 2006 Apr 12. PMID: 16611832.
18. Camello C, Lomax R, Petersen OH, Tepikin AV. Calcium leak from intracellular stores--the enigma of calcium signalling. *Cell Calcium.* 2002 Nov-Dec;32(5-6):355-61. doi: 10.1016/s0143416002001926. PMID: 12543095.
19. Tu H, Nelson O, Bezprozvanny A, Wang Z, Lee SF, Hao YH, Serneels L, De Strooper B, Yu G, Bezprozvanny I. Presenilins form ER Ca²⁺ leak channels, a function disrupted by familial Alzheimer's disease-linked mutations. *Cell.* 2006 Sep 8;126(5):981-93. doi: 10.1016/j.cell.2006.06.059. PMID: 16959576; PMCID: PMC3241869.
20. Vanden Abeele F, Bidaux G, Gordienko D, Beck B, Panchin YV, Baranova AV, Ivanov DV, Skryma R, Prevarskaya N. Functional implications of calcium permeability of the channel formed by pannexin 1. *J Cell Biol.* 2006 Aug 14;174(4):535-46. doi: 10.1083/jcb.200601115. Erratum in: *J Cell Biol.* 2013 May 27;201(5):777. PMID: 16908669; PMCID: PMC2064259.
21. Snipas M, Kraujalis T, Maciunas K, Kraujaliene L, Gudaitis L, Verselis VK. Four-State Model for Simulating Kinetic and Steady-State Voltage-Dependent Gating of Gap Junctions. *Biophys J.* 2020 Oct 20;119(8):1640-1655. doi: 10.1016/j.bpj.2020.08.032. Epub 2020 Sep 2. PMID: 32950074; PMCID: PMC7642245.
22. Ceriani F, Pozzan T, Mammano F. Critical role of ATP-induced ATP release for Ca²⁺ signaling in nonsensory cell networks of the developing cochlea. *Proc Natl Acad Sci U S A.* 2016 Nov 15;113(46):E7194-E7201. doi: 10.1073/pnas.1616061113. Epub 2016 Nov 2. PMID: 27807138; PMCID: PMC5135323.
23. Donati V, Peres C, Nardin C, Scavizzi F, Raspa M, Ciubotaru CD, Bortolozzi M, Pedersen MG, Mammano F. Calcium Signaling in the Photodamaged Skin: In Vivo Experiments and Mathematical Modeling. *Function (Oxf).* 2021 Dec 1;3(1):zqab064. doi: 10.1093/function/zqab064.

(This page is intentionally left blank)

4 RESULTS AND DISCUSSION

4.1 Results

The simulation was performed to show both conditions studied experimentally, namely with and without usage of HC blockers [1]. The results for HC without blocker for different final Ca^{2+} concentrations are shown in figure (4.1).

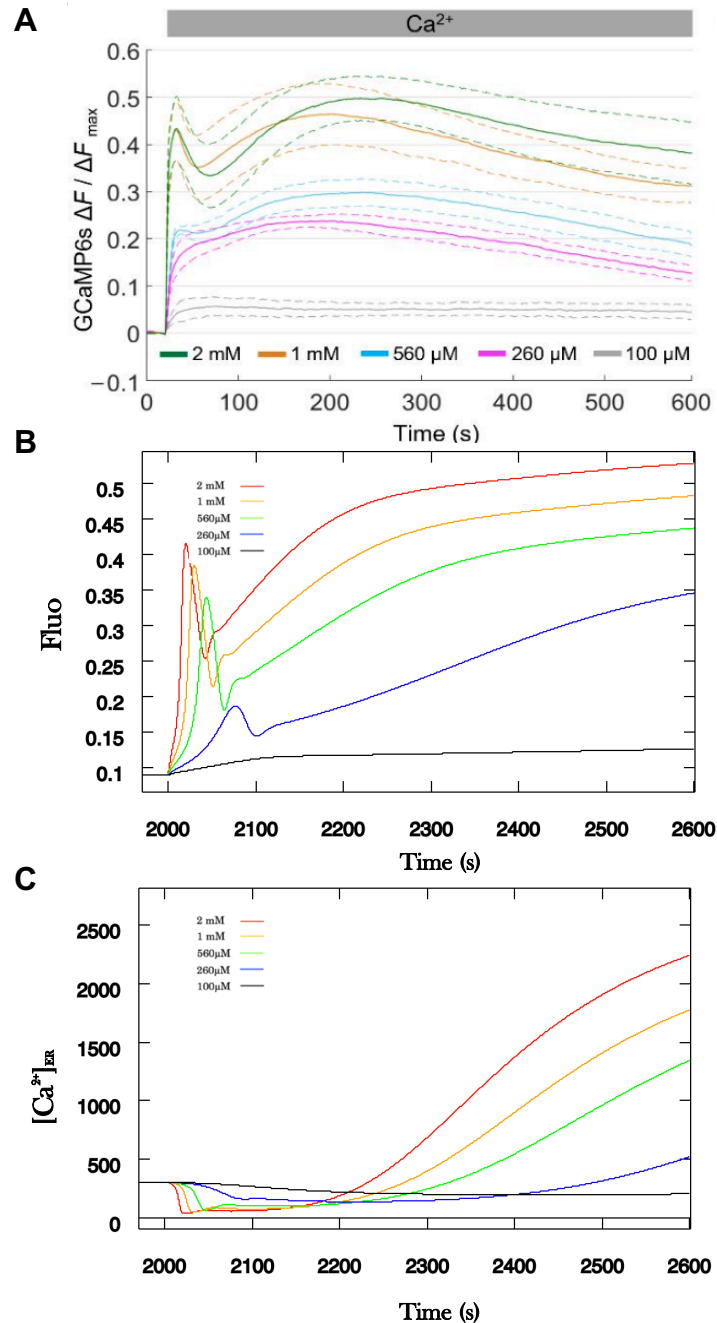


Figure 4.1 Simulation results for HC without blocker. (A) the experimental results of mean Ca^{2+} uptake traces (solid line) \pm s.e.m (dashed line) obtained in HaCaT-Cx26-GCaMP6s. (B) fluorescence signal (fluo) as a function of time. (C) concentration of Ca^{2+} in ER as a function of time.

In case of HC with blocker, which we considered the blocker could inhibit flux through the channel by factor of 90% with respect to the case that HC without blocker, the simulation results obtained for all experiments are depicted in figure (4.2).

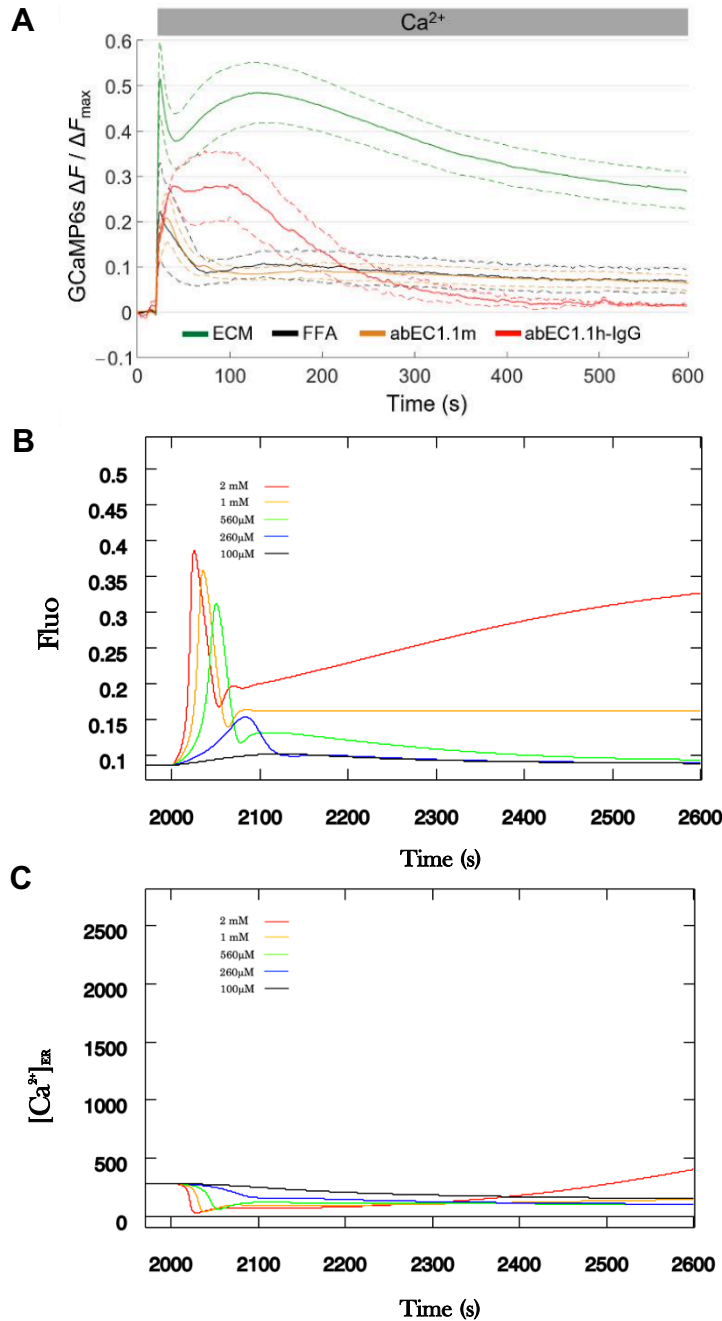
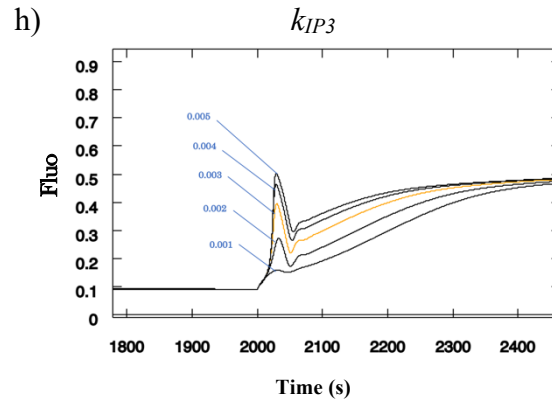
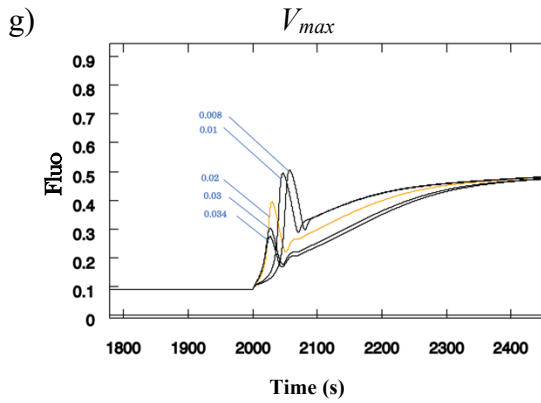
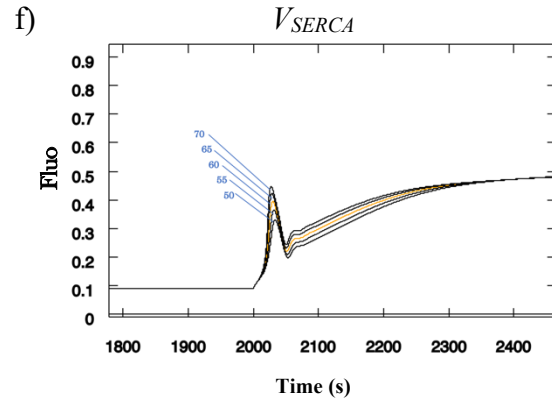
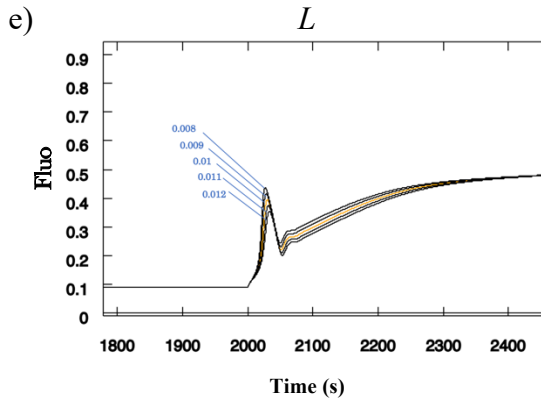
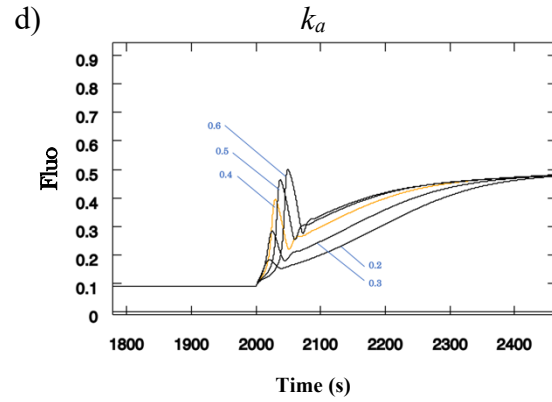
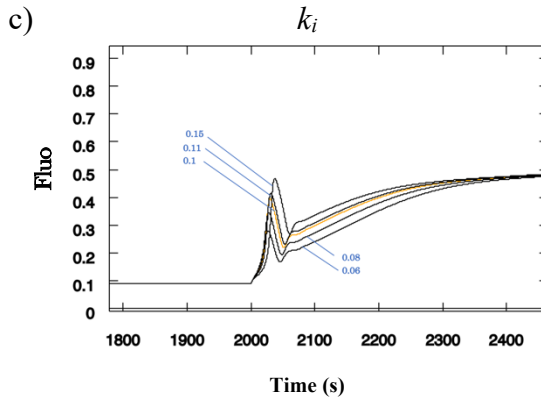
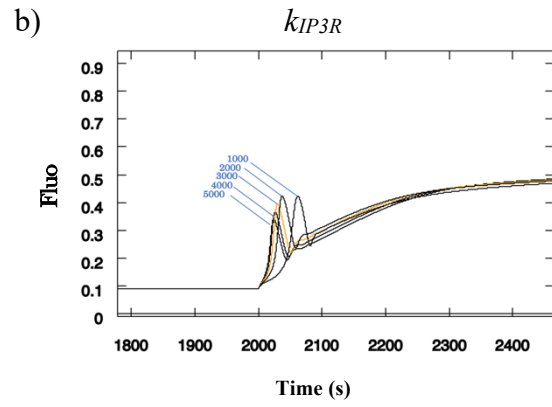
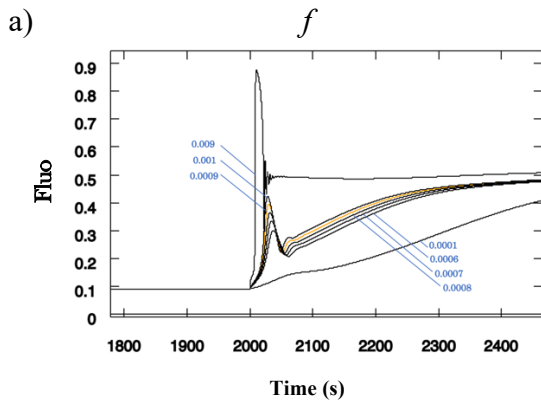


Figure 4.1 Simulation results for HC with blocker. (A) the experimental results of mean Ca²⁺ uptake traces (solid line) \pm s.e.m (dashed line) obtained in HaCaT-Cx26-GCaMP6s. (B) fluorescence signal as a function of time. (C) concentration of Ca²⁺ in ER as a function of time.

To analyze which model's parameters were contributed to form the traces, and could massively influence them, all parameters listed in chapter 3 were checked by increasing and decreasing their values. The Simulation results are shown in figure (4.3) and (4.4)..



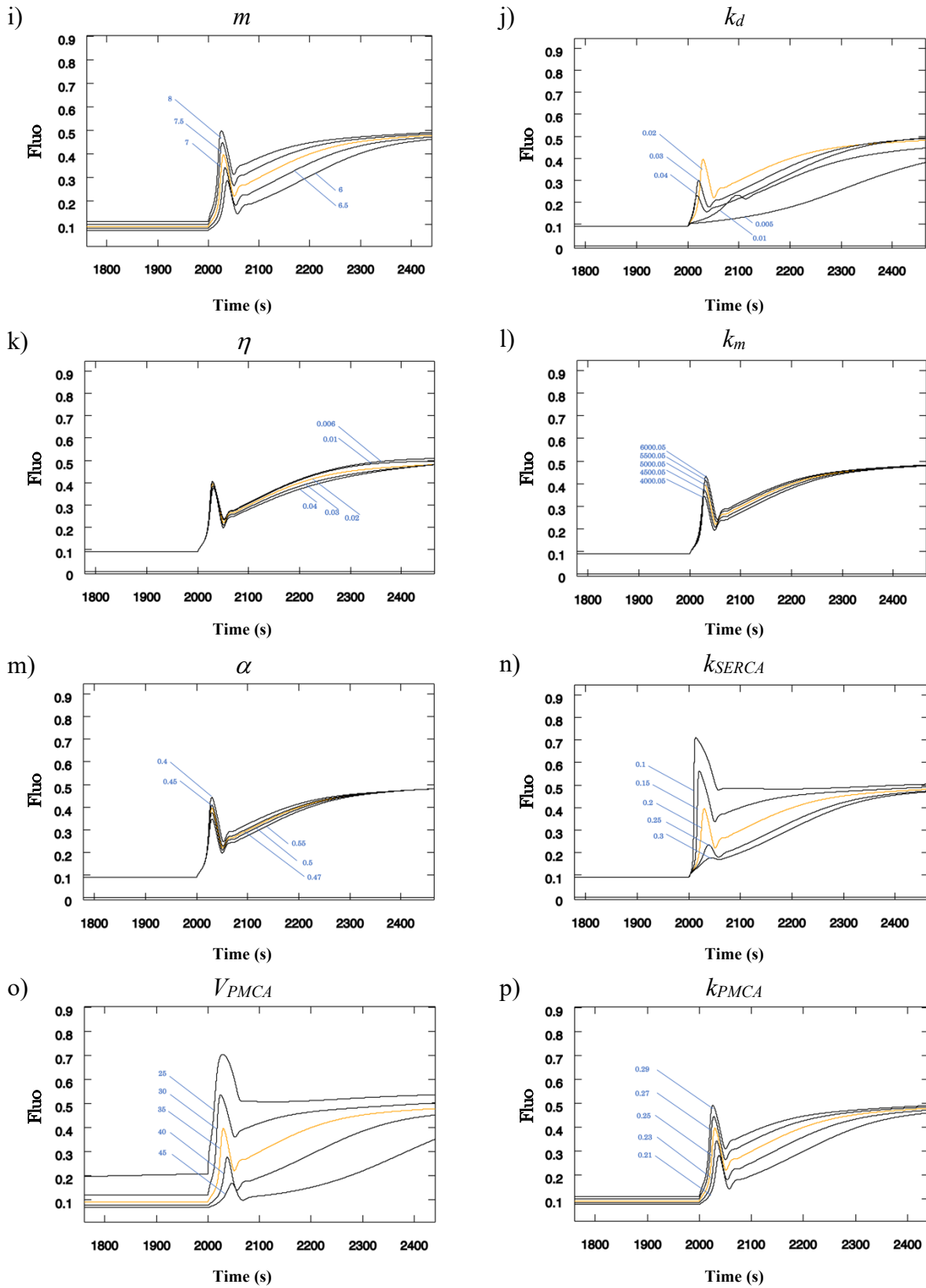
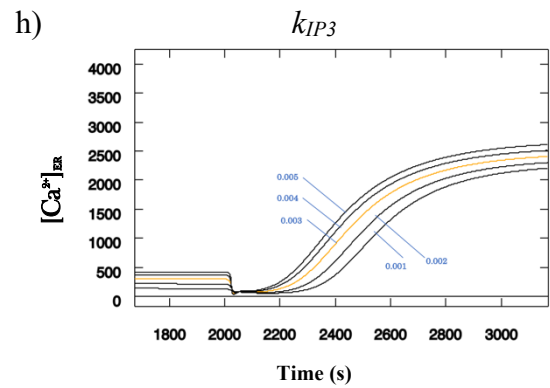
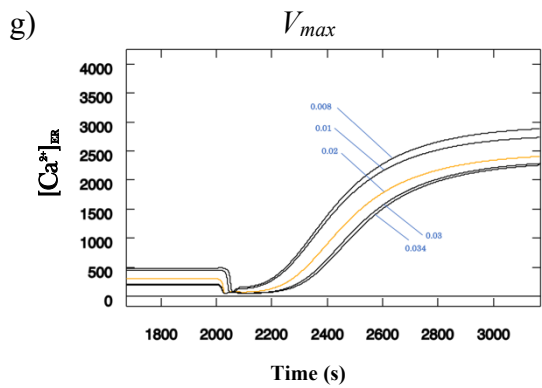
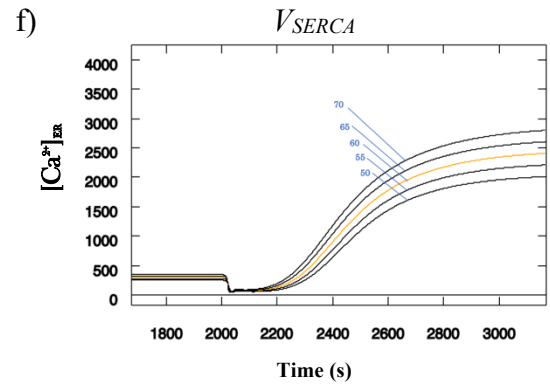
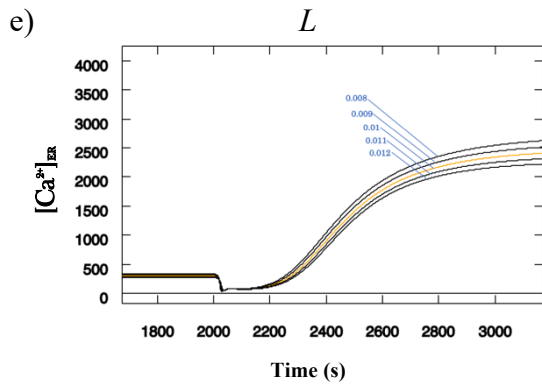
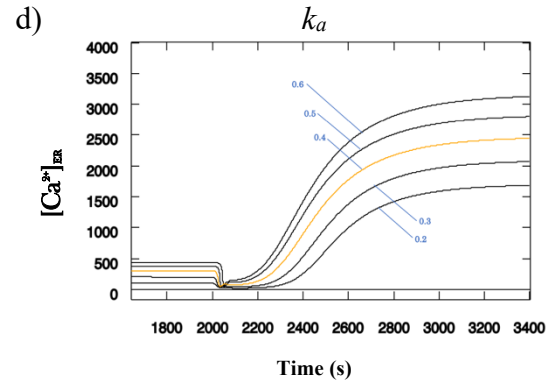
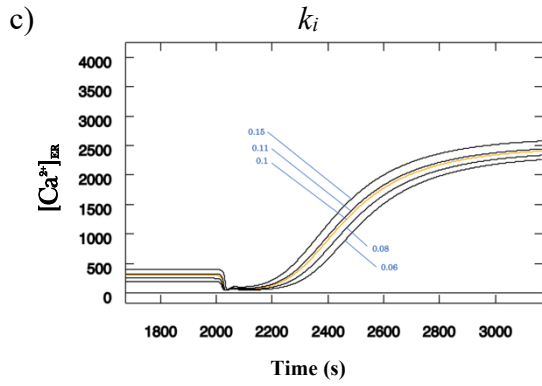
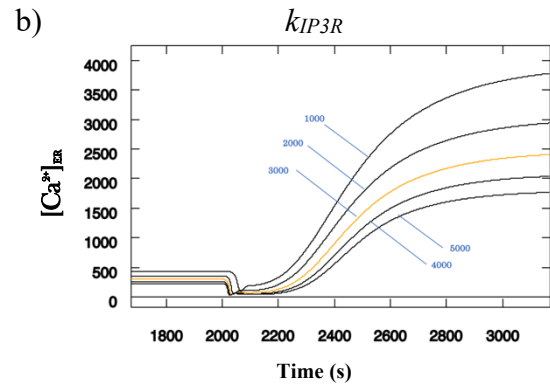
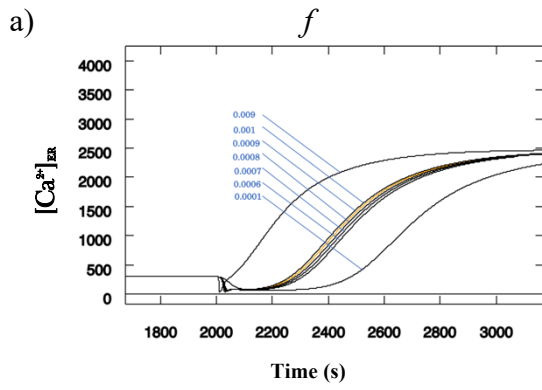


Figure 4.3 Simulation results for fluorescence signal as a function of time for changing individual parameter. For all figures are for HC open (without blocker) case with final Ca^{2+} concentration 1mM . Orange curve shows the result for set of control parameters, and black curves showing results when an individual parameter changed.



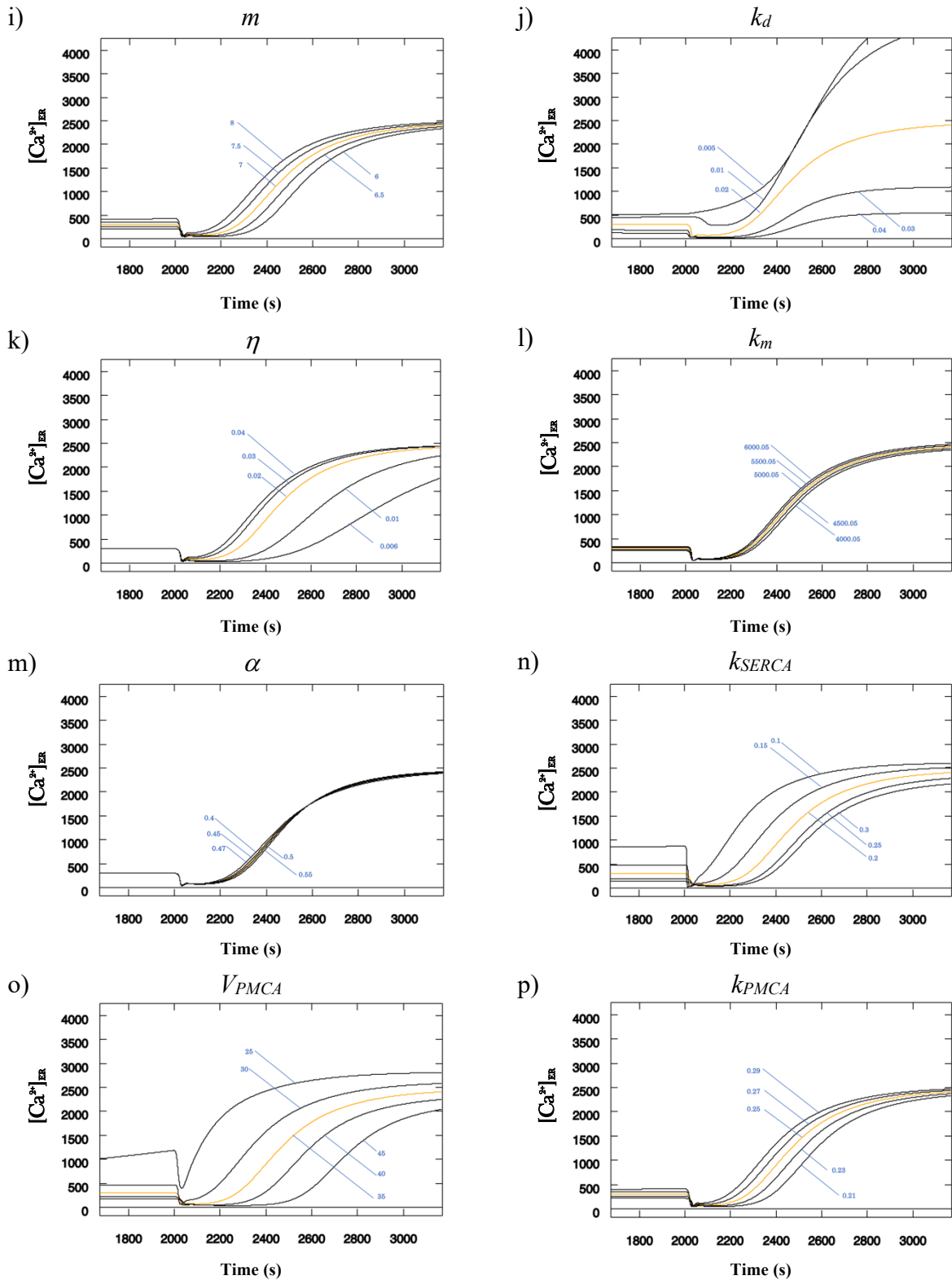


Figure 4.4 Simulation results for ER Ca^{2+} concentration as a function of time for changing individual parameter.

For all figures are for HC open (without blocker) case with final Ca^{2+} concentration 1mM . Orange curve shows the result for set of control parameters, and black curves showing results when an individual parameter changed.

we selected those parameters that were affected trace significantly, and ran the simulation for different final Ca^{2+} concentrations (all experiments). The simulation results for fluorescence signal

as a function of time and ER Ca^{2+} concentration as a function of time, for both with and without usage of HC blocker are depicted in figure (4.5) and (4.6) respectively.

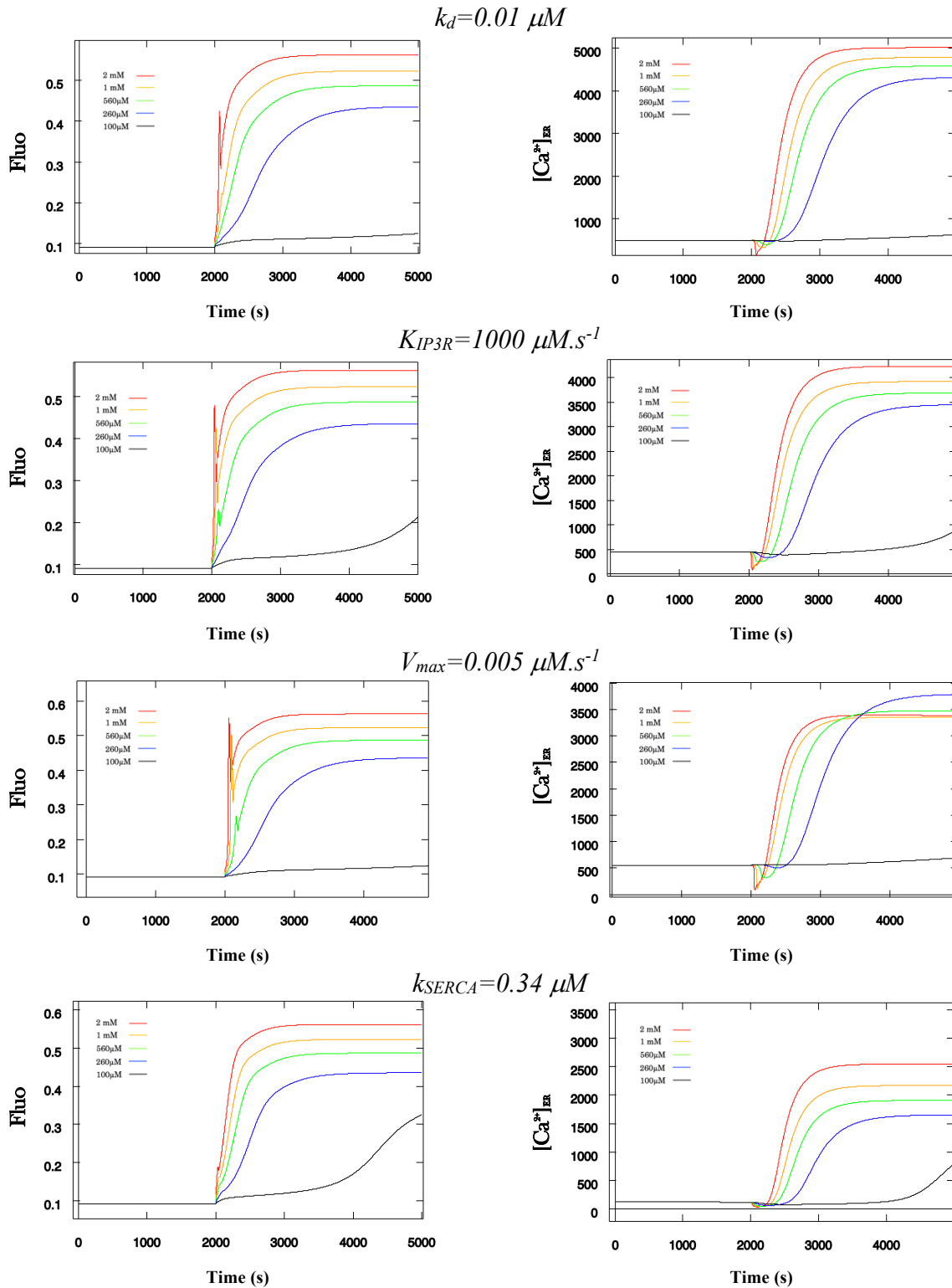


Figure 4.5 Results of different final Ca^{2+} concentrations, when HC is open for parameters with specific values. Left column shows the fluorescence signal as function of time. Right column shows the Ca^{2+} concentration in ER as a function of time.

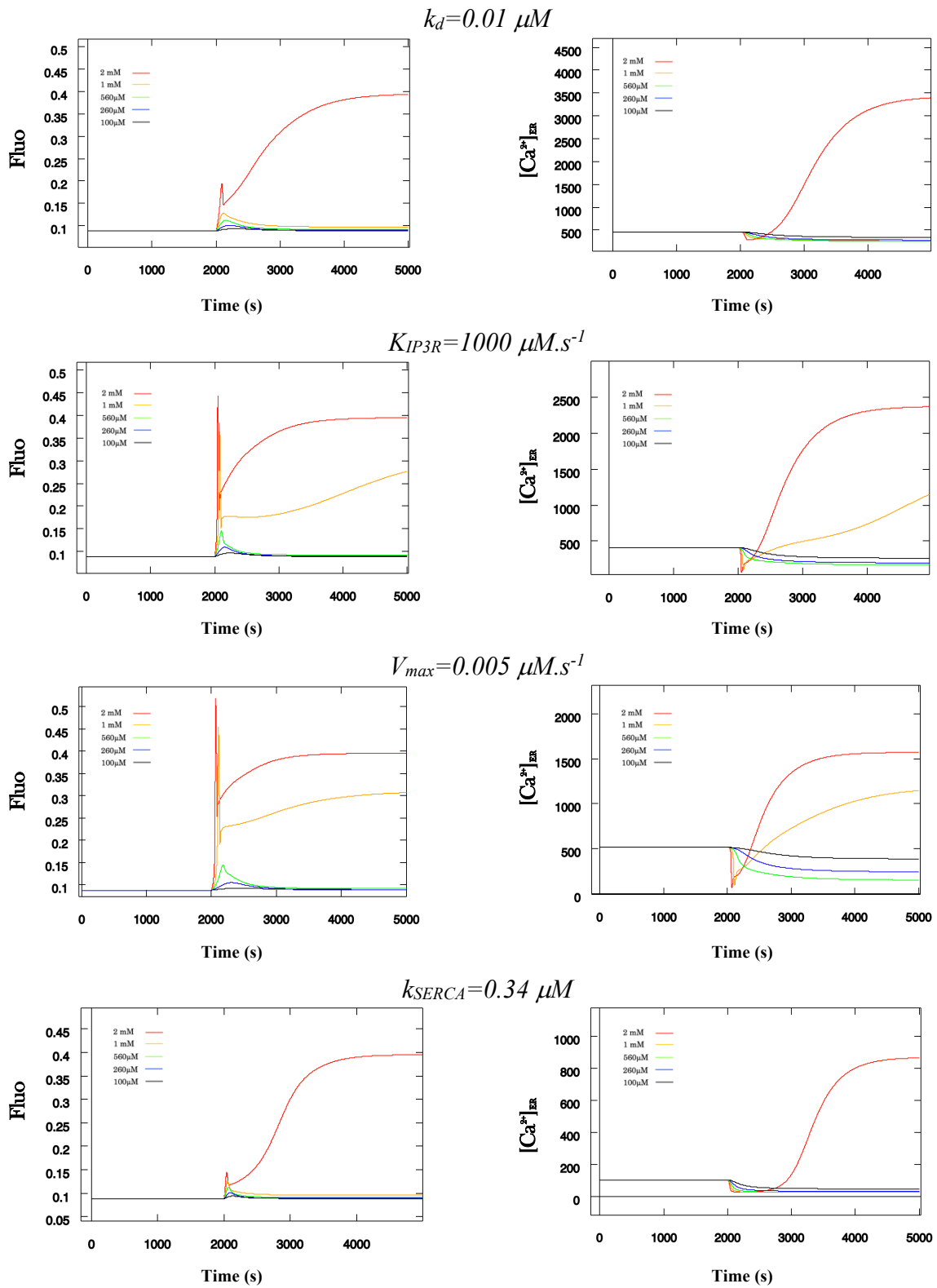


Figure 4.6 Results of different final Ca^{2+} concentrations, when HC is blocked for parameters with specific values. Left column shows the fluorescence signal as function of time. Right column shows the Ca^{2+} concentration in ER as a function of time.

4.2 Discussion

Mathematical and computational modeling of the ion channels and membrane transporters are widely acknowledged for examining each transporter's mechanism, the interactions between different transporters, estimating the changes in outcomes, reproducing and analyzing the experimental data, and predicting any new phenomena caused by membrane disorders. Mathematical models are also useful for identifying drug targets and recognizing key control points that would be useful for drug screening trials.

In current thesis work, we mathematically simulated Ca^{2+} dynamics correspond to complex responses measured experimentally by fluorescence microscopy in HaCaT cells challenged by a sudden increase of the extracellular Ca^{2+} concentration. Comparison of the results of changing different model's parameters with our control parameters for HC open are explained in follow.

It is obvious that increasing ten times in the fraction of free cytosolic Ca^{2+} makes a big increase in the Ca^{2+} level which is then followed by a decrease to half of that value and, starts oscillations for few seconds before reaching the steady level for the rest of experiment time. From ER graph for changing f , we could observe that the level of Ca^{2+} in ER were increased as the fraction of free Ca^{2+} increased. This can be due to the fact that excess of cytosolic Ca^{2+} is removed by Ca^{2+} stores in cell as well as by pumps in PM.

Changing maximal rate of IP_3R release ($k_{\text{IP}_3\text{R}}$) doesn't change the level of cytosolic Ca^{2+} markedly, however, the first spike after release of bolus of CaCl_2 was achieved with a delay for lower values of $k_{\text{IP}_3\text{R}}$. This can be explained by looking at Ca^{2+} level in ER which it shows that the high level of Ca^{2+} was achieved for low value of $k_{\text{IP}_3\text{R}}$. This means the ER is uptaking Ca^{2+} through SERCA while release of Ca^{2+} through IP_3R is slow, therefore, concentration of Ca^{2+} is high in ER.

As it mentioned in chapter 1, IP_3 is made by hydrolysis of PIP_2 by PLC. Consequently, it binds to IP_3R causes release of Ca^{2+} from ER to cytosol. From the simulation result for k_i , we observed that increasing the activation of IP_3R by IP_3 causes the increase in cytosolic Ca^{2+} level. IP_3R is activated not only by IP_3 but also by Ca^{2+} . It means that both of them should be existed sufficiently to activate IP_3R . Therefore, changing the activation of each of them results in change in cytosolic Ca^{2+} level. However, if there would be a lack of the Ca^{2+} ions in cytosol, ER will pump out Ca^{2+} via leak channel, and consequently Ca^{2+} level will start to increase and bind to IP_3R to open it and make further release of Ca^{2+} . This is what we obtained by our simulation where Ca^{2+} level in the beginning is low and as time passes the level goes high.

Considering the equation for flux on Ca^{2+} through leak channel, we know that leak rate is inversely related to the cytosolic Ca^{2+} . By looking at Ca^{2+} level in ER and cytosol as this parameter was changed, it can be clearly seen that, levels didn't change markedly. The reason would be the release of Ca^{2+} from this channel is not fast as uptake of Ca^{2+} from cytosol by SERCA and PMCA. Therefore, the level of Ca^{2+} by changing this value doesn't show significant changes in the level. Other explanation is that Ca^{2+} release from the ER does not only affect cytosolic Ca^{2+} but also can influence the concentration of the Ca^{2+} in other organelles. A prime example are the mitochondria, which can be in close apposition with the ER so that a preferential transfer of Ca^{2+} can occur from the ER to the mitochondrial matrix [2-4].

The SERCA pump uses the chemical energy produced from the conversion of ATP into ADP to transport Ca^{2+} across the membrane from the cytosol to the ER, against a concentration gradient [5,6]. From simulation results shown we didn't see change in level of Ca^{2+} in ER and cytosol as pump rate parameter changes. The reason is that when Ca^{2+} are transported into the ER through the SERCA pump, they are bound to pump proteins on the cytosolic side of the membrane. Although the Ca^{2+} are bound to the pump protein, they do not contribute to the Ca^{2+} concentration inside the cytosol or to the Ca^{2+} concentration inside the ER, therefore, the Ca^{2+} is being buffered by the SERCA pump. Because there is a large amount of pump protein present, the pump is able to bind a large amount of Ca^{2+} and so the buffering effect of the pump is significant [6].

It is well understood that CaSR in PM directly activates PLC, and in turn PLC generates IP_3 which then releases Ca^{2+} from intracellular stores and stimulates Ca^{2+} influx. Therefore, maximal rate of IP_3 production by PLC depends on the agonist concentration and does not related directly to intracellular Ca^{2+} concentration. What we observe from the simulation is that changing the rate of IP_3 production to higher values, causes decrease in intracellular Ca^{2+} level as well as ER Ca^{2+} concentration level. The latter can be explained by the fact that binding of IP_3 and Ca^{2+} to IP_3R on ER causes depletion of this Ca^{2+} store. Looking at equation (3.3), the first term is responsible for the sensitivity of PLC to extracellular Ca^{2+} concentration while the second term shows the IP_3 degradation rate which still doesn't relate to intracellular Ca^{2+} concentration. However, mathematically, lowering V_{\max} causes first term becomes small, so solving the differential equation shows the IP_3 level decreases. If there wouldn't be enough IP_3 to activate IP_3R , the excess of Ca^{2+} in ER will be removed by leak channel which causes increase in cytosolic Ca^{2+} level. Increasing V_{\max} causes more IP_3 and depletion of the Ca^{2+} store through IP_3R , however, cell remove excess of cytosolic Ca^{2+} by PMCA and SERCA, thus, resulting in reduction of the intracellular Ca^{2+} concentration.

In general, IP₃ degradation rate sets the time frame over which IP₃ accumulation are integrated as input signal. The lifetime of IP₃ determines whether regeneration of IP₃ production could underline propagation of Ca²⁺ waves. Consequently, the waves can cross cells without diminishing or slowing and are those form generated by a process in which a messenger is regeneratively produced [7]. The lifetime and diffusion constant of IP₃ in cytoplasm together determine its spatial range of action which was measured by several studies [8-11]. However, information about how quickly IP₃ is degraded in a single cell most recently was determined [12].

In Wang et al study, the delay to Ca²⁺ release was used to infer the lifetime of IP₃ in an individual cell [12]. They showed that Ca²⁺ release is slower at lower doses of agonist and the latency is longer. Additionally, higher concentration of agonist causes greater activation of PLC and faster generation of IP₃. Therefore, they concluded that latency will decrease with increasing muscarinic receptor occupancy. Experimental results indicate that muscarinic receptors expressed in human keratinocytes regulate their viability, proliferation, migration, adhesion, and terminal differentiation, hair follicle cycling, and secretion of humectants, cytokines, and growth factors [13]. The relationship between inverse muscarinic receptor occupancy and latency will be an exponential with time constant, as it is indicated by Wang et al [12]. Ca²⁺ itself might contribute to setting the latency. Study showed that latency if caused by gradual accumulation of small amount of Ca²⁺ that feedback positively to cause regenerative Ca²⁺ induce Ca²⁺ release [14]. Ca²⁺ could also functions to shorten latency by enhancing IP₃ action to cause more Ca²⁺ release, analogous to the role of depolarization in the initiation of an action potential. In our simulation changing IP₃ degradation rate changes cytosolic Ca²⁺ level significantly. The marked change was for lowering the rate which caused cytosolic Ca²⁺ level reaches to steady level very slowly. This is in agreement with the explanation of Wang that Ca²⁺ release begins when IP₃ level reaches threshold level.

Inhibition of IP₃ receptor by increasing cytosolic free Ca²⁺ concentration may contribute to terminating Ca²⁺ releases but it may not be the only mechanism [15]. In fact, IP₃- evoked Ca²⁺ release is quantal. The mechanism of quantal Ca²⁺ release is not known however two categories of mechanism have been proposed. The first model is that submaximal concentration of IP₃ completely empty the stores that are most sensitive to IP₃, and higher IP₃ concentrations then recruit the less sensitive stores [16-18]. Second model suggests that IP₃R activity attenuates before Ca²⁺ stores are fully depleted [19,20]. The mechanisms that might curtail IP₃R mediated Ca²⁺ release are included IP₃ medicated inactivation, inhibition by increase cytosolic Ca²⁺, loss of the electrochemical gradient of Ca²⁺ for Ca²⁺ release as Ca²⁺ ions leave ER without compensatory charge movement, and regulation of IP₃R by luminal Ca²⁺. The latter mechanism proposes that

opening of an IP₃R requires binding of IP₃ and of Ca²⁺ at both the cytosolic and luminal sides of the IP₃R, as it mentioned earlier [19, 21]. Regulation by luminal Ca²⁺ predicts that as ER Ca²⁺ level falls, the sensitivity of IP₃R to cytosolic IP₃ and Ca²⁺ decline, and Ca²⁺ release then terminates with Ca²⁺ trapped in the ER. Rossi et al showed that incremental response to low IP₃ concentration are accompanied by rapid inactivation of IP₃R [22]. Also, it is clear that the rapid activation of IP₃R by IP₃ is followed by slower inactivation and slower recovery. This mechanism would permit incremental response only if inactivating requires most IP₃ binding site to be occupied. What we have observed from our simulation when k_d (model parameters for IP₃R inactivation by IP₃) were changed confirming that increasing IP₃ rate decreases the flux of Ca²⁺ through IP₃R. In contrast lowering IP₃ inactivation rate, as it mentioned above may reduce the Ca²⁺ level as it might be low IP₃ concentration to bind the receptor.

Mechanism of inhibition of IP₃R is though feed by Ca²⁺ as it crosses an open channel, but even there are local Ca²⁺ signals would be intercepted, which did not promote quantal response. Many studies suggest that IP₃R inactivation is directly connected to rapid activation of IP₃R by IP₃ which is followed by slow inactivation rather than via feedback effect from increase in cytosolic Ca²⁺ concentration [23-25]. Our model shows that changing the inactivation of IP₃R by Ca²⁺ parameter doesn't change the level of cytosolic Ca²⁺ concentration, while ER Ca²⁺ concentration level for low η values is small and reaches to a steady level very slowly.

As it mentioned previously, PLC's role in signal transduction is its cleavage of PIP₂ into DAG and IP₃. Activator of each PLC vary but typically include small G protein, Ca²⁺ and phospholipids. From simulation results we can see that change in k_m doesn't affect cytosolic Ca²⁺. Meaning that it doesn't have a direct effect on changing the Ca²⁺ level.

Excess of cytosolic Ca²⁺ is removed by SERCA pump as well as PMCA. From formula we wrote for SERCA flux we can see that Ca²⁺ affinity of SERCA pump (K_{SERCA}) inversely related to the flux. This can be seen from the results that decreasing this parameter caused the Ca²⁺ level in cytosol increases. PMCA and NCX are two other mechanism responsible to Ca²⁺ extrusion. The NCX has low Ca²⁺ affinity, but high capacity for Ca²⁺ transport, whereas PMCA have a high affinity to Ca²⁺ but low transport capacity. Therefore, PMCA has been attributed a housekeeping role in sustaining cytosolic Ca²⁺. It is clear that as maximal PMCA current increases more Ca²⁺ extrude from cytosol. The ER Ca²⁺ level graph for changing this parameter shows that decreasing V_{PMCA} increases Ca²⁺ level in ER. This is obvious as SERCA pump works in a similar manner to remove excess of Ca²⁺. In other words, in a cell all compartments and channels are working in cooperative way to maintain Ca²⁺ level. PMCA are autoinhibited under low Ca²⁺ concentration.

Calmodulin binding to a unique regulatory domain release the autoinhibition and activates pumps. Binding Ca^{2+} to calmodulin causes a conformational change that permits Ca^{2+} /calmodulin to bind various target protein, thereby switching their activities on or off. If cytosolic Ca^{2+} is high so it triggers binding of it to calmodulin causes activation of PMCA pump. Therefore, changing in affinity of the PMCA would be related to the calmodulin which is related to cytosolic Ca^{2+} . From our result it can be seen that increasing k_{PMCA} caused Ca^{2+} level increase. Since it reduces the outflux through PMCA.

From our analysis we can conclude that parameters that have had large contribution in change of cytosolic Ca^{2+} level are including k_d (IP_3R inactivation by IP_3), $k_{\text{IP}_3\text{R}}$ (maximal IP_3R release rate), K_{SERCA} (Ca^{2+} affinity of SERCA pumps), and V_{max} (Maximal rate of PLC production). It should be noted that only first peak is affected by the changes of these parameter. Means that what we see from the experimental results traces is that the first peak is for the behavior of ER to efflux of Ca^{2+} due to dynamic of IP_3 in cell.

Other goal of the experiment was to simulate also the behavior of the system in case HC is blocked. Running the simulation for different concentrations with control parameter, while considering HC is blocked, shows that the first peak is still existed while the second hump reduced. Looking at graphs for HC close while cytosolic Ca^{2+} model parameters are changed; it can be easily seen that the first peak has changed while the second hump disappeared. In other words, we didn't observe any significant change on the second peak as the cytosolic Ca^{2+} model parameters were changed. Therefore, we conclude that the appearance of the second peak is the result of the inflow of Ca^{2+} through HC.

4.3 Conclusion

Our mathematical simulation of Ca^{2+} dynamic could fit well with experimental data for both cases, HC open and close. Guided by simulation, we were able to identify peculiar biphasic elevation of cytosolic Ca^{2+} observed experimentally by changing different model's parameters. We conclude that the first peak that was observed experimentally is due to the releases of Ca^{2+} from ER and second peak was the results of Ca^{2+} influx from extracellular milieu to cytosol as well observed by our mathematical model.

4.4 References

1. Nardin C, Tettey-Matey A, Donati V, Marazziti D, Di Pietro C, Peres C, Raspa M, Zonta F, Yang G, Gorelik M, Singh S, Cardarelli L, Sidhu SS, Mammano F. A Quantitative Assay for Ca²⁺ Uptake through Normal and Pathological Hemichannels. *Int J Mol Sci*. 2022 Jun 30;23(13):7337. doi: 10.3390/ijms23137337. PMID: 35806342; PMCID: PMC9266989.
2. Rizzuto R, Brini M, Murgia M, Pozzan T. Microdomains with high Ca²⁺ close to IP₃-sensitive channels that are sensed by neighboring mitochondria. *Science*. 1993 Oct 29;262(5134):744-7. doi: 10.1126/science.8235595. PMID: 8235595.
3. Csordás G, Thomas AP, Hajnóczky G. Quasi-synaptic calcium signal transmission between endoplasmic reticulum and mitochondria. *EMBO J*. 1999 Jan 4;18(1):96-108. doi: 10.1093/emboj/18.1.96. PMID: 9878054; PMCID: PMC1171106.
4. Lemos FO, Bultynck G, Parys JB. A comprehensive overview of the complex world of the endo- and sarcoplasmic reticulum Ca²⁺-leak channels. *Biochim Biophys Acta Mol Cell Res*. 2021 Jun;1868(7):119020. doi: 10.1016/j.bbamcr.2021.119020. Epub 2021 Mar 30. PMID: 33798602.
5. Vandecaetsbeek I, Vangheluwe P, Raeymaekers L, Wuytack F, Vanoevelen J. The Ca²⁺ pumps of the endoplasmic reticulum and Golgi apparatus. *Cold Spring Harb Perspect Biol*. 2011 May 1;3(5):a004184. doi: 10.1101/cshperspect.a004184. PMID: 21441596; PMCID: PMC3101839.
6. Higgins ER, Cannell MB, Sneyd J. A buffering SERCA pump in models of calcium dynamics. *Biophys J*. 2006 Jul 1;91(1):151-63. doi: 10.1529/biophysj.105.075747. Epub 2006 Apr 14. PMID: 16617079; PMCID: PMC1479058.
7. Winfree, A. T. when time breaks down the Three-Dimensional Dynamics of Electrochemical Waves and Cardiac Arrhythmias, Princeton University press, NJ, 340 pp.
8. Allbritton NL, Meyer T, Stryer L. Range of messenger action of calcium ion and inositol 1,4,5-trisphosphate. *Science*. 1992 Dec 11;258(5089):1812–1815
9. Irvine RF, Anggård EE, Letcher AJ, Downes CP. Metabolism of inositol 1,4,5-trisphosphate and inositol 1,3,4-trisphosphate in rat parotid glands. *Biochem J*. 1985 Jul 15;229(2):505–511.
10. Stauderman KA, Harris GD, Lovenberg W. Characterization of inositol 1,4,5-trisphosphate-stimulated calcium release from rat cerebellar microsomal fractions. Comparison with [3H]inositol 1,4,5-trisphosphate binding. *Biochem J*. 1988 Oct 15;255(2):677–683.
11. Breer H, Boekhoff I, Tareilus E. Rapid kinetics of second messenger formation in olfactory transduction. *Nature*. 1990 May 3;345(6270):65–68.
12. Wang SS, Alousi AA, Thompson SH. The lifetime of inositol 1,4,5-trisphosphate in single cells. *J Gen Physiol*. 1995 Jan;105(1):149-71. doi: 10.1085/jgp.105.1.149. PMID: 7730788; PMCID: PMC2216926.
13. Grando SA. Muscarinic receptor agonists and antagonists: effects on keratinocyte functions. *Handb Exp Pharmacol*. 2012;(208):429-50. doi: 10.1007/978-3-642-23274-9_18. PMID: 22222709.
14. Dupont G, Berridge MJ, Goldbeter A. Latency correlates with period in a model for signal-induced Ca²⁺ oscillations based on Ca²⁺-induced Ca²⁺ release. *Cell Regul*. 1990 Oct;1(11):853–861
15. Wiltgen SM, Dickinson GD, Swaminathan D, Parker I. Termination of calcium puffs and coupled closings of inositol trisphosphate receptor channels. *Cell Calcium*. 2014 Sep;56(3):157-68. doi: 10.1016/j.ceca.2014.06.005. Epub 2014 Jun 26. PMID: 25016315; PMCID: PMC4162808.
16. Ferris C.D., Cameron A.M., Haganir R.L., Snyder S.H. Quantal calcium release by purified reconstituted inositol 1,4,5-trisphosphate receptors. *Nature*. 1992;356:350–352. -
17. Hirose K., Iino M. Heterogeneity of channel density in inositol-1,4,5-trisphosphate-sensitive Ca²⁺ stores. *Nature*. 1994;372:791–794.

18. Oldershaw K.A., Richardson A., Taylor C.W. Prolonged exposure to inositol 1,4,5-trisphosphate does not cause intrinsic desensitization of the intracellular Ca²⁺-mobilizing receptor. *J. Biol. Chem.* 1992;267:16312–16316
19. Irvine R.F. “Quantal” Ca²⁺ release and the control of Ca²⁺ entry by inositol phosphates—A possible mechanism. *FEBS Lett.* 1990;263:5–9
20. Parys J.B., Missiaen L., De Smedt H., Casteels R. Loading dependence of inositol 1,4,5-trisphosphate-induced Ca²⁺ release in the clonal cell line A7r5. Implications for the mechanism of quantal Ca²⁺ release. *J. Biol. Chem.* 1993;268:25206–25212.
21. Marchant J.S., Taylor C.W. Cooperative activation of IP₃ receptors by sequential binding of IP₃ and Ca²⁺ safeguards against spontaneous activity. *Curr. Biol.* 1997;7:510–518.
22. Rossi AM, Riley AM, Dupont G, Rahman T, Potter BVL, Taylor CW. Quantal Ca²⁺ release mediated by very few IP₃ receptors that rapidly inactivate allows graded responses to IP₃. *Cell Rep.* 2021 Nov 2;37(5):109932. doi: 10.1016/j.celrep.2021.109932. PMID: 34731613; PMCID: PMC8578705.
23. Hajnóczky G., Lin C., Thomas A.P. Luminal communication between intracellular calcium stores modulated by GTP and the cytoskeleton. *J. Biol. Chem.* 1994;269:10280–10287.
24. Stehno-Bittel L., Lückhoff A., Clapham D.E. Calcium release from the nucleus by InsP₃ receptor channels. *Neuron.* 1995;14:163–167
25. Mak D.-O., McBride S., Raghuram V., Yue Y., Joseph S.K., Foskett J.K. Single-channel properties in endoplasmic reticulum membrane of recombinant type 3 inositol trisphosphate receptor. *J. Gen. Physiol.* 2000;115:241–256.

(This page is intentionally left blank)